DYNAMIC EMMA: INVESTIGATING WATERSHED FLOW PATHWAYS USING GEOCHEMISTRY AND TIMING AT PANOLA MOUNTAIN RESEARCH WATERSHED, GEORGIA

By

RICHARD HOLLAND CARY

(Under the Direction of John F. Dowd)

ABSTRACT

Investigating storm runoff generation in watersheds is an area of ongoing hydrologic research. Geochemical tracer studies, such as static end-member mixing analysis (EMMA) and hysteresis loop analysis, have been used to evaluate these processes. We propose a new method called “Dynamic EMMA” (DEMMA) that incorporates both hysteresis loops and geochemical tracer studies to quantify runoff contributions from watershed flow pathways during a storm. This approach involves estimating relative tracer concentrations of four end-members, along with estimating the percentage of total stream discharge from each end-member. The method has been applied to storms from a 22 year dataset from Panola Mountain Research Watershed (PMRW), Georgia. Using DEMMA, two distinct watershed responses to rain events have been identified at PMRW, one where hysteresis rotation is clockwise, and another where the rotation is counter-clockwise. These responses appear to be related to a threshold of approximately 50 mm of total rain per storm.

INDEX WORDS: EMMA, flow pathways, hysteresis, mixing model, storm runoff

DYNAMIC EMMA: INVESTIGATING WATERSHED FLOW PATHWAYS USING GEOCHEMISTRY AND TIMING AT PANOLA MOUNTAIN RESEARCH WATERSHED, GEORGIA

by

RICHARD HOLLAND CARY

B.S, The University of Georgia, 2003

A Thesis Submitted to the Graduate Faculty of The University of Georgia in Partial Fulfillment of the Requirements of the Degree

MASTER OF SCIENCE

ATHENS, GEORGIA

2011

DYNAMIC EMMA: INVESTIGATING WATERSHED FLOW PATHWAYS USING GEOCHEMISTRY AND TIMING AT PANOLA MOUNTAIN RESEARCH WATERSHED, GEORGIA

by

RICHARD HOLLAND CARY

Major Professor: John F. Dowd

Committee: Norman E. Peters
C. Rhett Jackson

Electronic Version Approved:

Maureen Grasso
Dean of the Graduate School
The University of Georgia
August 2011

ACKNOWLEDGEMENTS

I would like to thank Dr. John Dowd for serving as my advisor for this project. Without the custom program the he developed for this project this research would not have been possible. I appreciate all of his many attempts to explain these concepts to me. I am sure that some of them will stick!

I also wish to thank Dr. Jake Peters and Dr. Rhett Jackson for serving on my committee. Their valuable insight and assistance helped immensely with the completion of this research. I also greatly appreciate the advice and support provided by Dr. Dave Wenner and Dr. Todd Rasmussen.

The extensive data on the Panola Mountain Research Watershed provided by the US Geological Survey enabled this project to proceed. It is truly an amazing resource for researchers.

I thank my parents, Richard and Marilynn Cary for their support in all aspects of my life. I appreciate all that you have done for me!

Finally, but not the least!, I thank my wife Liz Cary for the truly amazing amount of effort, assistance, and encouragement she has given me. If not for her, I likely would not have entered graduate school, much less completed it!

TABLE OF CONTENTS

LIST OF TABLES

Page

LIST OF FIGURES

Page

CHAPTER 1: INTRODUCTION

Numerous hydrochemical studies have been conducted to investigate the contributions of watershed flow pathways during rainstorms. While this research has identified pre-event water as the dominant contribution to stream flow during storms (Pinder and Jones 1969; Sklash and Farvolden 1979; Sklash 1990), it has not been able to determine the actual flow mechanisms or their timings (Buttle 1994). Understanding these processes is important from a watershed management perspective, because which areas of the watershed that generate flow has implications for both flood control and stream ecological health.

Hydrograph separations have been used to divide a storm hydrograph into event (new) and pre-event (old) waters (Pinder and Jones 1969). Pre-event water has been further divided into base flow and soil water (Kennedy *et al.* 1986; DeWalle *et al.* 1988). Hydrograph separations can provide insight into the timing and source of inputs to stream discharge and the amount contributed from these sources.

One method used to generate hydrograph separations is end-member mixing analysis (EMMA) (Christopherson *et al.* 1990; Hooper *et al.* 1990; Burns *et al.* 2001). EMMA assumes that stream water is made up of a mixture of waters supplied by distinct components of the watershed, each with distinctive concentrations of natural geochemicals (Figure 1). The geochemical signature of the stream can be used to determine the contributions of these watershed components to total stream flow. One drawback of EMMA is its use of a fixed end-member composition, which likely varies over time. This may lead to results that do not accurately represent the flow contributions of each component (or end-member) during a storm (Hooper 2001).

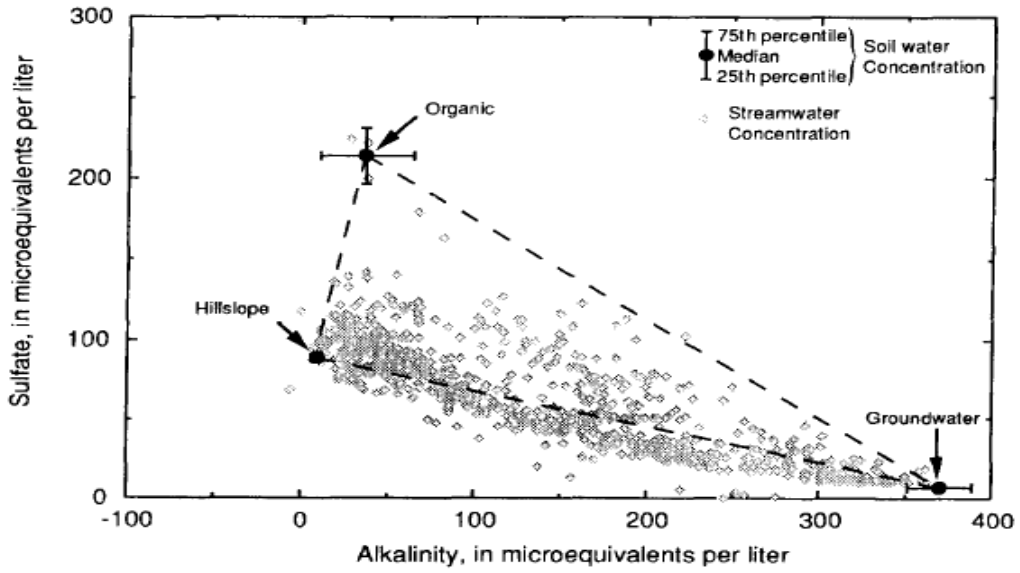

Figure 1. Example of EMMA (Hooper *et al.* 1990).

Another method used to investigate storm runoff generation processes is the analysis of the hysteresis of concentration-discharge (C/Q) loops (Evans and Davies 1998; Chanat *et al.* 2002). Hysteresis of stream solutes occurs during storm events when the variation in stream solute concentrations is different for the same discharge on the rising and falling limbs of the hydrograph (Walling and Webb 1986). Techniques that involve the analysis of these loops utilize the temporal variations in stream tracer concentrations with respect to stream discharge along with approximate tracer concentrations supplied by each component to show hysteresis between the rising and falling limbs of the hydrograph. The C/Q loop can then be matched to a hysteresis loop taxonomy, such as the one developed by Evans and Davies (1998) (Figure 2). This taxonomy provides an indication of which component of the watershed dominates flow contributions during the storm hydrograph. This method also has limitations, mainly that it cannot quantify the percentage of contribution coming from each component, and that it cannot provide the tracer concentration of each end-member.

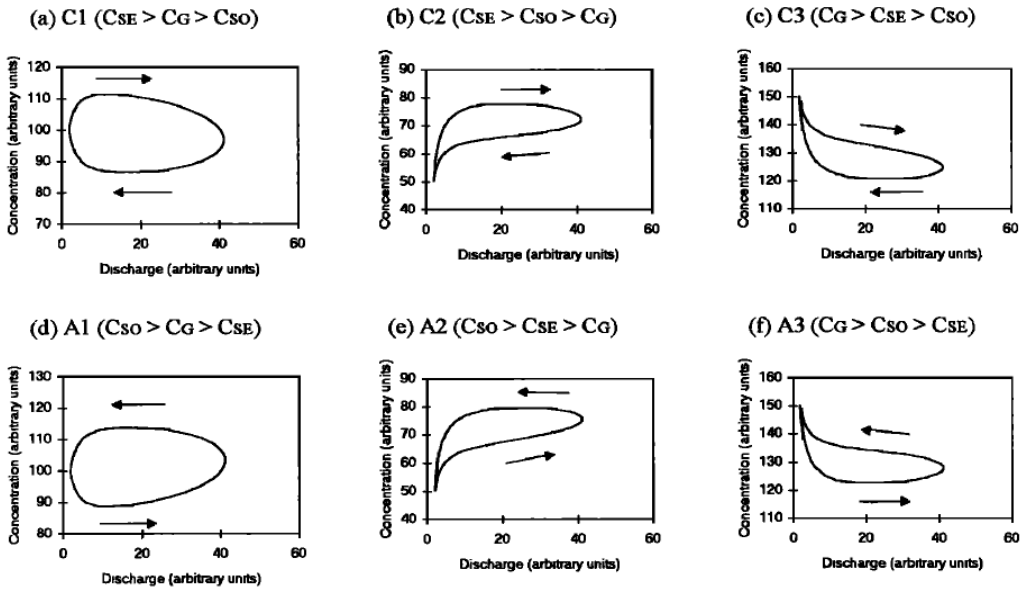

Figure 2. Example of C/Q hysteresis loop taxonomy from Evans and Davies (1998).

In this paper, we propose a new method that incorporates elements of both EMMA and hysteresis loop analysis, which we apply to data collected at Panola Mountain Research Watershed (PMRW). This method uses a range of measured end-member tracer concentration values for four watershed components along with estimates of flow pathway contributions and their timing to fit actual hysteresis loops for two natural geochemical tracers. By analyzing the results generated from this method, we can investigate the flow pathways operating at PMRW.

CHAPTER 2: LITERATURE REVIEW

One of the most widely used hydrologic models utilized today, the curve number method (USDA 1986), is based on the assumption that the bulk of storm runoff enters the stream via overland flow. This theory was built upon the work of Horton (1933 and 1945), who focused on the importance of soil erosion and infiltration rates on the movement of water on the ground surface. He theorized that this infiltration excess overland flow was the primary contributor of storm water in a stream. The underlying assumption in his work is that subsurface water movement is far too slow to contribute to storm flow. Horton's research was well-accepted and other flow pathways were virtually ignored for many years.

General Hillslope Hydrology

A major concern with models based on Horton's research is that overland flow is rarely observed in the field. This discrepancy led researchers at the Coweeta Research Watershed, North Carolina to evaluate the contributions of soil water to stream flow by measuring water flow through a 3x3x45 ft soil-filled trough (Hewlett 1961; Hewlett and Hibbert 1963). Surprisingly, water drained from the trough for 140 days after application, causing them to conclude that subsurface flow was likely a major storm runoff generation process. Hewlett and Hibbert (1967) also developed the concept of the variable source area (VSA), which states storm runoff is generated by a relatively small portion of the watershed that expands and contracts during the course of the storm, depending on the amount of rain and antecedent conditions. As part of the same research, Hewlett and Hibbert also introduced the concept of quick and delayed storm flow as a way of describing the timing of watershed response to storms (Figure 3).

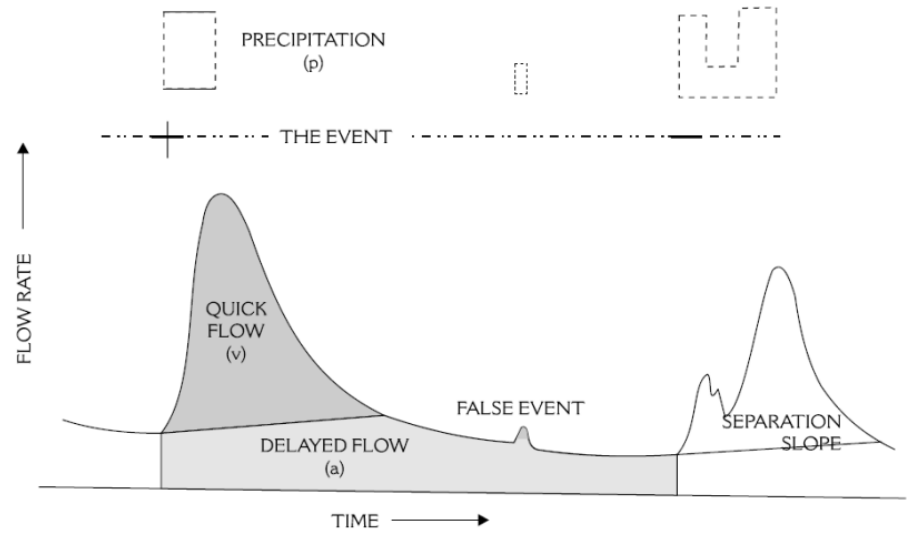

Figure 3. Hydrograph separation into quick and delayed flow created by Hewlett and Hibbert (1967). Figure recreated by McDonnell (2009).

In following hydrologic work, numerous researchers were able to note the dominance of pre-event water in storm and snow-melt runoff generation (Dincer *et al.* 1970; Martinec 1975; Fritz *et al.* 1976; Sklash and Farvolden 1979). Using natural isotopes as tracers, these researchers were able to show the dominance of groundwater in storm runoff generation in multiple watersheds. Sklash and Farvolden (1979) theorized that "groundwater ridging" might be a process that could explain how large amounts of groundwater could enter the stream so quickly. In areas near the stream, small amounts of water reaching the capillary fringe cause the water table to rapidly rise, which increases the hydraulic gradient and causes more discharge into the stream.

The Maimai Catchment, located in North Westland, New Zealand, has been the site of many innovative hydrologic research projects. Mosley (1979) proposed the concept of macropores as a possible flowpath for event water to quickly enter the stream. A few years later, Pearce *et al.* (1986) questioned Mosley's findings after noticing that isotopic tracer concentrations indicated that storm runoff at Maimai was dominated by pre-event ("old") water rather than event ("new") water. They concluded that their results clearly showed that

macropores were not rapidly delivering event water to the stream. McDonnell (1990) brought these two seemingly contradictory theories together. He asserted that under most conditions macropores quickly transmit pre-event water to the steam. However, during high intensity storms, bypass flow, which causes macropores to deliver event water to the stream through unsaturated or partially saturated soil, also plays a significant role in runoff generation.

As part of a hillslope stability experiment, Torres *et al.* (1998) identified another major storm runoff generation process. Their work showed that unsaturated zones that are very close to saturation respond quickly to pressure waves caused by changes in rainfall intensity, resulting in the rapid movement of stored soil water and leading to stream discharge. In an experiment that involved sprinkler application of water to intact soil cores, Rasmussen *et al.* (2000) showed that, at near-saturated conditions, each pass of the sprinkler resulted in a pressure wave that propagated through the soil core. As this pressure wave moved through the unsaturated zone, it caused water to be ejected from the base of the soil core much more quickly than the pore water velocity would suggest. These two projects provided a possible process for rapid pre-event storm runoff generation.

Hydrologic Methods

Mixing Models

One method that hydrologists have utilized to evaluate storm flow generation pathways is hydrograph separation. Early techniques to divide hydrographs involved using the recession limb to graphically separate the hydrograph into 2 components. In an effort to quantify the groundwater contributions to the hydrograph, Pinder and Jones (1969) used the concentrations of natural geochemical tracers to divide the hydrograph into direct runoff and groundwater runoff using a 2 component mixing model (Equation 1):

$$C_{tr} = \frac{Q_{dr}C_{dr} + Q_{gw}C_{gw}}{Q_{tr}} \qquad \text{Equation 1}$$

where C is concentration, Q is discharge, tr is total runoff, dr is direct runoff, and gw is groundwater. Using this method, they linked total stream discharge and stream tracer concentrations to the concentrations and volumes added by groundwater and event water. Pinder and Jones concluded that groundwater runoff composed 32-42% of peak discharge in the stream.

Much of the continuing work with mixing models used natural geochemical and isotopic tracers with two component mixing models. However, DeWalle *et al.* (1988) noted the traditional two component model yielded erroneous results (contributions of up to 160% "old" water) at Fish Run, Pennsylvania. Instead, they utilized a three component model (groundwater, soil water, and channel precipitation), which better accounted for stream constituent concentrations and flow paths of storm runoff. In addition, Sklash (1990) and Buttle (1994) have published extensive reviews of methods involving mixing models.

In a study at PMRW, Hooper *et al.* (1990) employed end-member mixing analysis (EMMA) to investigate contributions of storm runoff from different components of the watershed. EMMA is an attempt to relate measurements of stream flow chemistry to observed soil- and ground-water chemistries and assumes that stream water is a mixture of the solutions. This method involves plotting stream water concentrations of one natural geochemical tracer against the stream water concentration of another. Then, end-members from different sources in the watershed are plotted over the stream tracer concentrations. By selecting the three end-members that best encompass the stream water values (Figure 1), the end-members that make up the stream water tracer concentration can then be identified. At the same time, Christophersen *et al.* (1990) applied EMMA to two other watersheds located in Norway and Wales. Through the use of EMMA, they were able to determine that their sampling methods did not include the end-members necessary to create the observed stream water concentrations. This illustrated the value of EMMA as a tool for proper identification of end-members for mixing models. Christophersen and Hooper (1992) modified this method by utilizing principal

component analysis (PCA) to determine the number of end-members needed for the mixing model and which end-members should be used.

Two of the original assumptions of EMMA were that the area associated with the end-members had a large spatial extent and that the end-member tracer concentrations did not change with time. Hooper (2001) reviewed his earlier work at PMRW by testing the validity of these assumptions. He found that the end-member tracer concentrations for the hillslope were not consistent with those from riparian areas. Additionally, the end-member tracer concentrations varied from those measured during his earlier research. Hooper concluded that using stream chemistry to investigate the workings of the entire watershed was impossible, but that variations in stream flow chemistry could be used to show the relative contributions of end-members from the riparian area.

Concentration-Discharge Analysis

Another method that many researchers have employed to investigate storm flow generation pathways is the analysis of the relationship between tracer concentration and stream discharge. Walling and Foster (1975) noted the cyclic patterns of ionic solutes in two catchments in Devon County, England. They also reported that the maximum or minimum concentration of solutes often did not coincide with the peak discharge. Walling and Foster speculated that this difference may be due to antecedent moisture conditions in the watershed and developed solute generation scenarios for high and low antecedent moisture conditions.

While conducting research on nutrient dynamics, Bond (1979) plotted nutrient concentration against stream discharge for a two year period. He noted that the data for each nutrient would create generally the same general plot year after year. He hypothesized that the nutrient concentration was controlled by the amount of stream discharge and the contributions of different components of the watershed. Bond developed hypothetical plots of concentration versus discharge that could be used to explain this response (Figure 4). Similarly, Johnson and

East (1982) created a set of “idealized” concentration-discharge (C/Q) plots for individual storms at Burbage Brook, England and a set of possible conditions that would cause them. By matching the shape and direction of actual plots of specific conductance versus stream discharge to their C/Q taxonomy, they were able to estimate contributions from groundwater, soil water and surface runoff.

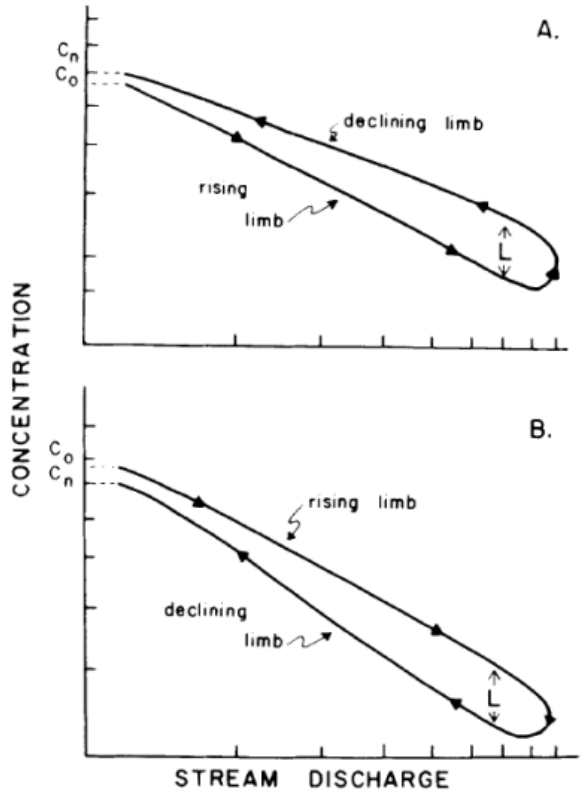

Figure 4. Counterclockwise (A) and clockwise (B) nutrient concentration patterns hypothesized by Bond (1979).

Using a synthetic hydrograph separated into two (event and pre-event) and three (event, soil water, and groundwater) components, Evans and Davies (1998) developed a taxonomy of hysteresis loops, which could be used to determine which watershed component dominated runoff at a given time during a storm (Figure 2). The taxonomy was developed by creating three hysteresis loop shapes for both the clockwise and counterclockwise directions. For example, a

hysteresis loop with a clockwise direction, concave curvature and a positive trend would be classified as type “C2”, where surface event water dominates at the start of the storm, followed by groundwater, and soil water towards the last part of the storm hydrograph. Some limitations associated with this method are that the synthetic hydrographs may not represent flow generation processes across all watersheds and that precise values for the contributions of components cannot be determined.

As an extension of the work of Evans and Davies (1998), Chanat *et al*. (2002) explored how changes in end-member behavior, such as variability in end-member volume, timing, and concentration, affected C/Q plot patterns. Specifically, they generated synthetic C/Q loops with different hydrograph separations and concentrations of a hypothetical solute, then classified these using the taxonomy developed by Evans and Davies, and, finally, identified the circumstances that could produce multiple C/Q plots for the same end-member rankings. Their results showed that while two of the six $C_{event\ water}$, $C_{groundwater}$, and $C_{soil\ water}$ rankings used by Evans and Davies would generate a unique C/Q plot, the other four rankings could produce multiple C/Q patterns. Additionally, Chanat *et al.* (2002) found that if the dominant runoff contributor continuously varied between event water and soil water, indeterminate C/Q loop shapes without clearly defined hysteresis would form. They also concluded that the process of using C/Q loops to evaluate runoff generation processes can be improved by using measurements of end-member concentrations and the knowledge of which end-member dominates the hydrograph for the watershed that is being studied.

Related Research at Panola Mountain Research Watershed

PMRW has been the site of many hydrologic research projects. Shanley and Peters (1988) utilized variations of temperature, isotopic signature, alkalinity, nitrate concentration, and sulfate concentration in stream water to evaluate storm runoff. They noted a rapid storm runoff response in the stream, and that large rain events generated enough runoff from the 3.6 ha

granite outcrop to produce a flood wave that traveled the length of the stream. They concluded that under dry antecedent conditions, storm runoff response was caused primarily by channel interception, and that rain events occurring under wet conditions resulted in an increase of the riparian zone water table, which increased the hydraulic gradient and produced more groundwater discharge in the stream.

Hooper *et al.* (1990) applied EMMA to PMRW using a three component mixing model composed of groundwater, organic horizon water, and hillslope water. They noted that the bedrock outcrop had little effect on stream chemistry. They found that storm runoff was dominated by groundwater, which is supplemented with hillslope water and shallow soil water during wet and dry antecedent conditions, respectively.

In an effort to investigate subsurface flow paths on hillslopes, McDonnell *et al.* (1996) excavated a 20 m long trench in the upper part of PMRW. After dividing the trench into 2 m sections, they determined the amount of accumulated area associated with each section based on the surface and bedrock topographies. During storm events, they collected runoff data from each trench section and found that the sections with the highest accumulated bedrock area generated the most runoff. They concluded that the bedrock topography controls subsurface flow.

By applying a two component mixing model with Cl^- as the tracer, Peters and Ratcliffe (1998) determined that Cl^- concentrations can be used to distinguish between “new” and “old” water contributions to stream flow. While they mainly focused on the differences in event and pre-event water, Peters and Ratcliffe also noted that soil water and groundwater had distinct Cl^- concentrations. They concluded that groundwater provides 75-79% of the storm runoff in the stream and that 45% of Cl^- in the watershed was from rain, with dry deposition accounting for the remainder.

In order to evaluate the relative roles of hillslope and riparian waters in storm runoff generation, Burns *et al.* (2001) applied EMMA to the 10 ha upper watershed at PMRW. They

found that peak stream discharge is dominated by runoff from the 3.6 ha bedrock outcrop in this sub-watershed, while the rising and falling limbs of the hydrographs were dominated by riparian groundwater. They also concluded that, although the two storms used in the study were preceded by wet antecedent conditions, the storm that occurred during the relatively drier conditions resulted in stream water that overall was dominated by runoff from the outcrop. Analysis of the storm occurring after a period of slightly wetter antecedent conditions revealed that overall storm runoff was dominated by riparian groundwater, followed by outcrop runoff. They hypothesized that the effectiveness of EMMA for use in determining runoff response relies heavily on more accurate identification and characterization of end-members.

Peters *et al.* (2003) analyzed 16 years of data from PMRW, which included 759 storms. They found water yield from storm runoff was most related to the maximum soil moisture. When storms reached a threshold of 37% soil moisture content value (this value is somewhat arbitrary because it was only measured at one location in the watershed), the water yields were significantly higher. Additionally, they found that, for medium and large sized storms with wet antecedent conditions, the correlation between water yields and wetness parameters was stronger than those preceded by dry conditions.

In an analysis of subsurface flow in a trench from 147-storms at PMRW, Tromp-van Meerveld and McDonnell (2006a) found a total precipitation threshold of 55 mm, where little subsurface flow occurred for storms below the threshold and significantly more subsurface flow was generated during storms above the threshold. They also observed seasonal changes in the distribution of flow from different portions of the trench. Specifically, flow through the trench face became more uniform with larger storms, wetter antecedent conditions, and during winter months. Additionally, they found that, while pipe flow was a major contributor of subsurface flow during winter storms, it was minimal during spring and summer rain events. They work suggested that bedrock topography may be less important in subsurface flow generation than previously thought. Instead, they hypothesized that subsurface flow from small storms with dry

antecedent conditions may be controlled by soil depth and that small storms with wet antecedent conditions produced subsurface flow controlled by both soil depth and bedrock topography.

As a follow-up to this research, Tromp-van Meerveld and McDonnell (2006b) attempted to investigate the cause of the 55 mm total precipitation threshold response at PMRW. In order to measure the extent and level of water table formation during rainstorms, they analyzed data from a large number of recording wells, piezometers, and crest stage gages. Based on their results, they developed a theory, called the "fill and spill hypothesis", in which percolating precipitation from small and medium sized storms start to fill bedrock depressions and create isolated saturated areas at the soil/bedrock interface. Larger storms continue to fill these saturated areas, allowing subsurface flow to spill over the bedrock depression. As total precipitation approaches the threshold value, more of these depressions fill and they become more hydrologically connected, generating much larger subsurface flows.

In order to test the accuracy of the widely held assumption that the bedrock at PMRW was impermeable, Tromp-van Meerveld *et al.* (2007) conducted sprinkler tests on the heavily instrumented hillslope area above the excavated trench. After accounting for losses due to flow around the trench edges, evapotranspiration, and flow through the trench, they concluded that as much as 91% of the applied water was lost due to leakage through the bedrock. Furthermore, they theorized that the subsurface saturation at the soil-bedrock interface, associated with their earlier fill and spill hypothesis, occurred not because the bedrock was impermeable, but instead was due to the lower infiltration rate of the bedrock compared to that of the soil. They determined that subsurface water flows both vertically into the bedrock and laterally over the bedrock.

Recent work involving PMRW has focused on modeling projects. In an attempt to evaluate subsurface storm flow thresholds, Lehmann *et al.* (2007) applied a percolation theory model of the soil-bedrock interface in order to relate subsurface connectivity and the observed

precipitation threshold. In addition to successfully reproducing the 55 mm precipitation threshold required to create a well-connected subsurface flow network, they also determined that 65% of water applied to the site was lost to flow through the bedrock. Clark *et al.* (2009) used recession analysis of discharge produced by >55 mm rain events in an effort to relate hillslope scale processes to the response of the watershed as a whole. They concluded that a model with linear reservoirs could account both for the linear relationship between precipitation and hillslope response and for the non-linear recession behavior at the watershed outlet. James *et al.* (2010) created a 3-D physics-based model of a PMRW hillslope using the TOUGH2 subsurface flow and transport simulator. Their model successfully replicated hillslope behaviors, such as variations in hillslope-scale storage, the expansion of a temporary water table at the soil-bedrock interface, and subsurface flow generation. Their results suggested that the contrast of soil to bedrock saturated hydraulic conductivity plays a key role in determining hillslope runoff response.

CHAPTER 3: METHODS

Site Description

PMRW is located approximately 25 km southeast of Atlanta, GA in the Panola Mountain State Conservation Park (Figure 5). The catchment covers 41 ha, of which 90% are covered by forest, with the remaining 10% consisting of exposed granite outcrops (Peters *et al.* 2003). Bedrock at the site is composed mainly of Panola Granite, which is a biotite-oligoclase-quartz, microcline granodiorite along with some scattered pods of amphibolitic gneiss (Higgins *et al.* 1988). The soils at the site are dominated by ultisols formed in colluvium and residiuum, which grade to inceptisols on steep slopes and at the base of the bedrock outcrop (Peters *et al.* 2003) Hillslopes comprise most of the catchment (>75%) and have shallow soils (<1 m). The riparian zone, which has the deepest soils (5 m) is relatively narrow (<50 m) and occupies less than 15% of the total catchment area.

Located in the southern Piedmont physiographic region, PMRW has a humid, subtropical climate, with average annual temperature of 16.3°C. Average annual precipitation is 1,220 mm, of which 70% is evapotranspired (Peters *et al.* 2003). Stream discharge fluctuates seasonally, generally with highest baseflows during the November-March dormant season and low baseflows during the May-October growing season (Peters *et al.* 2003; Tromp-van Meerveld *et al.* 2007).

Data Collection

The analysis herein uses data collected from PMRW during a 23-year period from October 1985 through September 2008, water years 1986 through 2008. Of the numerous wells and lysimeters present at PMRW, data from 13 groundwater (GW) wells installed at varying depths (Table 1) throughout the watershed were used, along with soil water data from four zero-tension lysimeters (Figures 5 and 6). Samples from these sites were collected weekly during the

periods when sampling occurred. Precipitation was recorded using tipping bucket rain gages. Wet/dry collectors were used to collect chemistry samples from two throughfall and two precipitation sites (Peters and Ratcliff 1998). Stream stage was recorded at 5 minute intervals during baseflow conditions and at 1 minute intervals during storms in a compound 90° V-notch weir, located at the mouth of the 41-ha watershed. An automatic sampler collected streamwater samples in the pool above the weir during rainstorms (Peters 1994). All water samples were analyzed for chloride (Cl^-) and silica (H_4SiO_4) using ion chromatography and either direct coupled plasma or inductively coupled plasma emission spectroscopy, respectively.

Table 1. Description of zero-tension lysimeters (ZW) and groundwater wells (GW).

Site Number	Depth (cm)	Screen Length (cm)	Screen Depth Below Land Surface (cm)
ZW105	0	N/A	N/A
ZW580	0	N/A	N/A
ZW617.015	15	N/A	N/A
ZW640	0	N/A	N/A
GW150	1981	None	N/A
GW311	236	152	160
GW312	244	152	168
GW321	91	61	61
GW322	122	30	107
GW325	219	30	204
GW520	221	152	145
GW530	372	61	341
GW670	366	152	290
GW691	457	61	427
GW693	411	61	381
GW760	250	152	174
GW801	398	146	325

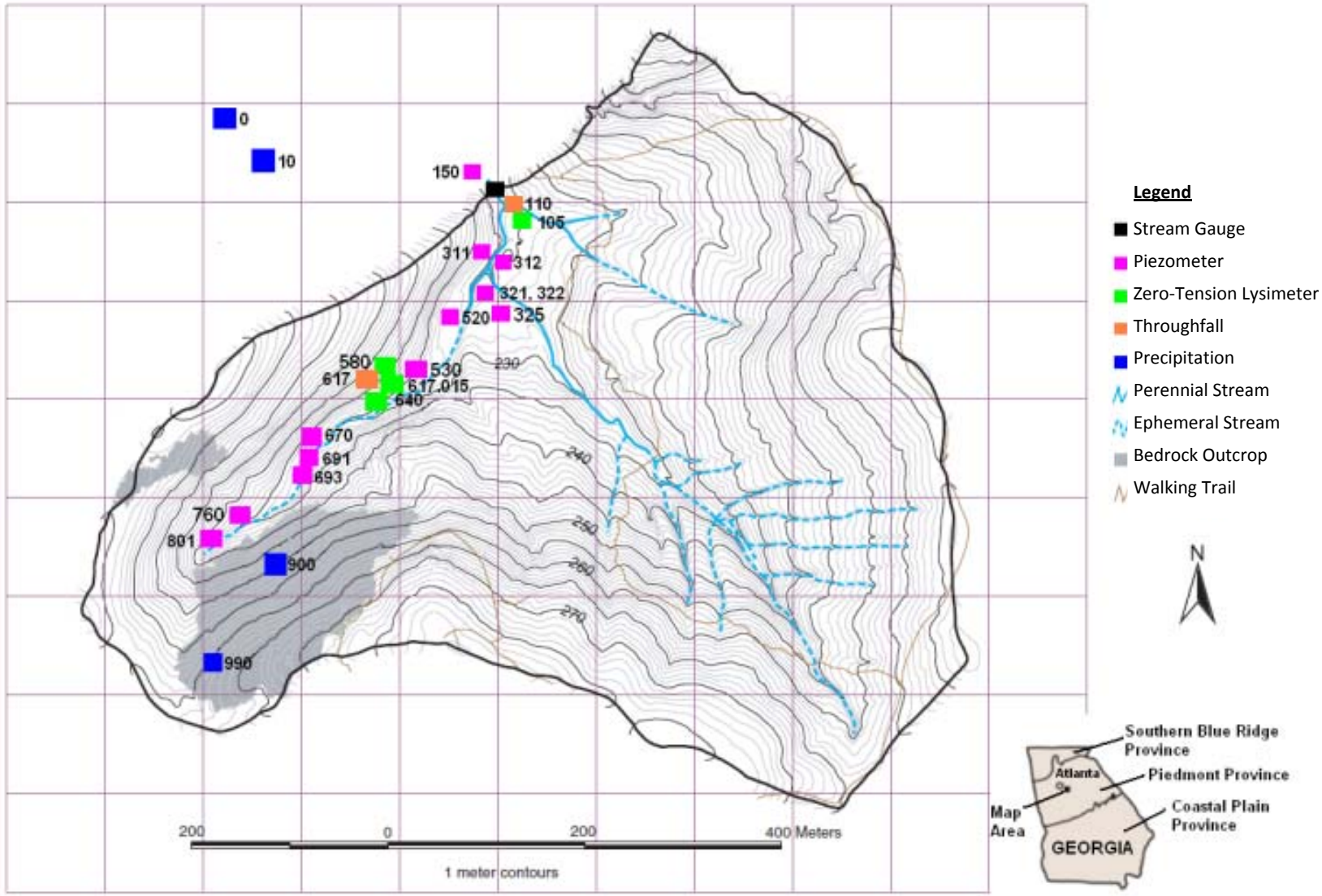

Figure 5. Map of PMRW showing location of sampling sites used in this study.

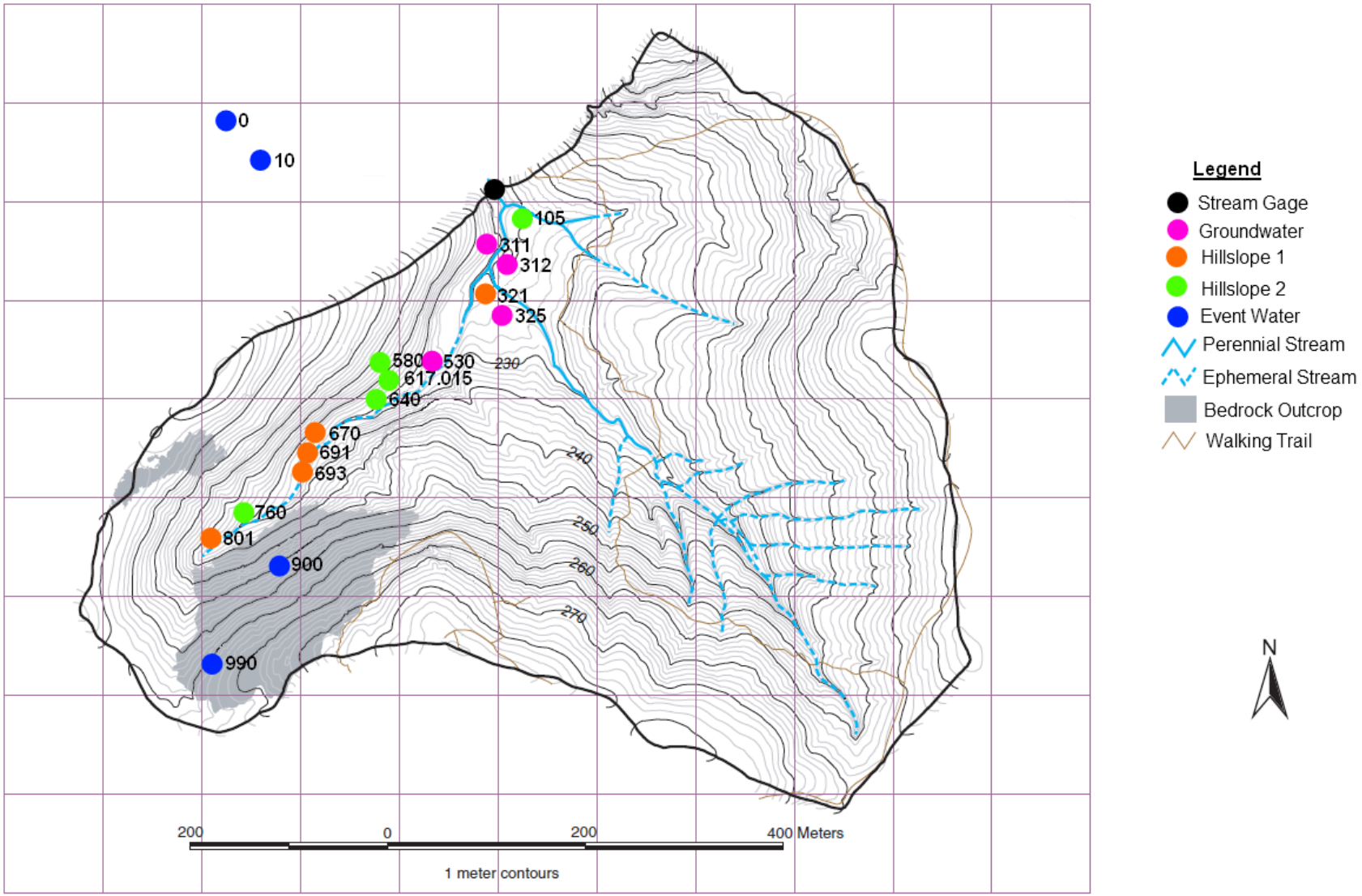

Figure 6. Map of PMRW showing location of sites used in the study grouped by end-member.

Data Analysis

End-member Identification and Characterization

Chloride and silica were selected as tracers for this study because they behave relatively conservatively at PMRW. Peters and Ratcliffe (1998) found that chloride is highly mobile at PMRW and that it is mineralogically inert and not affected by ion exchange processes. Hooper *et al.* (1990) noted that the presence of gibbsite at PMRW implies that silica has a higher mobility than at sites without the occurrence of this aluminum hydroxide mineral. They also noted that silica concentrations increase with depth in the soil profile and found no evidence of silica mobilization or precipitation.

At PMRW, chloride concentrations in precipitation are typically low compared to soil water and groundwater, which have relatively similar concentrations. Peters and Ratcliffe (1998) asserted that this is caused by concentration of chloride due to evaporation and evapotranspiration of water in the soil. Silica concentrations are extremely low in precipitation, but increase as water has more contact with weathering minerals; the longer water has contact with minerals in the watershed, the higher the silica concentration (Burns et al. 2003).

Chloride and silica concentration data from selected sites were plotted on a bivariate graph (Figure 7). Four distinct populations are noted: deep groundwater, shallow groundwater (GW), hillslope 1 water (H1), and hillslope 2 water (H2). Deep groundwater consists of water that is supplied from bedrock fractures, and is measured approximately 20 m in depth. Shallow groundwater represents water located within or near the saprolite located in the lower watershed riparian area, and is measured from four piezometers located that are between 219 to 372 cm deep. Hillslope 1 water consists of soil water from the B horizon in the lower watershed and of deeper soil water in the upper watershed. This is measured from one piezometer located in the lower part of the watershed at 91cm, and four piezometers in the upper part of the watershed that range from 366 to 457 cm. Hillslope 2 water represents shallow soil water and is measured with four zero-tension lysimeters 0-15 cm deep located in

the riparian area and one piezometer located in the upper part of the watershed which is 250 cm deep.

Deep groundwater flowing through fractured bedrock would have to flow through the weathered bedrock/saprolite to reach the stream channel, causing the deep groundwater to mix with the shallow groundwater and become diluted that is with respect to weathering products. Additionally, stream silica concentrations never reach values approaching those of the deep groundwater, indicating that deep groundwater is not a significant contributor to stream flow. Therefore, deep groundwater was not used as a flow component in the analysis. Event water (EW), which consists of runoff from the bedrock outcrop, direct precipitation or rather throughfall as rain falls through the deciduous forest canopy onto the stream channel, and runoff from the adjacent riparian zone, was used as the fourth end-member (Figure 8).

Based on the results of the relations between silica and chloride, the piezometers, lysimeters, and rainfall collectors were assigned to one of the four identified end-members (Table 2 and Figure 6). As noted previously, GW 150 was not used as an end-member. GW 322 and 520 also were not considered as part of an end-member group because they had tracer concentrations that fell between those of the GW and H1 end-members, indicating that they were a mixture of these two end-members. Box-whisker plots were made from tracer concentrations of all samples associated with each end-member (Figures 9 & 10). The expected end-member tracer concentrations were determined by using the range between the first and third quartiles (Table 3). These values showed that GW samples generally had the highest concentration for both tracers, with chloride and silica concentrations decreasing in the order of H1, followed by H2, with the lowest concentrations in EW. It should be noted that prior to entering the stream, runoff from the four end-members mix somewhat in the riparian area. This mixing may cause the actual end-member tracer concentrations to differ slightly from those that have been identified.

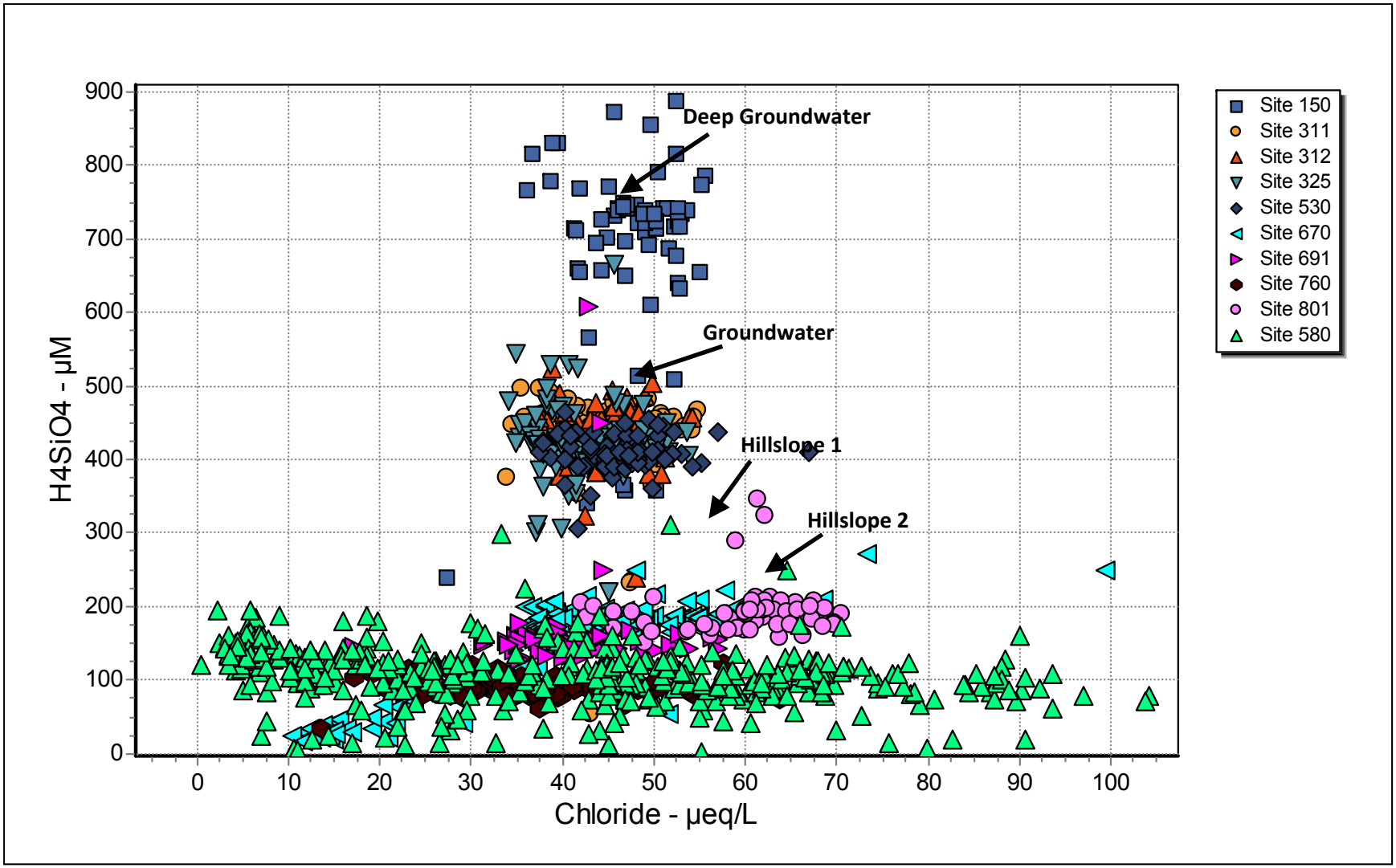

Figure 7. Chloride versus silica concentrations for selected sample sites.

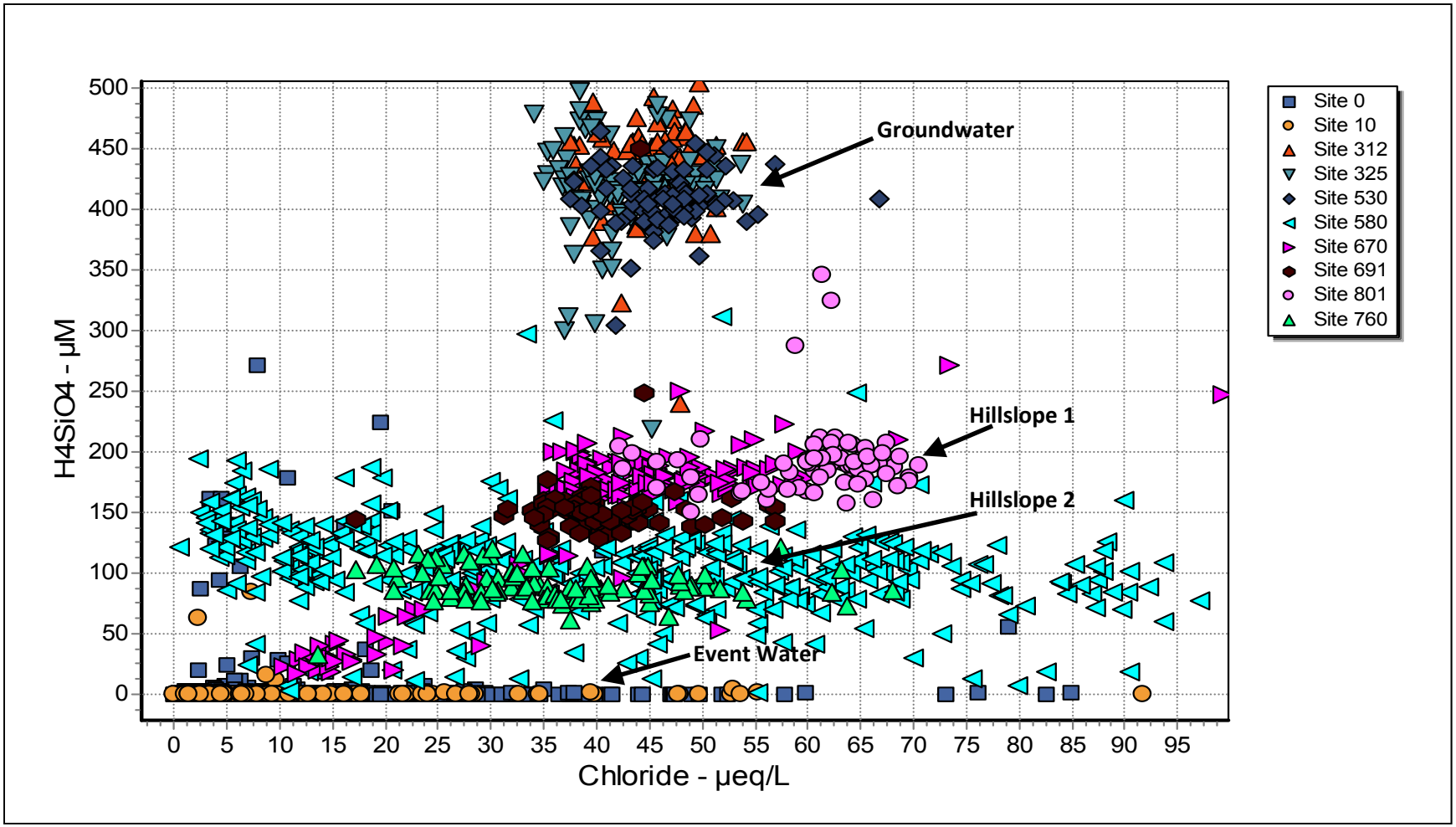

Figure 8. Chloride versus silica concentrations for end-members identified at PMRW.

Table 2. Piezometers, lysimeters, and rainfall collectors associated with end-members.

End-Member	Site Identification
Groundwater	GW 311, GW 312, GW 325, GW 530
Hillslope Water 1	GW 321, GW 670, GW 691, GW 693, GW 801
Hillslope Water 2	GW 760, ZW 105, ZW 580, ZW 617.015, ZW 640
Event Water	PW 0, PW 10, PW 900, PW 990

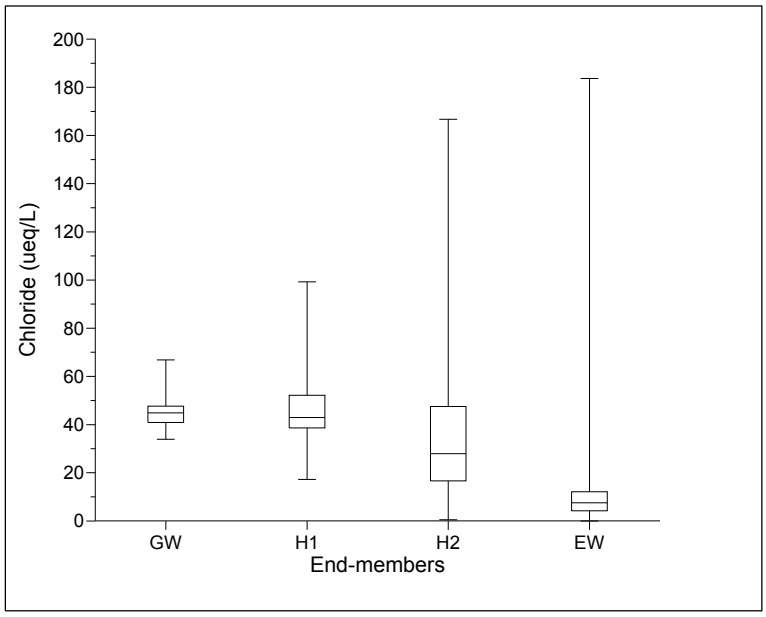

Figure 9. Box-whisker plots of chloride concentrations of samples from the four end-members at PMRW.

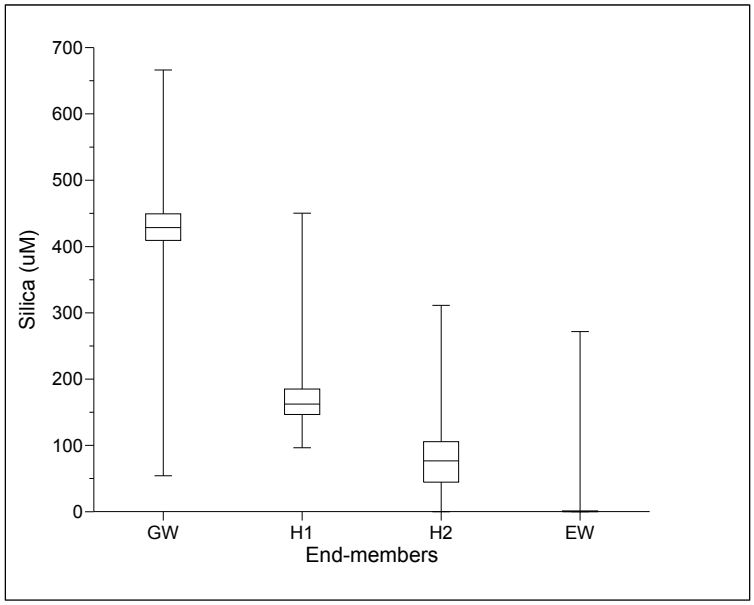

Figure 10. Box-whisker plots of silica concentrations of samples from the four end-members at PMRW.

Table 3. Range of expected tracer concentration values determined by first and third quartiles.

End-member	Chloride (µeq/L)	Silica (µM)
GW	41-48	409 - 449
H1	39-52	146 - 185
H2	17-48	44 - 105
EW	4-12	0.1 - 1.2

Storm Suitability

During the23-year sampling period at PMRW, the start and end times of 139 storms were identified. Of those storms, the hydrographs of 41 of them had single peaks and these storms were used in this analysis. Twenty-three of these storms were selected for use with the DEMMA based on the ease of applying the method to them. Storm characteristic data for the 18 storms with single peak hydrographs that were not analyzed with DEMMA are also included to better investigate causes of hysteresis loop behavior.

Storms were excluded if too few stream water samples were taken or if the sample distribution did not provide adequate coverage throughout the storm. Additionally, storms were excluded based on their hysteresis behavior. In order to evaluate DEMMA, the storms with the simplest hysteresis patterns were selected. Some storms had C/Q hysteresis loops that crossed-over themselves, creating a stylized “fish” shape (Figure 11) that would be difficult to duplicate. Possible explanations for this hysteresis shape include erratic precipitation towards the end of the storm and a longer than usual stop time for the storm. Rarely, the hysteresis of the two tracers would rotate in opposite directions (Figure 12). This behavior may be due to a possible fifth end-member with high tracer concentrations that does not normally contribute to stream discharge or a threshold response that has not fully developed. In this case, DEMMA cannot be used because the estimated hysteresis loop will always be going in the wrong direction for one tracer, making it impossible to create an accurate fit. Storms with weak hysteresis, which indicated that the mixture of contributions from end-members were the same

on the rising and falling limbs of the hydrograph, were not used due to the difficulty of generating the proper estimated hysteresis loop shape with DEMMA.

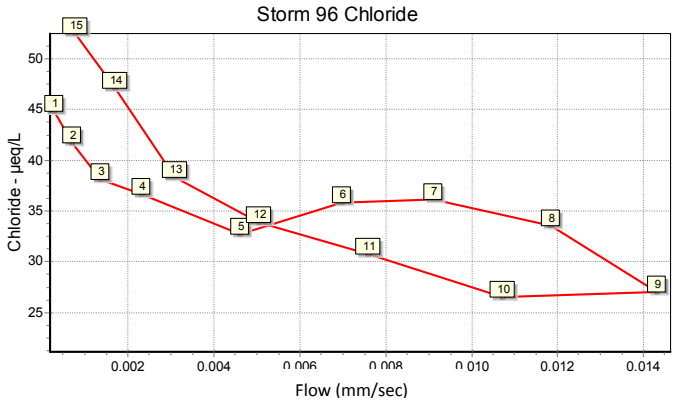

Figure 11. Storm 96 (January 19-20, 2002) is an example of a storm that was excluded from this study because its observed hysteresis crosses-over itself.

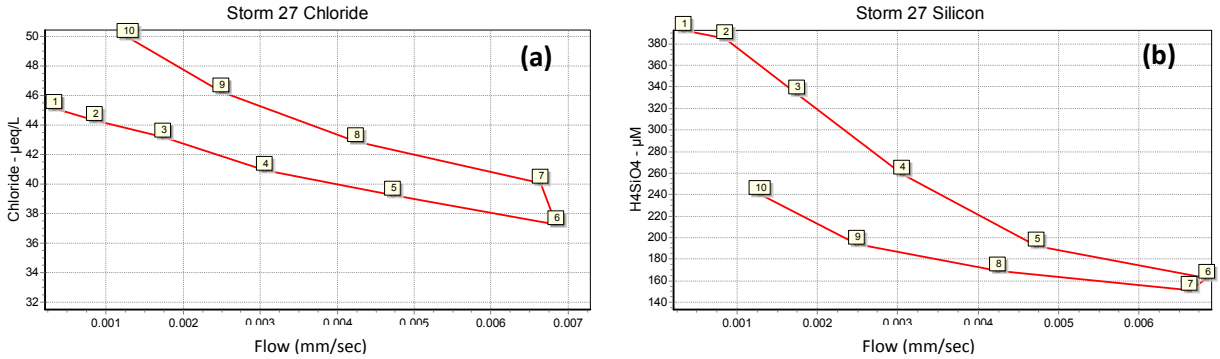

Figure 12. Storm 27 (September 20, 1993) is an example of a rain event in which the C/Q hysteresis loops for chloride (a) and silica (b) rotate in opposite directions.

DEMMA

DEMMA begins by subdividing the storm hydrograph into four components using assumptions about how these components should behave (Figure 13a). End-member concentrations for either chloride or silica are used with these components to construct synthetic chemical concentrations using a four component mixing model:

$$C_S Q_S = C_{GW} Q_{GW} + C_{H1} Q_{H1} + C_{H2} Q_{H2} + C_{EW} Q_{EW} \qquad \text{Equation 2}$$

where C is concentration, Q is discharge, S is stream water, GW is shallow groundwater, H1 is hillslope water 1, H2 is hillslope water 2, and EW is event water. The timing of component contributions can be adjusted for each end-member using a beta grading function:

$$X(i) = \left(\frac{i-1}{n}\right)^{\beta}, \quad i = 1, \ldots, N \qquad \text{Equation 3}$$

where X(i) is a point on the time axis of the hydrograph, n is the number of line segments, N is the number of points (1+n), and β is the nonlinear grading value. Additionally, a minimum Q value, representing baseflow, can be defined for each component. An important note to consider is that the percent contributions of end-members can be affected by the minimum Q values depending on the start and stop times for the storm.

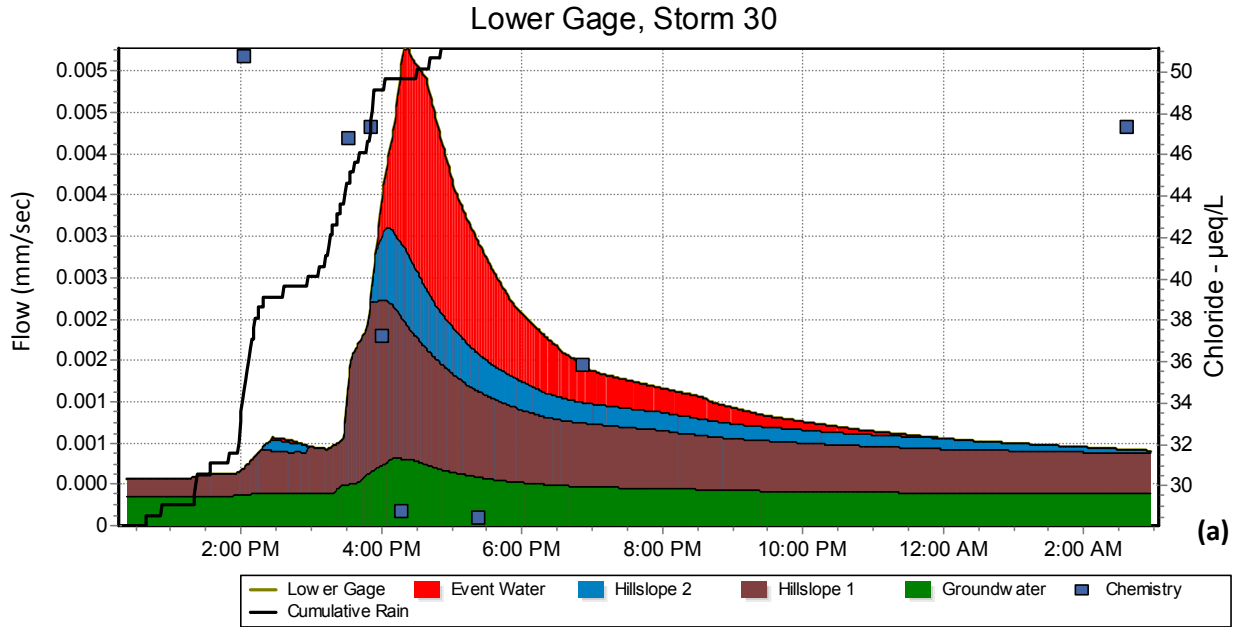

(a)

End-member	Chloride (µeq/L)	Silica (µM)	Runoff Percent
Groundwater	55	375	24.9
Hillslope 1	44	149	44.1
Hillslope 2	28	68	11.5
Event Water	9	2	19.5

(b)

Figure 13. Hydrograph separation (a) and table of end-member concentrations and component contributions (b) resulting from DEMMA of a rainstorm on December 10, 1993.

The results of the mixing model are plotted versus the total discharge to construct a synthetic hysteresis loop (Figure 14a). This loop is compared to the sample values on the observed hysteresis loop for that tracer using root mean square error (RMSE). The hydrograph components and end-member concentrations are adjusted to achieve a "best" fit. Next, the observed hysteresis loop and the calculated hysteresis loop for the other tracer is plotted. The values for component flow contribution, minimum flow, and beta-grading are preserved from the previous fit with the first tracer. Appropriate end-member concentration values are entered for the second tracer are again adjusted until the estimated hysteresis loop "best" fits the observed hysteresis of the second tracer (Figure 14b). This process is continued by switching back and forth between the tracers and adjusting the values until the best overall fit is achieved. An example of the application of DEMMA to Storm 30 which occurred on December 10, 1993 is shown in Figures 12 and 13.

Applying DEMMA to PMRW

Applying DEMMA to a typical storm at PMRW with clockwise hysteresis begins by setting the minimum discharge value for the GW and H1 end-members, usually with .0002 mm for GW and with the remainder of the baseflow being applied to H1. The percent contributions for GW are then lowered to approximately 10%, followed by 50% for H1, and 30% for H2. These percent contributions for the H1, H2, and EW end-members are the percent of the remainder of stream discharge after the previous percent contribution has been removed from the total discharge. For this example, GW would provide 10% of the total discharge, H1 would supply 50% of the remaining 90% of discharge, equaling 45% of total discharge, and H2 would supply 13.5% of the total discharge. Any remaining stream discharge is then automatically assigned to the EW end-member. Additionally, the beta grading values are then adjusted to cause the timing of flow from the GW, H1, and H2 end-members to occur earlier in the storm. These values are set to 1.1, 1.15, and 1.2, respectively.

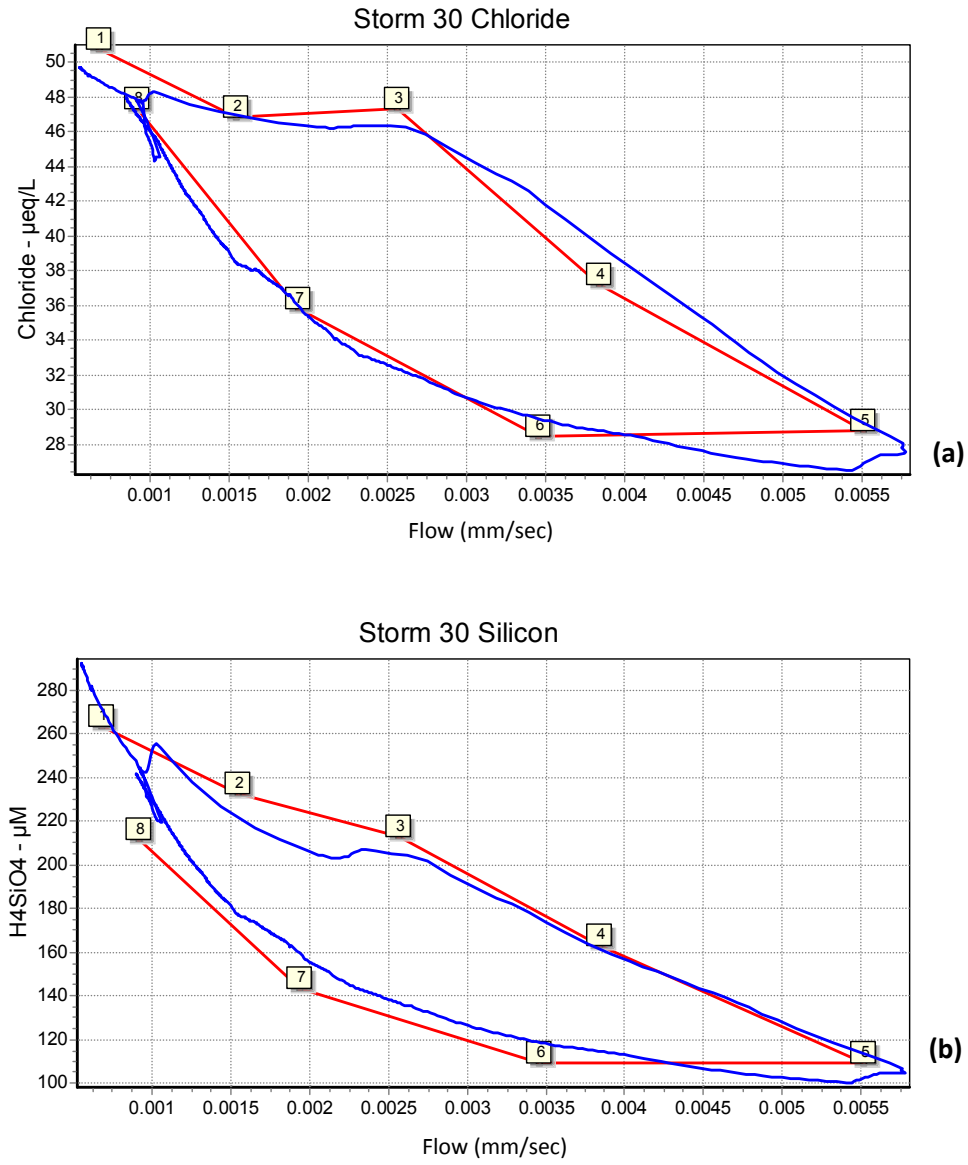

Figure 14. Estimated hysteresis loops for chloride (a) and silica (b) for Storm 30, which occurred on December 10, 1993. The numbered squares represent sample number in chronological order, the red line represents the observed hysteresis loop and the blue line is the synthetic hysteresis loop.

Next, values are set for the 4 end-member tracer concentrations. This is done using the median values identified for each end-member (Table 3). This step will cause the estimated hysteresis loop to now be plotted over the observed hysteresis plot. It is very likely that the shape of the estimated hysteresis loop will not be appropriate and that it will need to be

adjusted, possibly significantly. This adjustment must keep the majority of beta-grading values greater than one or else the estimated hysteresis loop will begin to rotate in the counter-clockwise direction. Once the proper shape is obtained, the percent contributions and end-member values are adjusted until a good fit is achieved for the current tracer. This process is repeated for the other tracer, and then continually repeated until the overall best fit realized.

The DEMMA process is similar for storms with counterclockwise hysteresis, with the main difference being the beta grading values. For counter clockwise storms, these values will generally be less than or equal to one.

Storm Characterizations

Additional storm data collected at PMRW include antecedent precipitation index (API), season, total rain, rainfall elapsed time by quartile and maximum 1 min, 5 min, and 30 min rainfall intensity. API was calculated with the equation developed by Kohler and Linsley (1951):

$$I = b_1P_1 + b_2P_2 + b_3P_3 + \ldots + b_iP_i \quad \text{Equation 4}$$

where P_i is the amount of precipitation that occurred i days prior to the storm (30 for this analysis) and b_i is a recession constant of 0.9. The season was determined by dividing the year into four seasons, wet (January1 – April 30), wet-to-dry (May 1 – May 31), dry (June 1 – November 30), and dry-to-wet (December 1 – December 31).

CHAPTER 4: RESULTS AND DISCUSSION

Storm Analysis

The initial analysis focused on storms with single peak hydrographs and revealed at least two different flow generation patterns occurring in the catchment. Generally, storms behave similarly to Storm 30, with clockwise hysteresis loops for chloride and silica (Figure 14). Tracer concentrations for these storms decrease relatively slowly during the rising limb of the hydrograph, followed by a gradual increase on the falling limb. In order to create an estimated hysteresis loop that fits the observed values, the timing of flow contributions for the pre-event components must be adjusted to occur during the rising limb of the hydrograph. This timing coincides with the occurrence of precipitation. Storms with clockwise C/Q hysteresis patterns were generally dominated by the H1 end-member, which had an average of 44.8% runoff contribution (Table 4 and Figure 15). Additionally, combining the runoff contributions from pre-event end-members (GW, H1, H2) shows that pre-event water contributes 69% of runoff during these storms (Figure 16). Peters and Ratcliffe (1998) found that 75% of runoff for storms at PMRW was from old water. It is interesting to note that, if the two clockwise storms with much higher EW contributions (Storms 53 and 79) are removed, the average contributions of pre-event water from the storms analyzed with DEMMA becomes 73.5%. The final results of the application of DEMMA to the storms with clockwise hysteresis are shown in Appendix A.

Table 4. End-member runoff contributions and RMSE values for storms with clockwise hysteresis loops.

Storm Number	% Runoff Contribution				RMSE	
	GW	H1	H2	EW	Chloride (µeq/L)	Silica (µM)
4	11.8	45.3	15.7	27.2	2.1	44.4
23	8.7	48.5	15.1	27.7	3.6	9.2
28	13.6	46.3	15.7	24.4	1.8	20.5
30	24.9	44.1	11.5	19.5	1.1	13.9
32	12.1	40.5	13.7	33.7	2.1	14.3
33	5.6	39.9	16.4	38.1	1.6	14.4
42	7.1	58.4	7.1	27.4	2.4	13.2
53	6.5	23.2	12.0	58.3	3.1	69.6
72	8.6	32.1	14.3	45.0	4.7	35.8
76	10.8	61.0	7.7	20.5	3.4	36.2
79	3.4	21.1	3.5	72.0	4.3	89.0
84	42.7	26.6	18.1	12.6	1.6	40.0
105	13.9	50.0	6.1	30.0	1.5	26.7
111	11.2	62.9	10.4	15.5	3.6	21.0
116	7.1	41.2	13.6	38.1	3.0	21.3
119	10.5	54.3	17.4	17.8	1.9	15.3
122	7.7	66.1	6.8	19.4	1.4	16.4
Average	12.1	44.8	12.1	31.0	2.5	29.5

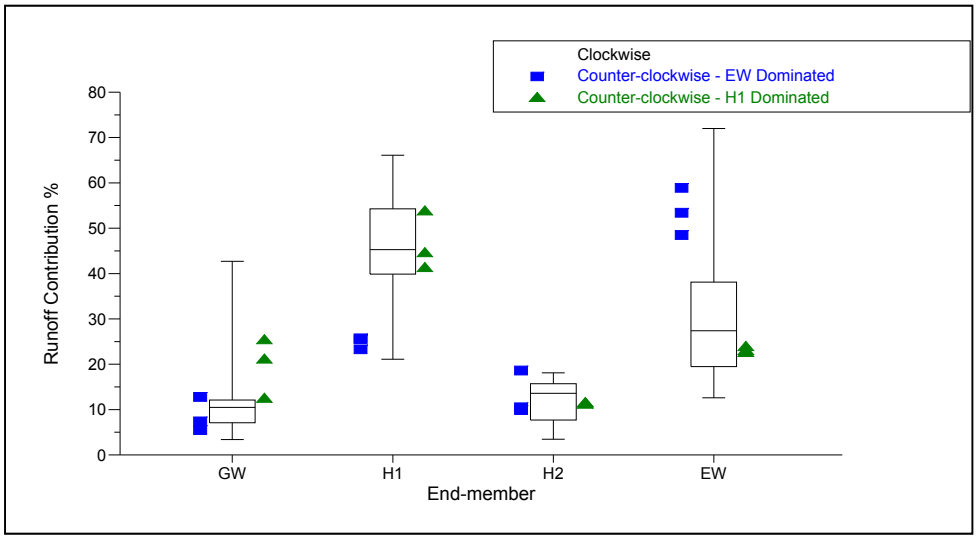

Figure 15. Percent runoff contributions from end-members used to analyze storms at PMRW with DEMMA. Box-whisker plots are used for storms with clockwise hysteresis, while individual points are used for counter-clockwise storms.

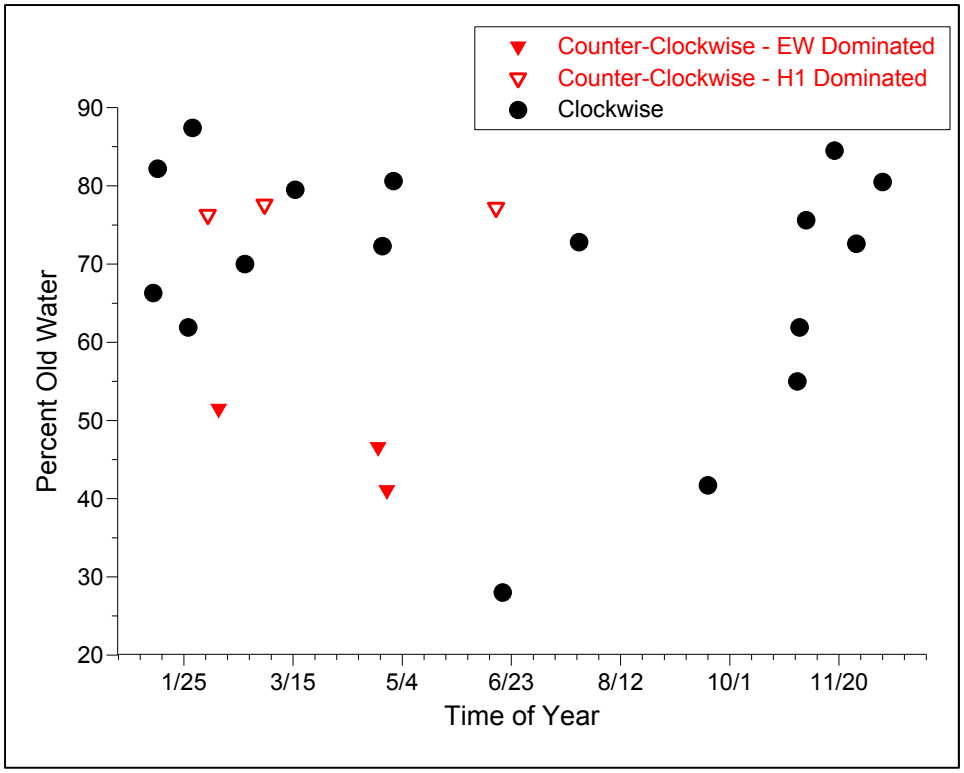

Figure 16. Percent old water runoff for storms analyzed with DEMMA. Storms occurred over a 23 year period.

RMSE was determined for each hysteresis fit by comparing the tracer concentration on the observed hysteresis loop at the times samples were taken to the estimated concentration at that time. The average RMSE for clockwise storms is 2.54 μeq/L for chloride and 29.5μM for silica (Table 4). It is important to consider that RMSE values may not accurately represent the fit because of the distribution of samples on the observed hysteresis loop, the shape of the hydrograph affecting the estimated hysteresis loop shape, and the difficulty matching the start and end of the observed hysteresis loop can make an otherwise good fit appear to be poor.

Clockwise vs. Counter-clockwise Hysteresis Rotation

Although the hysteresis rotation for most storms at PMRW is clockwise, the C/Q patterns of a few rainstorms are counter-clockwise, as seen for Storm 44 (Figure 17). Percent runoff contributions are dominated by the H1 and EW end-members (Figure 18). Of the six storms,

three are dominated by H1 with 77% of runoff contributed by pre-event water. The remaining three storms are dominated by EW with pre-event water contributing 46% of stream flow. Generally, DEMMA achieved good fits for counter-clockwise storms, with average RMSE values for chloride and silica of 4.3 μeq/L and 48.5 μM, respectively (Table 5). Compared to clockwise storms, the counter-clockwise RMSE values are higher, showing how they were more difficult to fit with DEMMA. Appendix B contains the results of applying DEMMA to storms with counter-clockwise hysteresis.

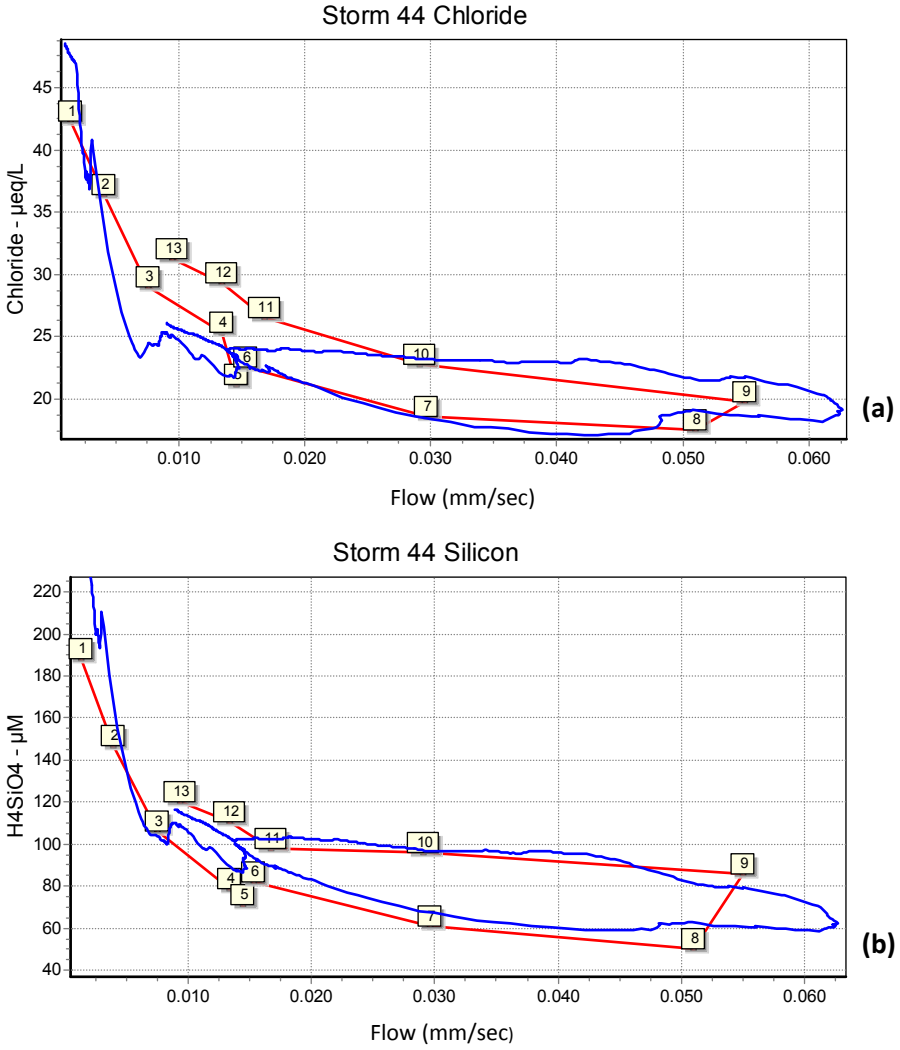

Figure 17. Estimated hysteresis loops for chloride (a) and silica (b) for Storm 44, which occurred on February 10, 1995. The numbered squares represent sample number in chronological order, the red line represents the observed hysteresis loop and the blue line is the synthetic hysteresis loop.

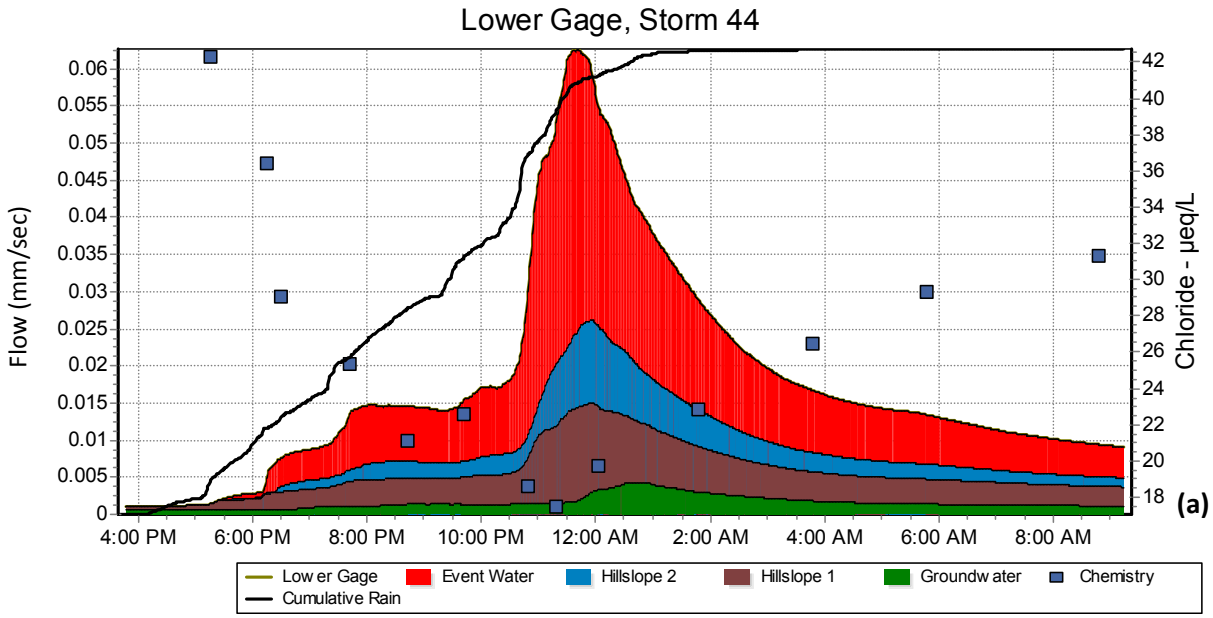

(a)

End-member	Chloride (µeq/L)	Silica (µM)	Runoff Percent
Groundwater	51	375	8.9
Hillslope 1	45	149	23.0
Hillslope 2	34	68	15.5
Event Water	5	2	52.6

(b)

Figure 18. Hydrograph separation (a) and table of end-member concentrations and component contributions (b) resulting from DEMMA of a rainstorm on February 10, 1995.

Table 5. End-member runoff contributions and RMSE values for storms with counter-clockwise hysteresis loops.

Storm Number	% Runoff Contribution				RMSE	
	GW	H1	H2	EW	Chloride (µeq/L)	Silica (µM)
22	12.8	23.3	10.5	53.4	8.5	55.2
44	7.4	25.5	18.6	48.5	3.5	28.6
58	5.5	25.7	9.9	58.9	4.2	55.6
87	25.2	41.1	11.3	22.4	3.6	51.5
97	20.9	44.4	11.0	23.7	2.9	64.7
113	12.3	53.6	11.3	22.8	2.8	35.2
Average	14.0	35.6	12.1	38.3	4.3	48.5

In order to investigate what might cause the storm hysteresis to rotate clockwise and counter-clockwise, a number of storm characteristics were analyzed, including total rainfall,

storm season, API, maximum rainfall intensity, and the temporal distribution of rain throughout the storm (Figures 19 - 26). It was initially thought that these rainstorms might have a large amount of new or tracer-diluted water supplied to the stream early during the rainstorm, which would rapidly decrease the overall tracer concentration in the stream and thus cause the counter-clockwise hysteresis loop. Analysis of total rainfall (Figure 19) indicates that this was not the case, and that there was a threshold value of approximately 50 mm of total rainfall above which the counter-clockwise hysteresis loops occurred. This threshold value is similar to the threshold value previously noted of 55 mm of rain required to generate significant subsurface flow at a trench in the upper part of PMRW (Tromp-van Meerveld and McDonnell 2006b). This suggests that during high volume storms, an additional source of water with a high tracer concentration becomes hydrologically connected to the stream and alters the stream water chemistry. Total rain plus API showed a similar threshold behavior to total rain, however it was less clearly defined (Figure 22). Analysis of the other storm characteristics did not appear to indicate any distinction between clockwise and counter-clockwise storms.

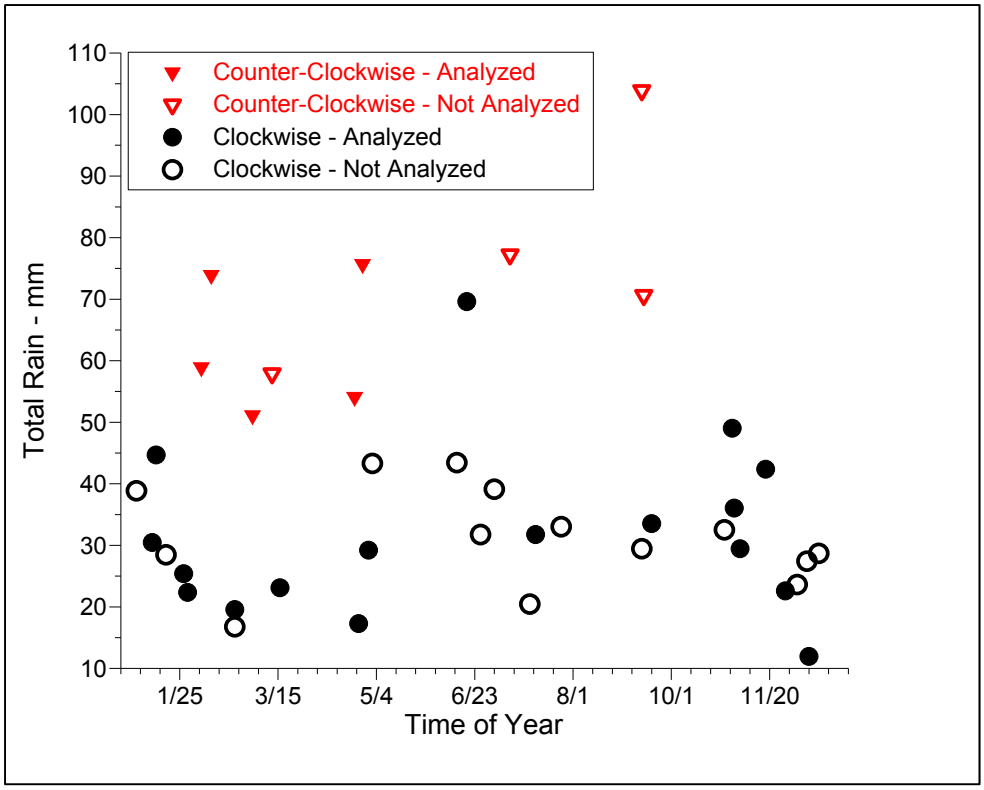

Figure 19. Total rainfall for 40 storms at PMRW. Storms occurred over a 23 year period.

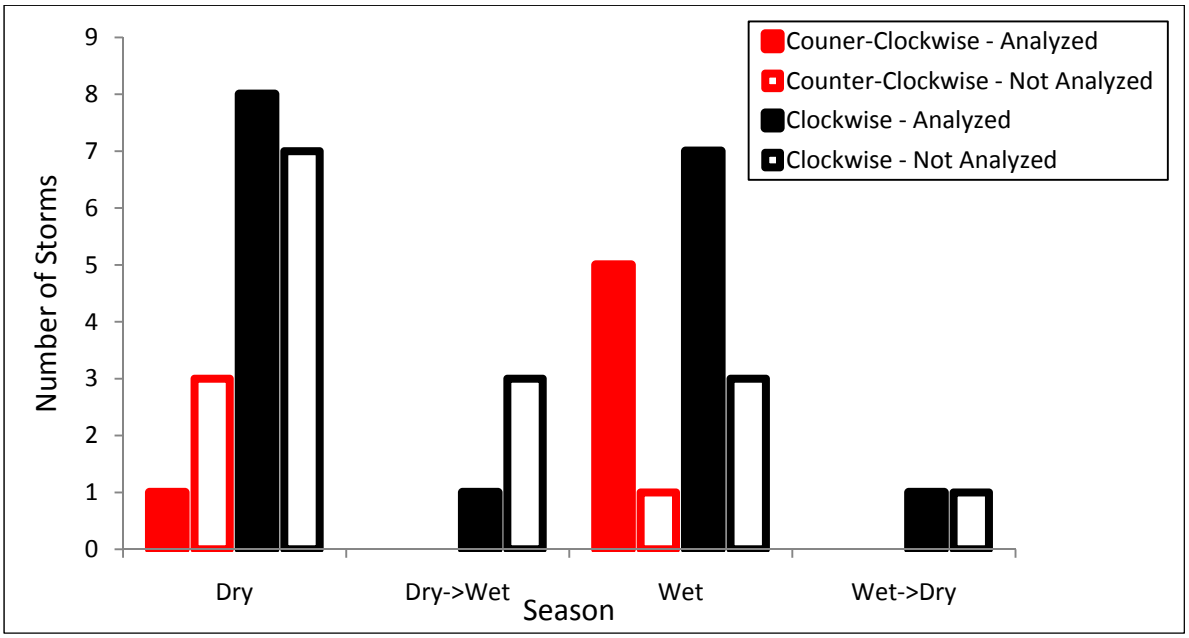

Figure 20. Seasonal distribution of 41 storms at PMRW.

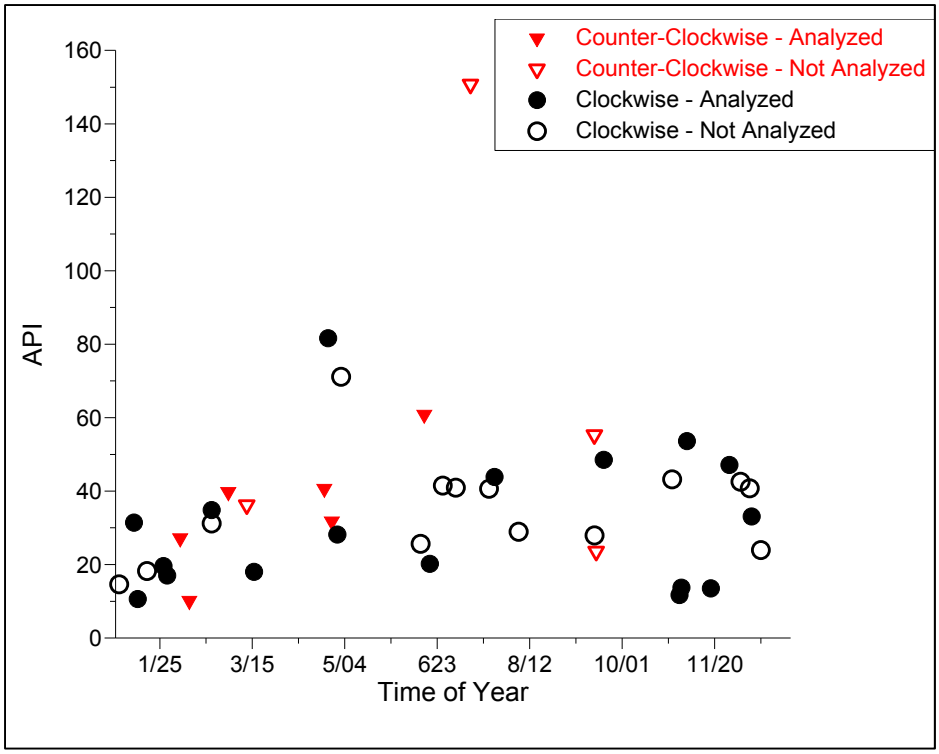

Figure 21. API of 41 storms at PMRW. Storms occurred during a 23 year period.

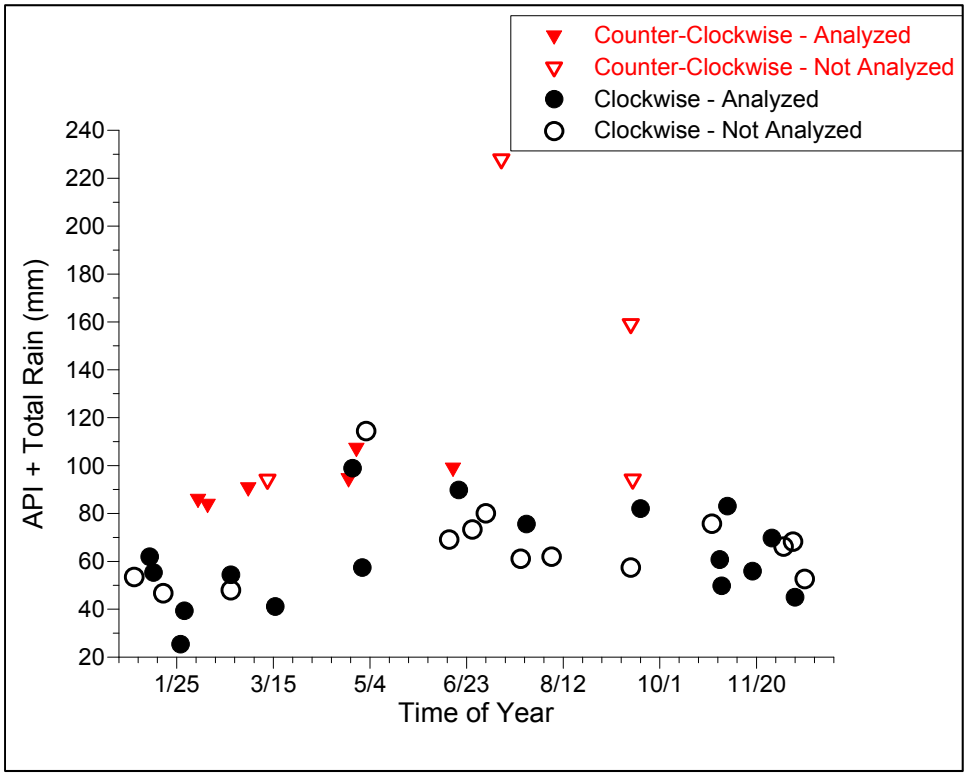

Figure 22. API plus total rain of 41 storms at PMRW. Storms occurred during a 23 year period.

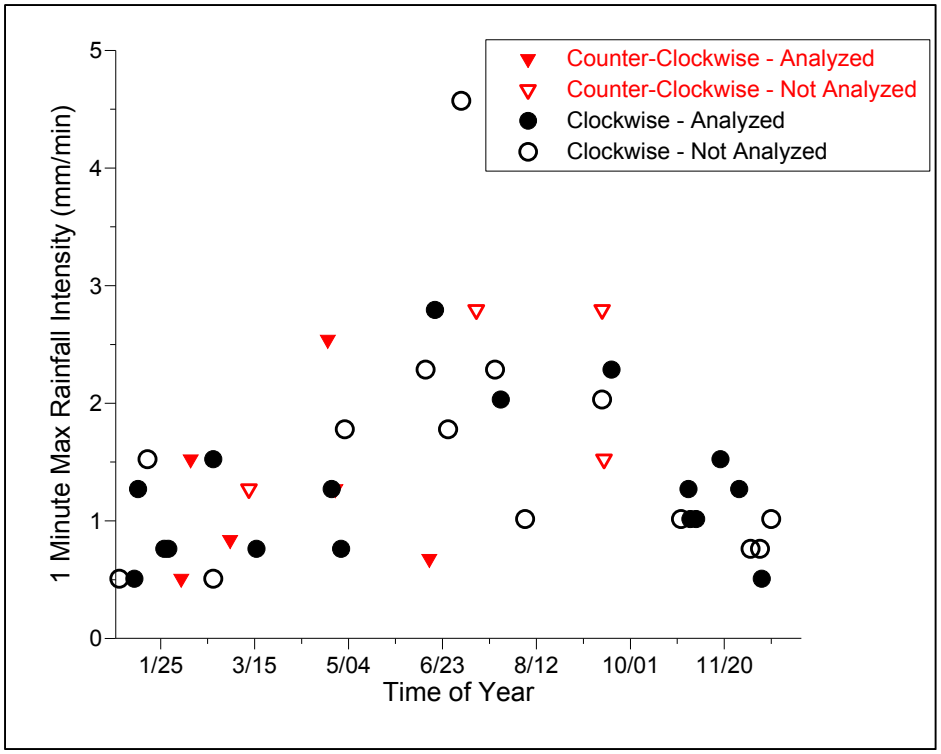

Figure 23. Maximum 1-minute rainfall rate of 41 storms at PMRW. Storms occurred during a 23 year period.

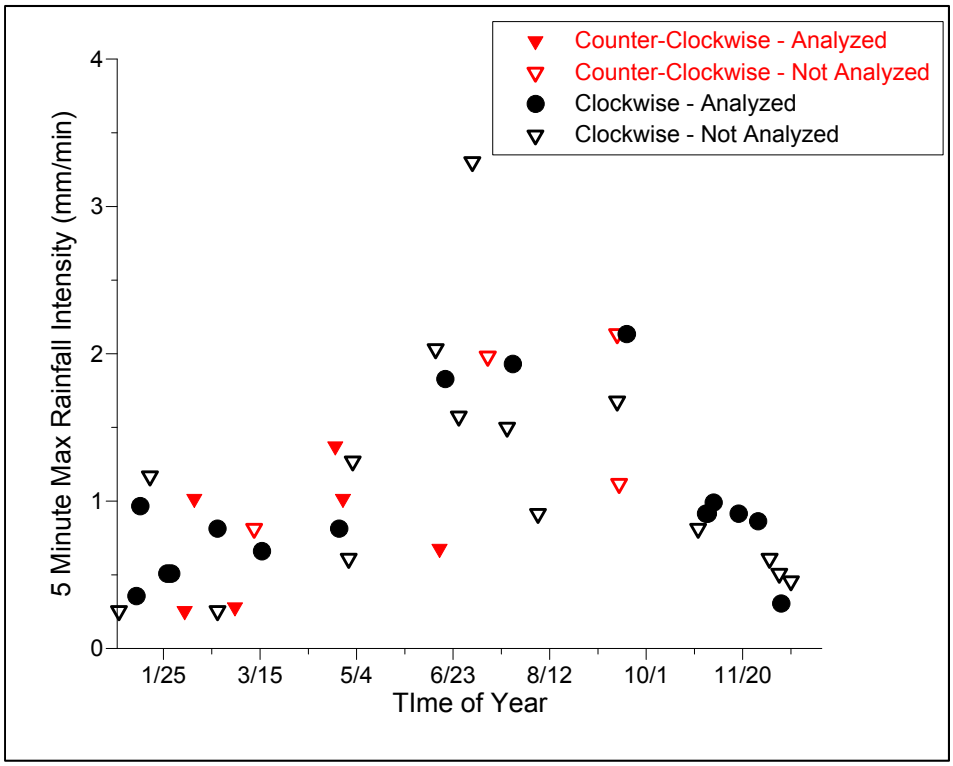

Figure 24. Maximum 5-minute rainfall rate of 41 storms at PMRW. Storms occurred during a 23 year period.

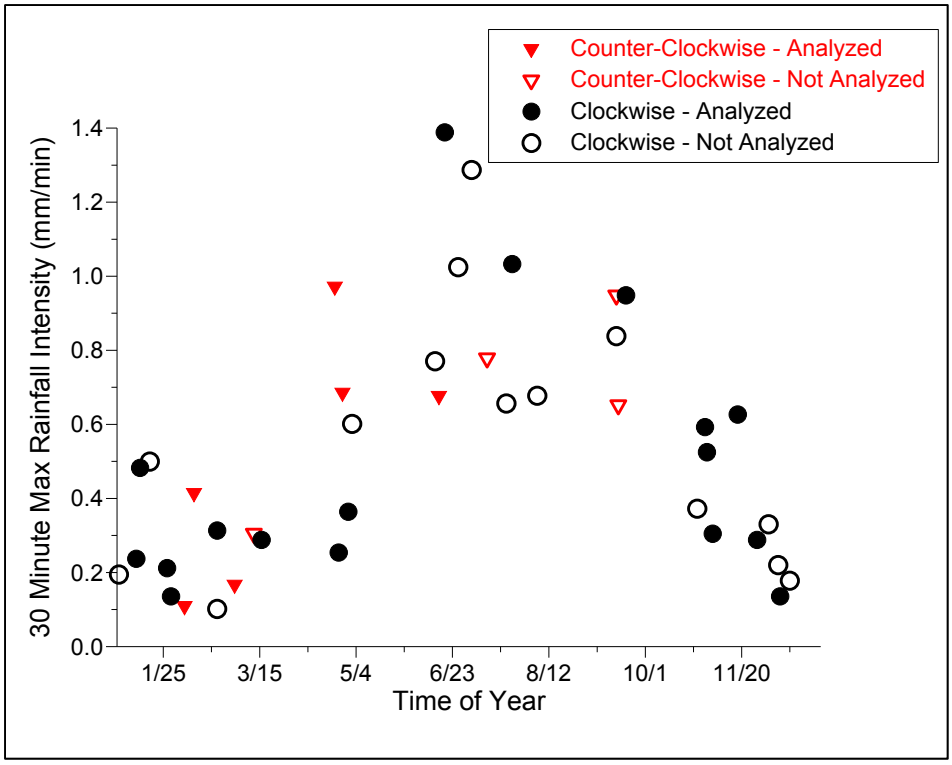

Figure 25. Maximum 30-minute rainfall rate of 41 storms at PMRW. Storms occurred during a 23 year period.

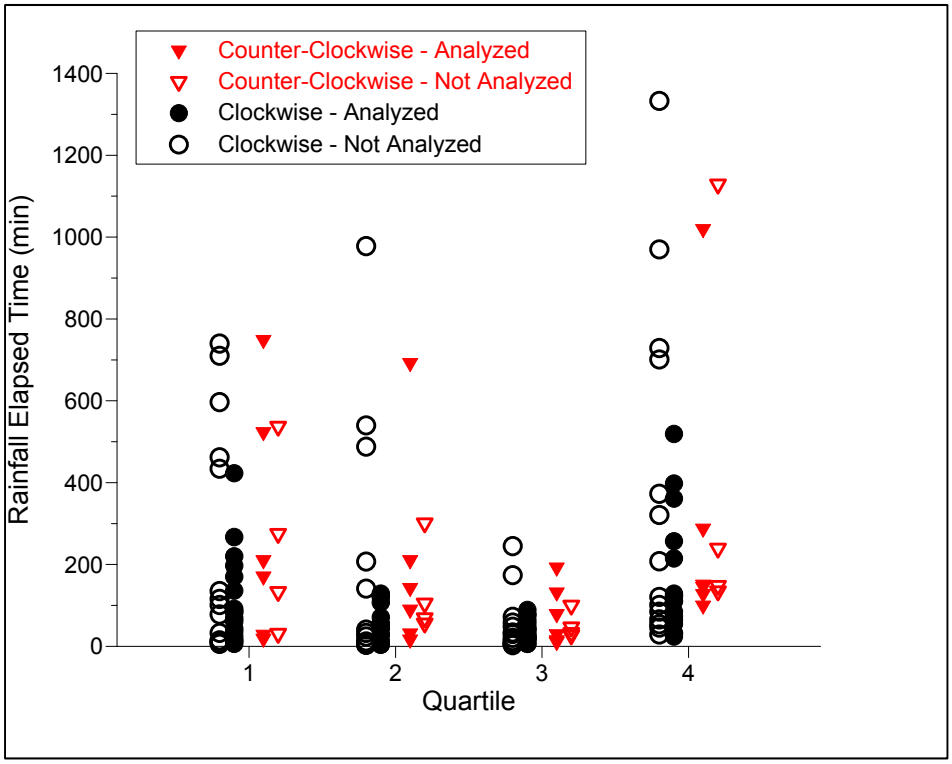

Figure 26. Rainfall duration by quartile of 41 storms at PMRW.

Based on the assumption that a threshold of 50 mm of total precipitation is controlling the two hysteresis loops behaviors at PMRW, a conceptual model of the runoff generation processes that are occurring throughout a storm for the two types of hysteresis loops was created (Figures 27 and 28). These models assume that the initial runoff processes are the same for each loop type until either the threshold is met or precipitation stops prior to reaching the threshold value. For a storm with clockwise hysteresis, baseflow generation occurs throughout the storm, and the rising limb of the hydrograph is dominated by runoff processes that are associated with precipitation, such as direct precipitation into the stream, pressure wave responses to rainfall, infiltration and saturation excess overland flow. As the storm continues, additional processes such as throughflow, return flow, macropore flow and preferential flow paths begin to generate runoff as the soil in the watershed continues to become more saturated. When precipitation ends, the contributions of these processes decrease until the flow in the stream returns to baseflow. The runoff processes for storms with counter-clockwise hysteresis are very similar, however once the 50mm threshold for total rainfall is met, an additional, currently unidentified source of high tracer concentration runoff begins supplying water to the stream. A process that might generate this high concentration runoff associated with the threshold could be an extreme expansion of the variable source area into parts of the watershed that normally do not generate much runoff. This unidentified source of runoff and the process that generates it will be the subject of future research at PMRW.

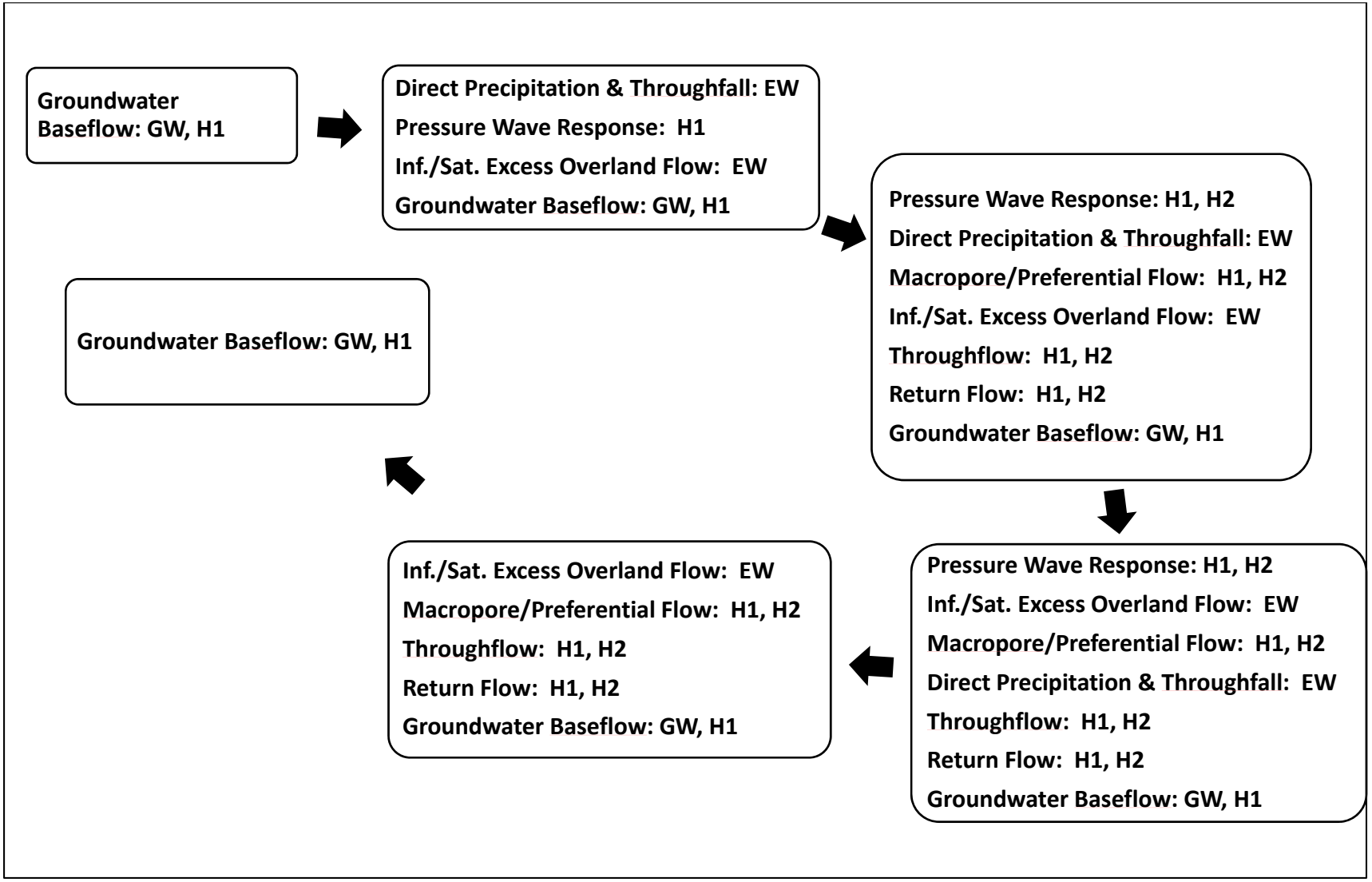

Figure 27. Conceptual runoff process model for storms with clockwise hysteresis at PMRW. Each box represents the runoff processes occurring at that point in the hysteresis loop and which end-members are associated with these processes.

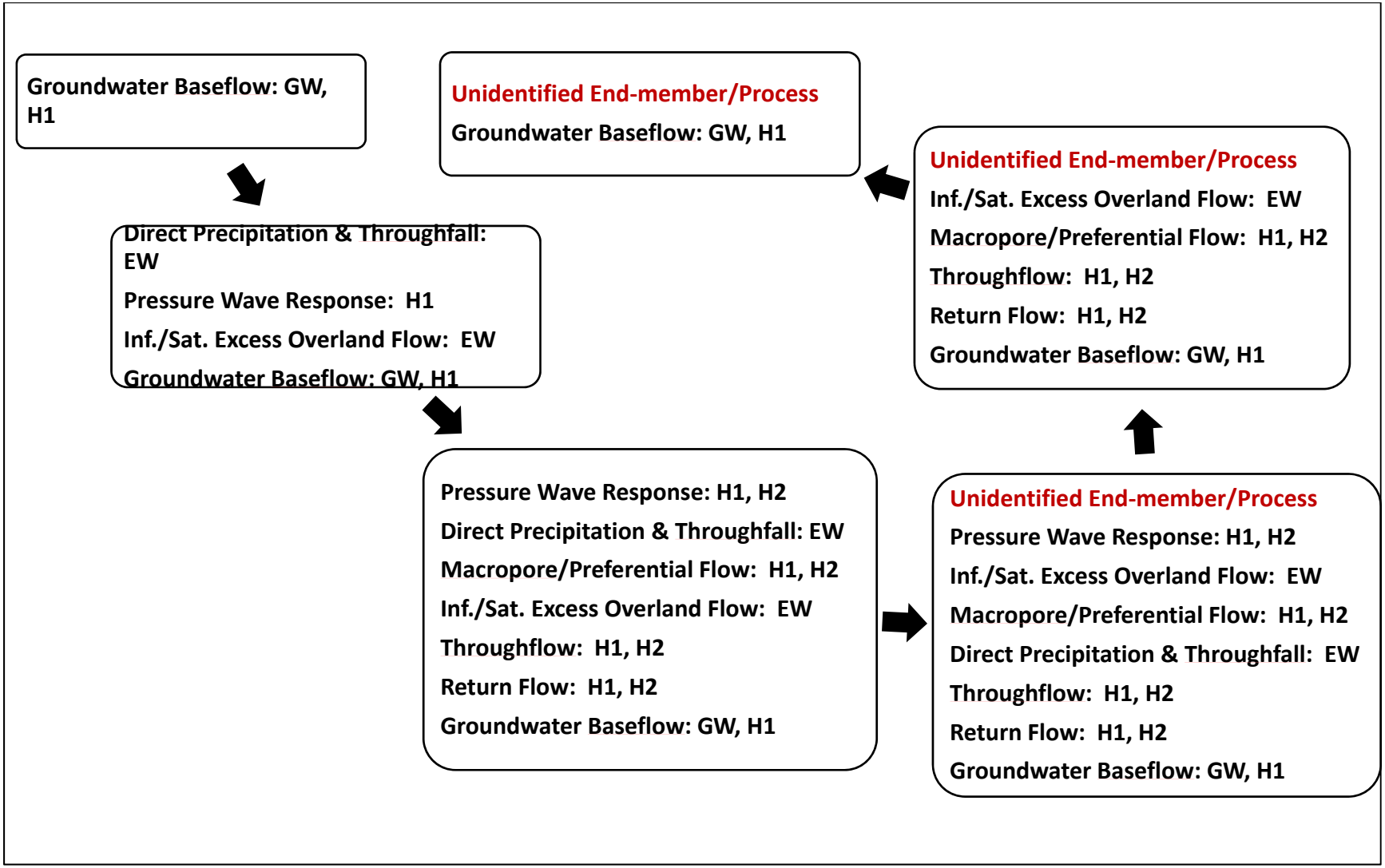

Figure 28. Conceptual runoff process model for storms with counter-clockwise hysteresis at PMRW. Each box represents the runoff processes occurring at that point in the hysteresis loop and which end-members are associated with these processes.

Sensitivity

During the course of this investigation, it became apparent that the timing of flow contributions, determined with beta grading, had the strongest effect on the shape and direction of the estimated hysteresis loop. Shifting the timing of the contributions of pre-event water so that they occur earlier during storms results in a clockwise hysteresis, while shifting the timing of the contributions of these end-members to later in the storm produces a counter-clockwise hysteresis loop. This is done by using beta grading values greater than one for storms with clockwise hysteresis and using beta grading values of less than one for storms with counter-clockwise hysteresis (Figure 29).

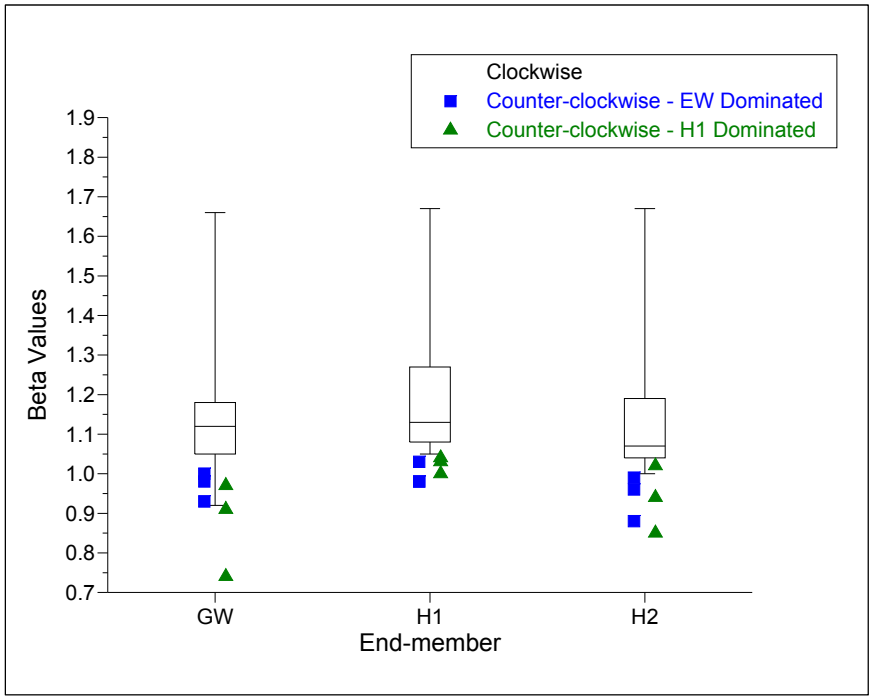

Figure 29. Range of beta grading values used to analyze storms at PMRW with DEMMA. Box-whisker plots are used for storms with clockwise hysteresis, while individual points are used for counter-clockwise storms.

The end-member tracer concentrations and runoff contributions also strongly influenced the estimated hysteresis loop. Altering the end-member tracer concentration determines the position of the estimated hysteresis loop. In general, it was possible to maintain similar end-

member tracer concentrations for both clockwise and counter-clockwise storms (Figures 30 and 31). Changing the percentage of runoff contributions can change the width of the hysteresis loop and, to some degree, its position. Setting minimum baseflow values for end-members, particularly GW and H1, was a useful tool to achieve reasonable fits at the start and end of hysteresis loops. Generally, for storms with counter-clockwise hysteresis, these values would be higher compared storms with clockwise hysteresis (Figure 32). While the beta grading had the strongest effect on the shape of the hysteresis loop, all four variables were important in generating the proper estimated hysteresis loop.

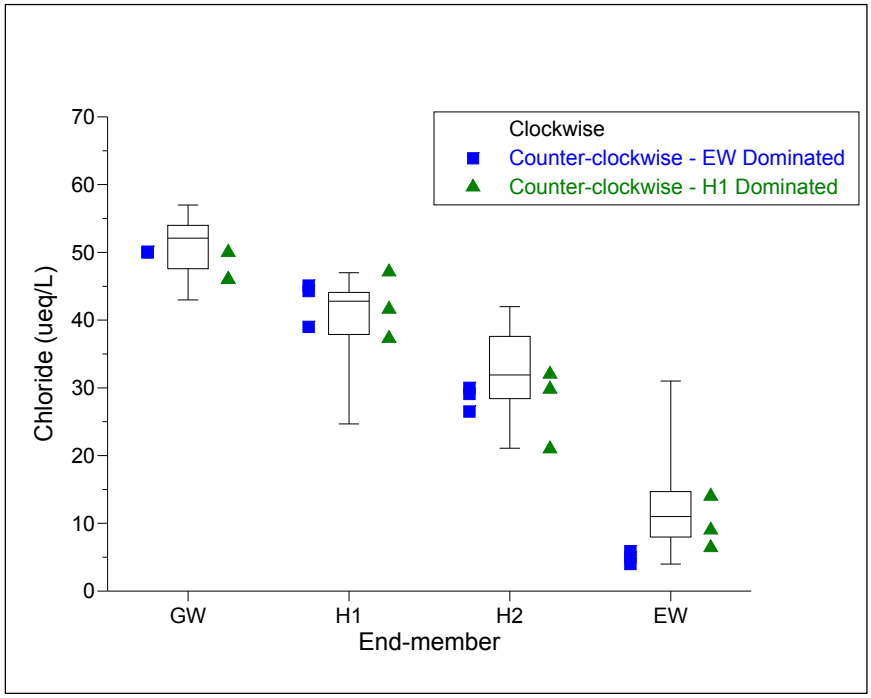

Figure 30. Chloride concentrations used to analyze storms at PMRW with DEMMA. Box-whisker plots are used for storms with clockwise hysteresis, while individual points are used for counter-clockwise storms.

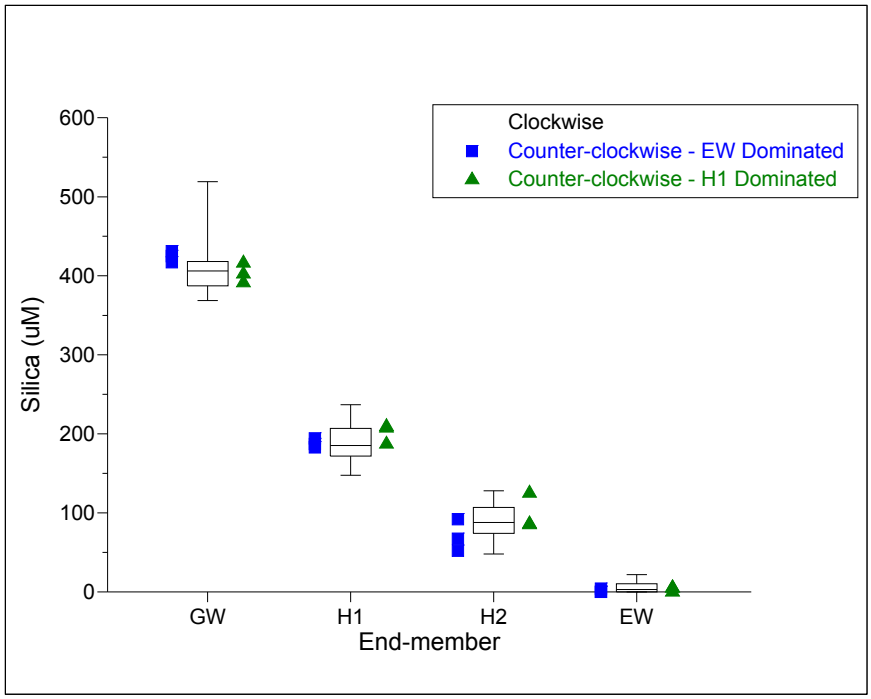

Figure 31. Silica concentrations used to analyze storms at PMRW with DEMMA. Box-whisker plots are used for storms with clockwise hysteresis, while individual points are used for counter-clockwise storms.

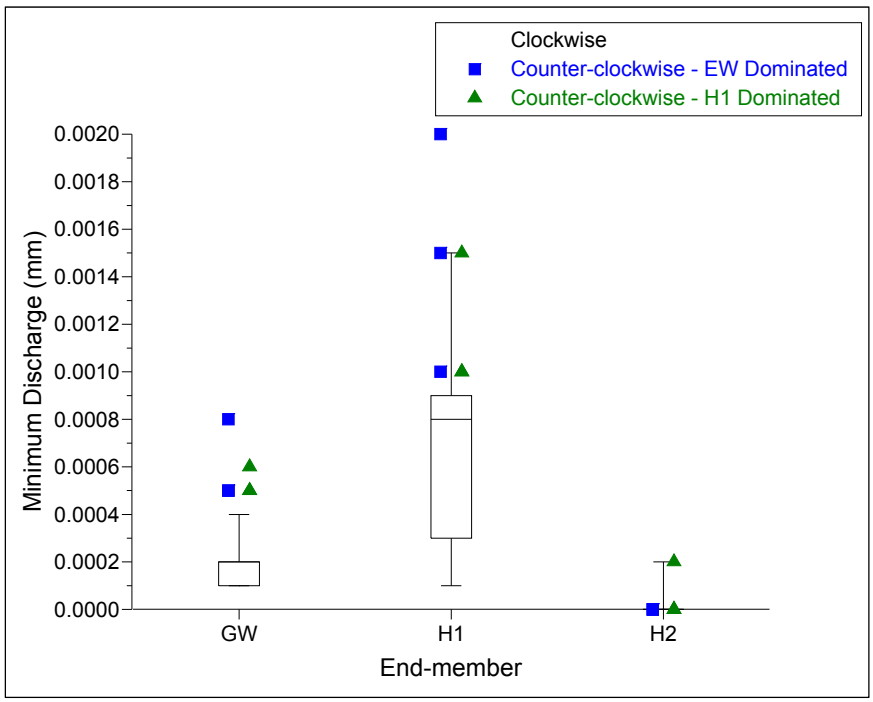

Figure 32. Minimum discharge values used to analyze storms at PMRW with DEMMA. Box-whisker plots are used for storms with clockwise hysteresis, while individual points are used for counter-clockwise storms.

CHAPTER 5: CONCLUSIONS

DEMMA has been used to investigate storm runoff generation processes at Panola Mountain Research Watershed. This method requires multiple tracers that have similar hysteresis shapes and rotation directions. DEMMA also requires water chemistry data collected over a long time period in order to properly identify and characterize the end-members present in the watershed and to analyze overall watershed processes. It would have been difficult to notice the clockwise and counter-clockwise hysteresis loop behavior at PMRW if the dataset available for the site had not covered such a long period of time.

Analysis of 41 single peak hydrographs has identified at least two flow generation patterns occur with different timing and contributions from the four watershed components. Results indicate that a threshold of 50 mm of total rainfall is related to these two patterns, where storms that have a total rainfall of less than 50 mm have clockwise hysteresis for tracer concentration and storms that reach 50 mm or more of total rainfall have counter-clockwise hysteresis. This finding is similar to that of Tromp-van Meerveld and McDonnell (2006b).

Peters and Ratcliffe (1998) found that 75% of storm runoff at PMRW came from old water. DEMMA at the site showed that 69% of storm runoff from storms with clockwise hysteresis was supplied by old or pre-event water. Half of the storms with counter-clockwise hysteresis had an average of 77% of runoff contribution from pre-event water while the other counter-clockwise storms had pre-event runoff contributions of 46%. This shows that, except in rare circumstances, storm runoff at PMRW is dominated by pre-event water.

CHAPTER 6: FUTURE RESEARCH

DEMMA could be the basis of a wide variety of future research. This work could include applying this method to other watersheds, including the 10-ha watershed at PMRW. Additional research with DEMMA could focus on using additional tracers in the hysteresis analysis to improve accuracy of the hydrograph separations. Furthermore, the analysis could be extended to include more complex multi-peak hydrographs. Currently, DEMMA cannot be used to analyze multi-peak storms due to a lack of method to modify values for the second peak separate from the first peak. This results in estimated hysteresis loops that achieve good fits for either the first or second peak but not for both (Figure 33). Optimization is another area that could improve DEMMA. This could be accomplished by investigating the sensitivity of parameters more in depth to reduce the number of parameters.

Further investigation of the causes and processes of the two hysteresis loop responses could lead to a better understanding of runoff at PMRW and in general. Collection of additional data at PMRW would be necessary in order to accomplish this. Stream tracer concentrations from the stream in the southeastern portion of the watershed should be analyzed to determine if this part of the watershed has a different tracer contribution. The range of end-member values in this part of the watershed should also be evaluated to further ensure that the proper end-member values are being used at PMRW. Additionally, investigating the end-member concentration variability throughout storms (particularly precipitation) and allowing these to vary accordingly during DEMMA could help with characterization of the threshold process. In order to determine if deep groundwater is contributing to stream flow during storms with counter-clockwise hysteresis, data from additional bedrock wells could be included in the analysis. An investigation of the spatial variability of tracer concentrations in stream water may identify the presence of localized differences in concentrations. Finally, a dense network of tensiometers could be installed from the stream riparian area to higher up the hillslope to determine the extent

that the variable source area expands during storms, particularly when the total rain threshold is met. Analysis of the characteristics of the two types of hysteresis loops at PMRW, such as the slopes of the hysteresis loops, the starting tracer concentrations, and the minimum tracer concentration values, could identify additional factors that may influence the two responses.

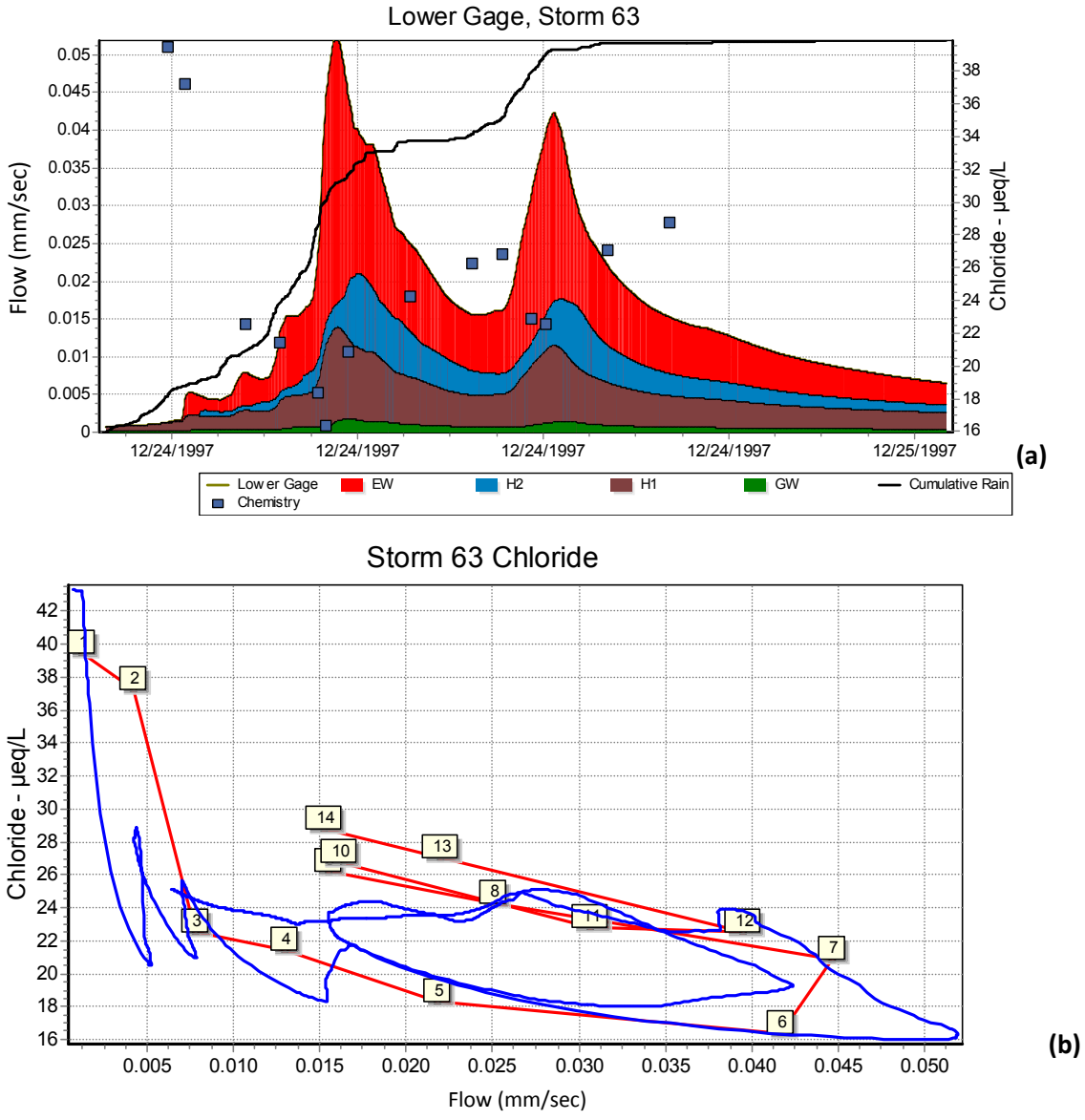

Figure 33. Example of hydrograph separation (a) and hysteresis loop (b) resulting from an attempt to fit a double-peak storm using DEMMA. The numbered squares represent sample number in chronological order and the blue line represents the synthetic hysteresis loop. Note that the position of the second estimated hysteresis loop does not match the second loop in the observed hysteresis.

Peters and Ratcliffe (1998) noted that chloride concentrations in precipitation decreased during storms, likely due to washout of particles in the lower atmosphere. DEMMA could be modified to incorporate end-members that vary over time. This feature would likely be applied primarily to the EW end-member, but could also be applied to H1 since it is increasingly likely that it is a mixture of pre-event and event waters as the storm progresses.

In order to facilitate future research with DEMMA at PMRW, some steps could be taken to increase the amount of data suitable for this method. Stream water and end-member samples could be analyzed for stable isotopes such as ^{18}O and ^{2}H to provide additional conservative tracers for use with the analysis. Ideally the temporal resolution of stream water sampling during storms could be increased to provide higher resolution C/Q hysteresis loops. Also, the sampling of piezomenters, lysimeters, and rainfall collectors could be conducted more frequently and at the same time when possible, to create a larger, more uniform, dataset.

LITERATURE CITED

Bond, H.W. 1979. Nutrient concentration patterns in a stream draining a montane ecosystem in Utah. *Ecology* 60(6): 1184-1196.

Burns, D.A., J.J. McDonnell, R.P. Hooper, N.E. Peters, J.E.Freer, C. Kendall, and K.J. Beven. 2001. Quantifying contributions to storm runoff through end-member mixing analysis and hydrologic measurements at the Panola Mountain Research Watershed (Georgia, USA). *Hydrological Processes* 15(10): 1903–1924.

Burns, D.A., N. Plummer, J.J. McDonnell, E. Busenberg, G.C. Casile, C. Kendall, R.P. Hooper, J.E. Freer, N.E. Peters, K. Beven, and P. Schlosser. 2003. The geochemical evolution of riparian groundwater in a forested piedmont catchment. *Ground Water* 41(7): 913-925.

Buttle, J.M. 1994. Isotope hydrograph separations and rapid delivery of pre-event water from drainage basins. *Progress in Physical Geography* 18(1): 16–41.

Cappellato, R., and N.E. Peters. 1995. Dry deposition and canopy leaching rates in deciduous and coniferous forests of the Georgia Piedmont: An assessment of a regression model. *Journal of Hydrology* 169: 131–150.

Carter, M.E.B. 1978. *A community analysis of the Piedmont deciduous forest of Panola Mountain State Conservation Park: Atlanta, Georgia.* M.S. thesis, Emory University, Atlanta, GA: pp. 126.

Chanat, J.G., K.C. Rice, and G.M. Hornberger. 2002. Consistency of patterns of concentration-discharge plots. *Water Resources Research* 38(8): doi:10.1029/2001WR000971.

Christopherson N., and R.P. Hooper. 1992. Multivariate analysis of stream water chemical data: the use of principal components analysis for the end-member mixing problem. *Water Resources Research* 28: 99–107.

Christopherson, N., C. Neal, R.P. Hooper, R.D. Vogt, and S.C.S. Andersen. 1990. Modeling streamwater chemistry as a mixture of soilwater endmembers—a step towards second-generation acidification models. *Journal of Hydrology* 116: 307–320.

Clark, M.P., D.E. Rupp, R.A. Woods, H.J. Tromp-van Meerveld, N.E. Peters, and J.E. Freer. 2009. Consistency between hydrological models and field observations: linking processes at the hillslope scale to hydrological responses at the watershed scale. *Hydrological Processes* 23: 311-319.

DeWalle D.R., B.R. Swistock, and W.E. Sharpe. 1988. Three component tracer model for stormflow on a small Appalachian forested catchment. *Journal of Hydrology* 104: 301–310.

Dincer, T., B.R. Payne, and T. Florkows. 1970. Snowmelt runoff from measurements of tritium and oxygen-18. *Water Resources Research* 6(1): 110-124.

Evans, C., and T.D. Davies. 1998. Causes of concentration/discharge hysteresis and its potential as a tool for analysis of episode hydrochemistry. *Water Resources Research* 34(1): 129–137.

Fritz, P., J.A. Cherry, K.U. Weyer, M.G. and Sklash. 1976. Runoff analyses using environmental isotopes and major ions. In *Interpretation of Environmental Isotope and Hydrochemical Data in Groundwater Hydrology*, IAEA, Vienna, 11 1-30.

Hewlett, J.D. 1961. Soil moisture as a source of base flow from steep mountain watershed. U.S. Forest Service Southeast Forest Experiment Station, Paper 132, pp. 11.

Hewlett, J.D. and A.R. Hibbert. 1963. Moisture and energy conditions within a sloping soil mass during drainage. *Journal of Geophysical Research* 63(4): 1801-1087.

Hewlett, J.D., and A.R. Hibbert. 1967. Factors affecting the response of small watersheds to precipitation in humid areas. *Forest Hydrology*, W.E. Sopper and H.W. Lull (editors), 275-290. Oxford, U.K.: Symposium Publications Division, Pergamon Press.

Higgins, M.W., R.L. Atkins, T.J. Crawford, R.F. Crawford III, R. Brooks, and R. Cook. 1988. The structure, stratigraphy, tectonostratigraphy and evolution of the southernmost part of the Appalachian orogen, U. S. Geological Survey Professional Paper, 1475: pp. 173.

Hooper, R.P. 2001. Applying the scientific method to small catchment studies: A review of the Panola Mountain experience. *Hydrological Processes* 15(10): 2039-2050.

Hooper, R.P., N. Christophersen, and N.E. Peters. 1990. Modeling streamwater chemistry as a mixture of soil-water end members: An application to the Panola Mountain watershed, Georgia, USA. *Journal of Hydrology* 116: 321–343.

Horton, R.E. 1933. The role of infiltration in the hydrologic cycle. *American Geophysical Union Transactions* 14: 446-460.

Horton,R.E. 1945. Erosional development of streams and their drainage basins: hydrophysical approach to quantitative morphology. *Bulletin of the Geological Society of America* 56(2): 75-3.

James, A., J.J. McDonnell, I. Tromp-van Meerveld, and N.E. Peters. 2010. Gypsies in the palace: Experimentalist's view on the use of 3-D physics based simulation of hillslope hydrological response. *Hydrological Processes* 24: 3878-3893.

Johnson, F.A., and J.W. East. 1982. Cyclical relationships between river discharge and chemical concentration during flood events. Journal of Hydrology 57: 93–106.

Kennedy, V.C., C. Kendall, G.W. Zellweger, T.A. Wyerman, and R.J. Avanzino. 1986. Determination of the components of stormflow using water chemistry and environmental isotopes, Mattole River basin, California. *Journal of Hydrology* 84: 10740.

Kohler, M.A., and R.K. Linsley. 1951. Predicting the runoff from storm rainfall. U.S. Department of Commerce Weather Bureau Research Paper #34. Washington, D.C.

Lehmann, P., C. Hinz, G. McGrath, H.J. Tromp-van Meerveld, and J.J. McDonnell. 2007. Rainfall threshold for hillslope outflow: an emergent property of flow pathway connectivity. *Hydrology and Earth System Science* 11: 1047–1063.

Martinec, J. 1975. Subsurface flow from snowmelt traced by tritium. *Water Resources Research* 11: 496-497.

McDonnell, J.J. 1990. A rationale for old water discharge through macropores in a steep, humid catchment. *Water Resources Research* 26(11): 2821-2832.

McDonnell, J.J. 2009. Classics in physical geography revisited: Hewlett, J.D. and Hibbert, A.R. 1967: Factors affecting the response of small watersheds to precipitation in humid areas. In Sopper, W.E. and Lull, H.W., editors, *Forest hydrology*, New York: Pergamon Press, 275-90. Progress in Physical Geography 33(2): 288-293.

McDonnell, J.J., J. Freer, R.P. Hooper, C. Kendall, D.A. Burns, and K.J. Beven. 1996. New method developed for studying flow on hillslopes. *EOS* 77(47): 465-472.

Mosley, M.P. 1979. Streamflow generation in a forested watershed, New Zealand. *Water Resources Research* 15: 795-806.

Pearce, A.J., M.K. Stewart, M.G. Sklash. 1986. Storm runoff generation in humid headwater catchments 1. Where does the water come from? *Water Resources Research* 22: 1263–1272.

Peters, N.E. 1994. Water-quality variations in a forested Piedmont catchment, Georgia, USA. *Journal of Hydrology* 156: 73–90.

Peters, N.E., and E.B. Ratcliffe. 1998. Tracing hydrologic pathways using chloride at the Panola Mountain Research Watershed, Georgia, USA. *Water Air and Soil Pollution* 105 (1–2): 263–275.

Peters, N.E., J. Freer, and B.T. Aulenbach. 2003. Hydrologic dynamics of the Panola Mountain Research Watershed, Georgia, USA. *Ground Water* 41(7): 973-988.

Pinder, G.F., and J.F. Jones. 1969. Determination of the groundwater component of peak discharge from the chemistry of total runoff. *Water Resources Research* 5(2): 438–445.

Rasmussen, T.C., R.H. Baldwin, and J.F. Dowd. 2000. Tracer vs. pressure wave velocities through unsaturated saprolite. *Soil Science Society of America Journal* 64(1): 75-85.

Shanley, J.B., and N.E. Peters. 1988. Preliminary observations of streamflow generation during storms in a forested Piedmont watershed using temperature as a tracer. *Journal of Contaminant Hydrology* 3: 349-365.

Sklash, M.G. 1990. Environmental isotope studies of storm and snowmelt runoff generation. In *Process Studies in Hillslope Hydrology*, M.G. Anderson and T.P.(editors),. Chichester: Wiley, 401-35.

Sklash, M.G., and R.N. Farvolden. 1979. The role of groundwater in storm runoff. *Journal of Hydrology* 43(1): 45–65.

Torres, R., W.E. Dietrich, D.R. Montgomery, S.P. Anderson, and K. Loague. 1998. Unsaturated zone processes and the hydrologic response of a steep, unchanneled catchment. *Water Resources Research* 34(8): 1865-1879.

Tromp-van Meerveld, H.J., and J.J. McDonnell. 2006a. Threshold relations in subsurface stormflow: 1. A 147-storm analysis of the Panola hillslope, *Water Resources Research* 42(2): W02410.

Tromp-van Meerveld, H.J., and J.J. McDonnell. 2006b. Threshold relations in subsurface stormflow: 2. The fill and spill hypothesis. *Water Resources Research* 42: W02411, DOI:10.1029/2004WR003800.

Tromp-van Meerveld, H.J., N.E. Peters, and J.J. McDonnell. 2007. Effect of bedrock permeability on subsurface stormflow and the water balance of a trenched hillslope at the Panola Mountain Research Watershed, Georgia, USA, *Hydrological Processes* 21: 750–769.

United States Department of Agriculture (USDA). 1986. Urban hydrology for small watersheds. Technical Release 55 (TR-55) (Second Edition). Natural Resources Conservation Service, Conservation Engineering Division.

Walling, D.E., and I.D.L. Foster. 1975. Variations in the chemical concentration of river water during flood flows, and the lag effect: Some further comments. *Journal of Hydrology* 26: 237–244.

Walling, D.E., and B.W. Webb (1986), Solutes in river systems. In *Solute Processes*, S. T. Trudgill (editor), J. Wiley, Chichester, U. K. pp. 251–327.

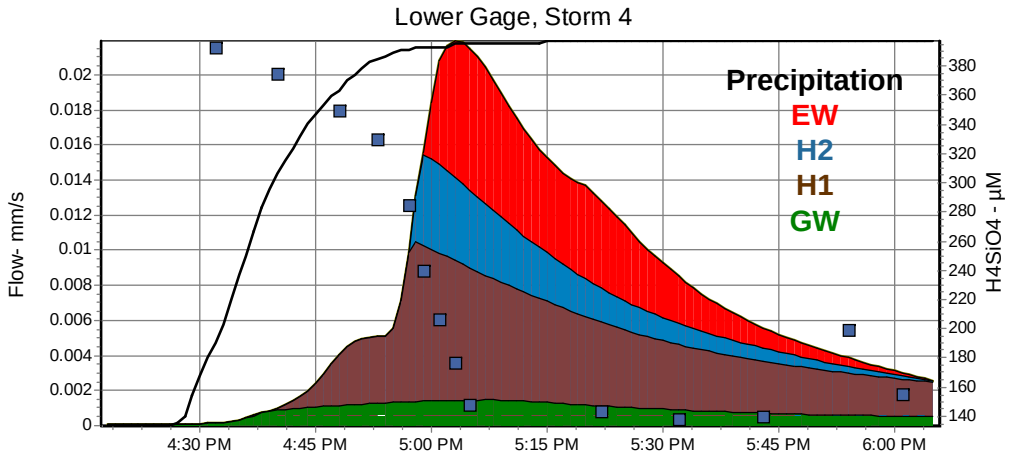

Storm 4, July 24, 1986			
	% Runoff	Cl^- (µeq/L)	H_4SiO_4 (µM)
GW	11.8	43.0	431.3
H1	45.3	32.7	236.9
H2	15.6	23.7	127.9
EW	27.2	7.7	22.0
RMSE	N/A	2.1	44.4

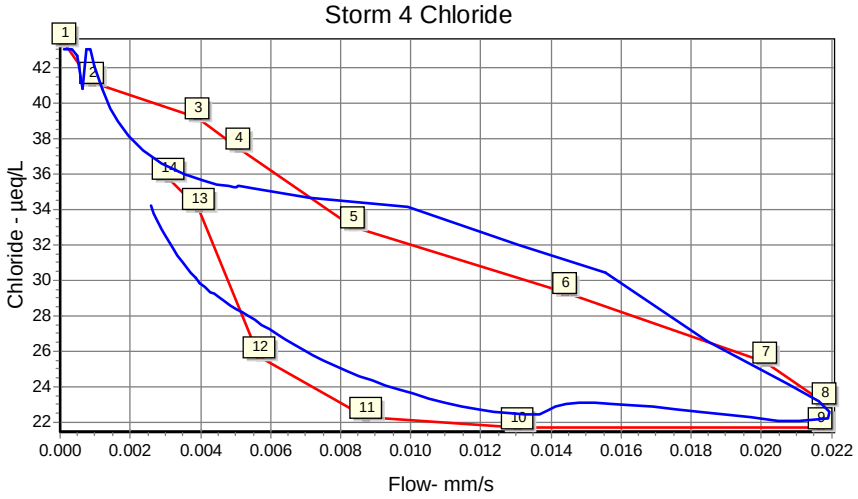

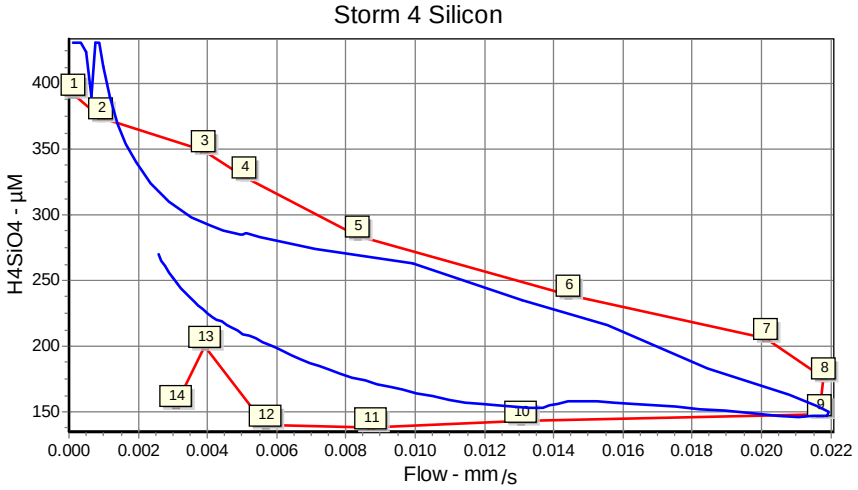

Miscellaneous Info:
Clockwise
API: 43.8
Total Rain: 32 mm
Max Flow Lower Gage: 150 L/sec

Rainfall Elapsed Time by Quartile (min)			
0-25%	25-50%	50-75%	75-100%
6	4	6	32

Figure 34. Results of DEMMA of Storm 4 (July 24, 1986).

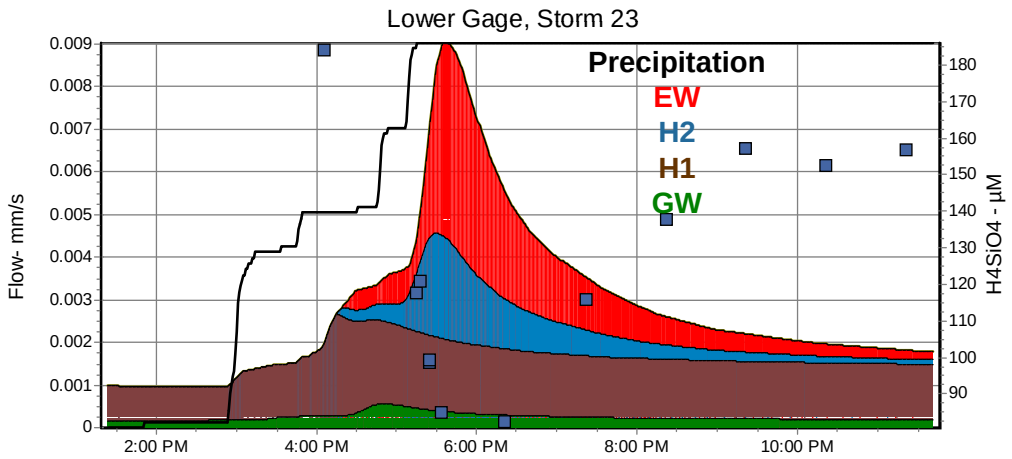

Storm 23, April 25, 1988			
	% Runoff	Cl^- (µeq/L)	H_4SiO_4 (µM)
GW	8.7	54.0	390.1
H1	48.6	46.4	147.5
H2	15.1	38.7	106.9
EW	27.7	12.1	8.0
RMSE	N/A	3.6	9.2

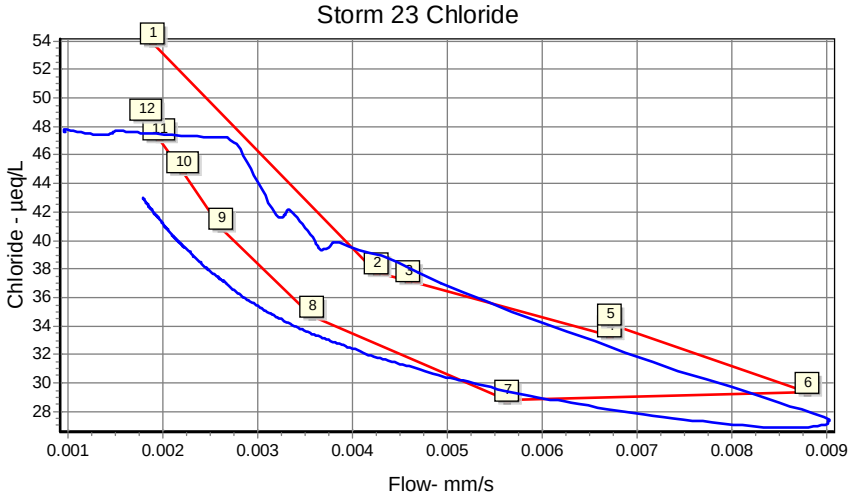

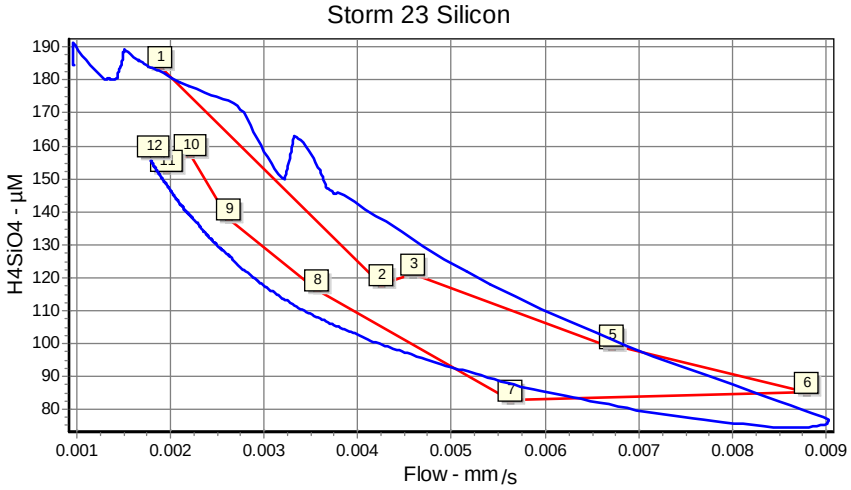

Miscellaneous Info:
Clockwise
API: 82
Total Rain: 17 mm
Max Flow Lower Gage: 62 L/sec

Rainfall Elapsed Time by Quartile (min)			
0-25%	25-50%	50-75%	75-100%
69	46	64	24

Figure 35. Results of DEMMA of Storm 23 (April 25, 1988).

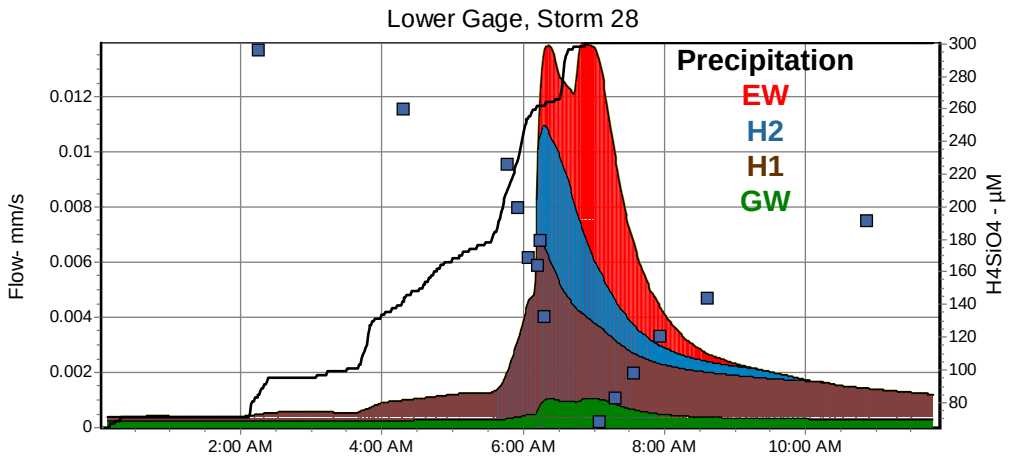

Storm 28, November 5, 1993			
	% Runoff	Cl^- (µeq/L)	H_4SiO_4 (µM)
GW	13.6	50.9	368.7
H1	46.3	43.3	185,2
H2	15.7	37.6	88.1
EW	24.4	14.7	1.0
RMSE	N/A	1.8	20.5

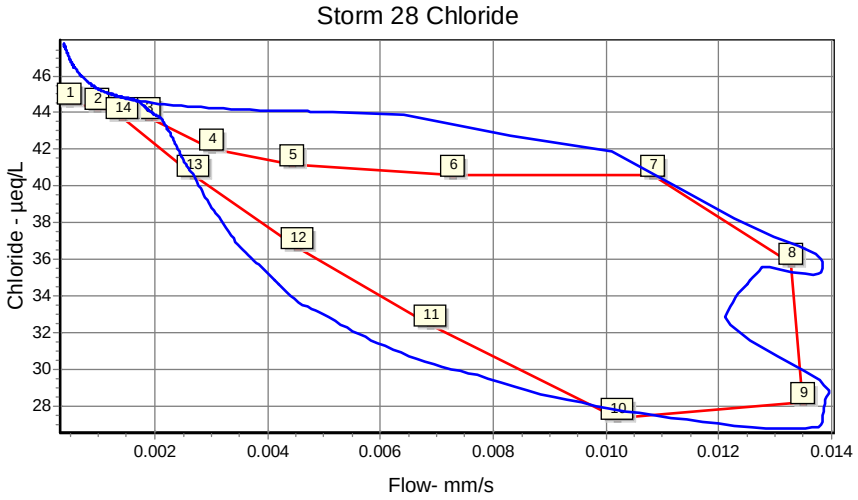

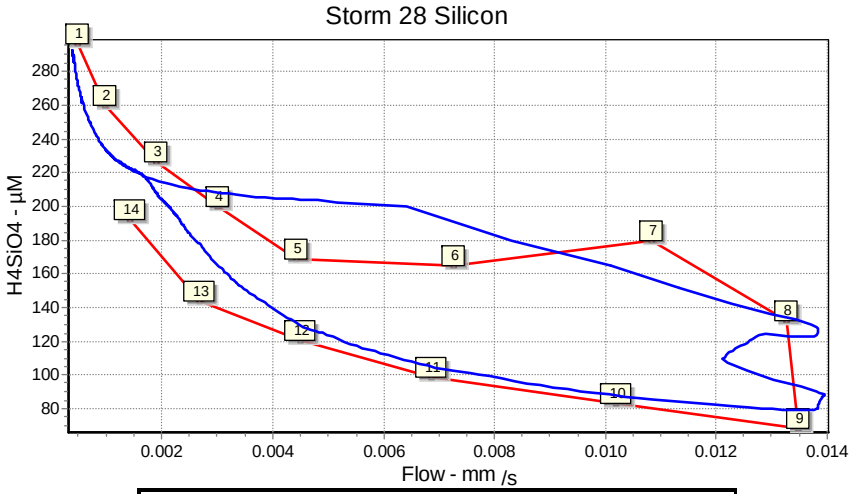

Miscellaneous Info:
Clockwise
API: 53.6
Total Rain: 29 mm
Max Flow Lower Gage: 95 L/sec

Rainfall Elapsed Time by Quartile (min)			
0-25%	25-50%	50-75%	75-100%
220	107	23	54

Figure 36. Results of DEMMA of Storm 28 (November 5, 1993).

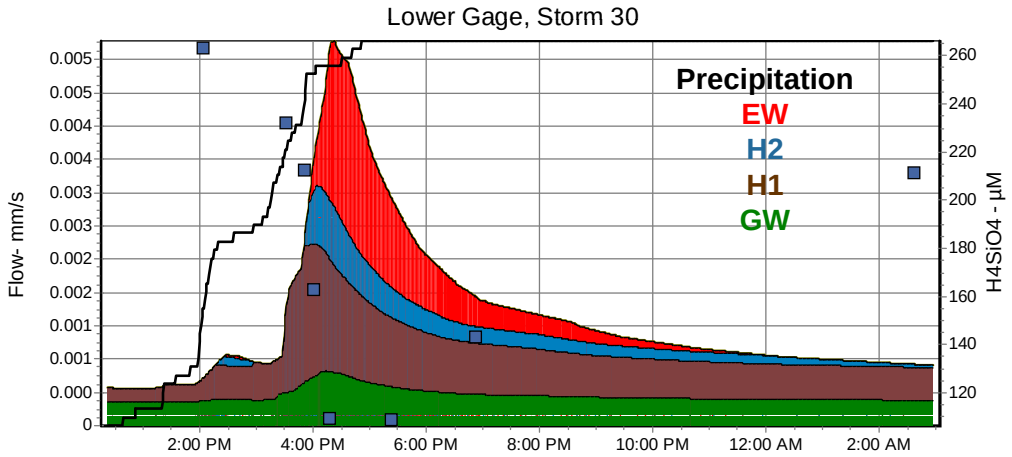

Storm 30, December 10-11, 1993			
	% Runoff	Cl^- (µeq/L)	H_4SiO_4 (µM)
GW	27.3	53.0	375.9
H1	41.7	44.1	148.9
H2	11.5	28.4	67.9
EW	19.5	9.0	2.1
RMSE	N/A	1.1	13.9

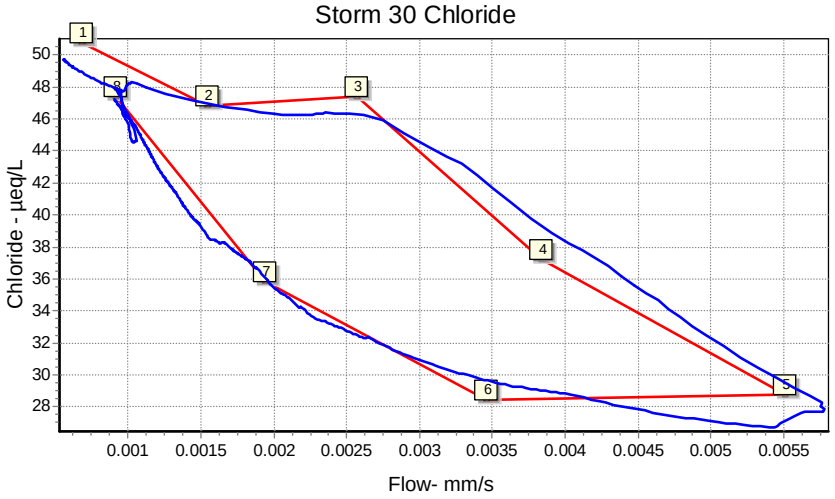

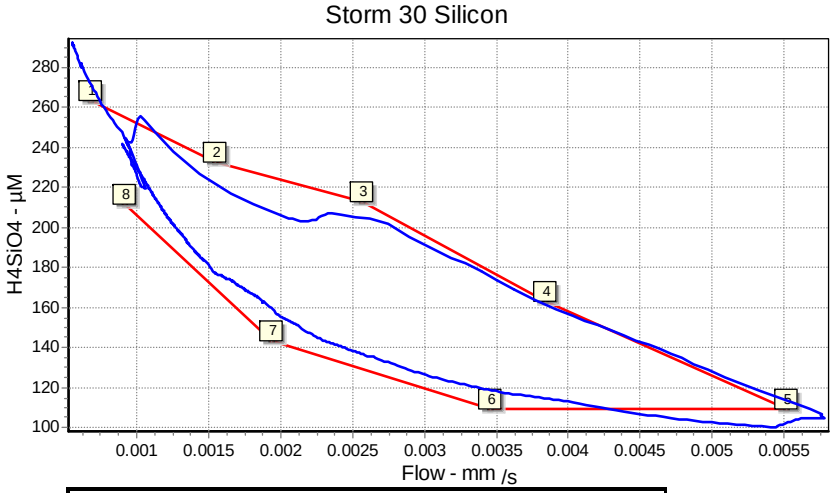

Miscellaneous Info:
Clockwise
API: 33.1
Total Rain: 12 mm
Max Flow Lower Gage: 40 L/sec

Rainfall Elapsed Time by Quartile (min)			
0-25%	25-50%	50-75%	75-100%
82	56	40	74

Figure 37. Results of DEMMA of Storm 30 (December 10-11, 1993).

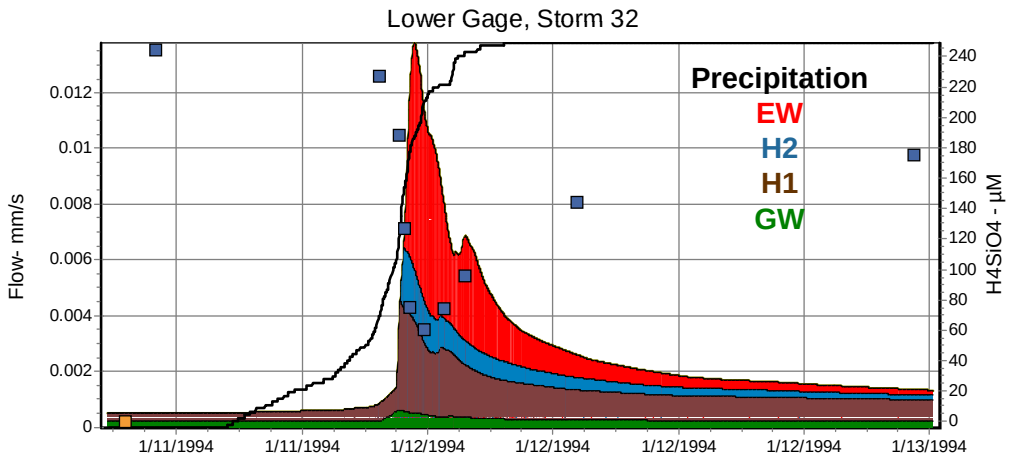

Storm 32, January 11-13, 1994			
	% Runoff	Cl^- (µeq/L)	H_4SiO_4 (µM)
GW	12.0	57.0	397.0
H1	40.5	45.0	160.0
H2	13.7	40.0	74.0
EW	33.7	31.0	7.0
RMSE	N/A	2.1	14.3

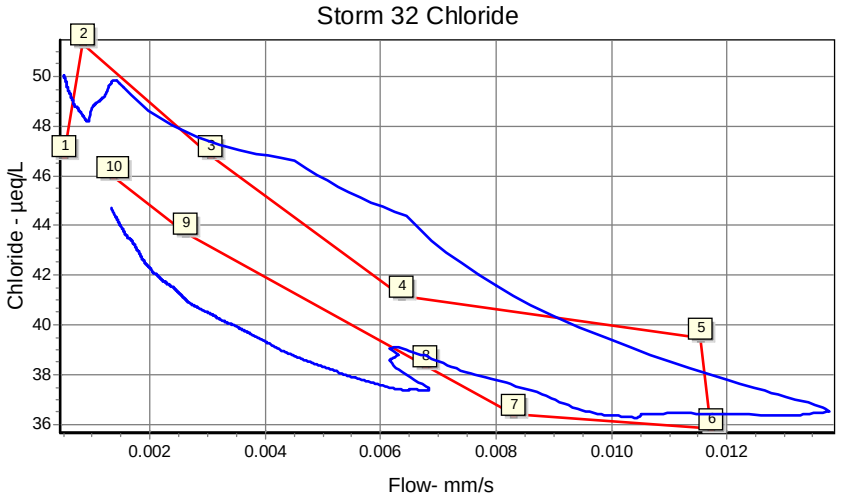

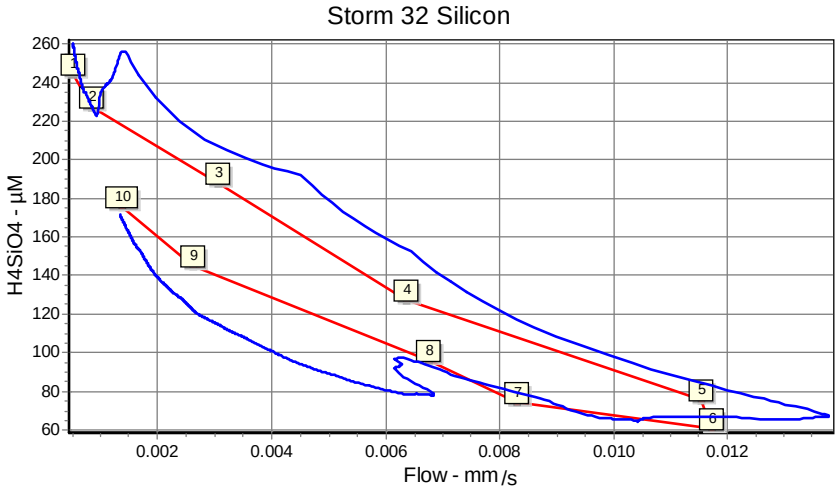

Miscellaneous Info:
Clockwise
API: 31.4
Total Rain: 30 mm
Max Flow Lower Gage: 94 L/sec

Rainfall Elapsed Time by Quartile (min)			
0-25%	25-50%	50-75%	75-100%
423	71	42	257

Figure 38. Results of DEMMA of Storm 32 (January 11-13, 1994).

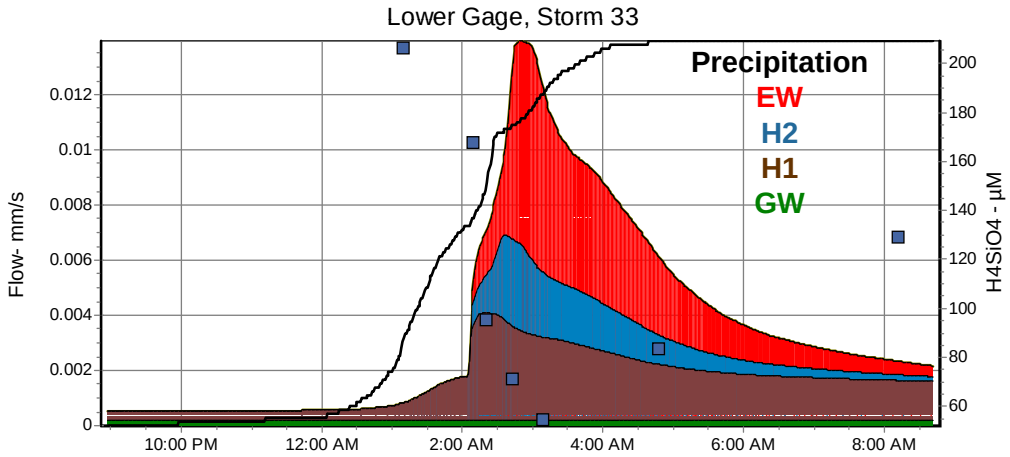

Storm 33, January 27-28, 1994			
	% Runoff	Cl^- (µeq/L)	H_4SiO_4 (µM)
GW	5.6	54.0	405.0
H1	39.9	45.0	172.0
H2	16.4	42.0	64.0
EW	38.1	27.5	0.0
RMSE	N/A	1.6	14.4

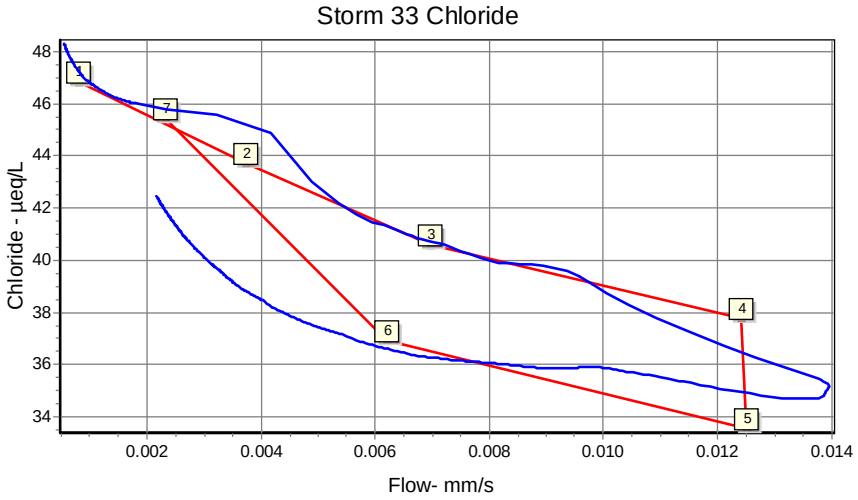

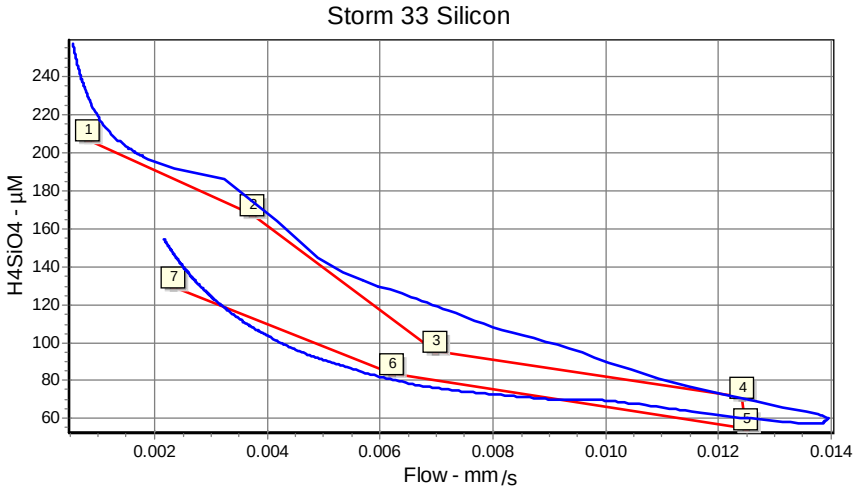

Miscellaneous Info:
Clockwise
API: 19.6
Total Rain: 25 mm
Max Flow Lower Gage: 95 L/sec

Rainfall Elapsed Time by Quartile (min)			
0-25%	25-50%	50-75%	75-100%
197	44	31	129

Figure 39. Results of DEMMA of Storm 33 (January 27-28, 1994).

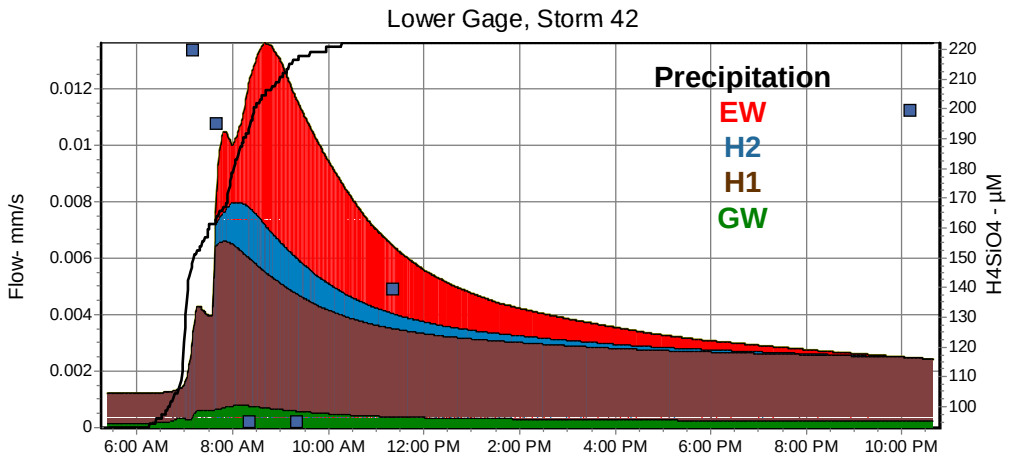

Storm 42, November 28-29, 1994			
	% Runoff	Cl^- (µeq/L)	H_4SiO_4 (µM)
GW	7.1	47.6	406.0
H1	58.4	40.9	189.9
H2	7.1	31.9	47.9
EW	27.4	8.1	0.0
RMSE	N/A	2.4	13.2

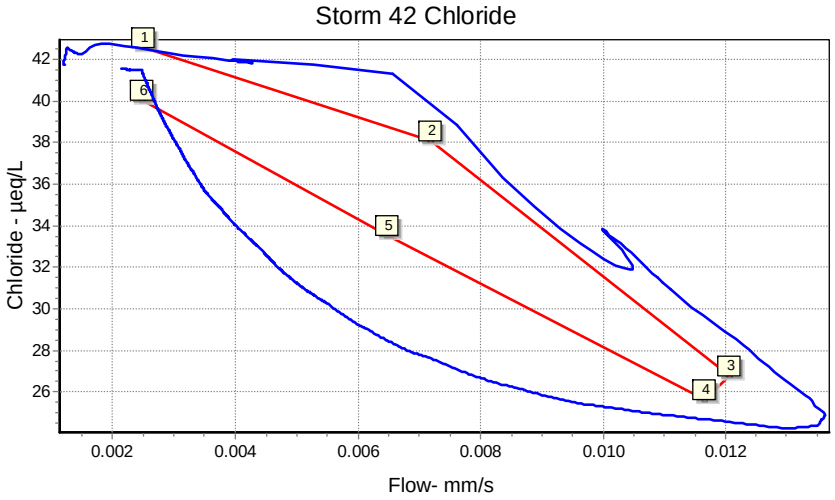

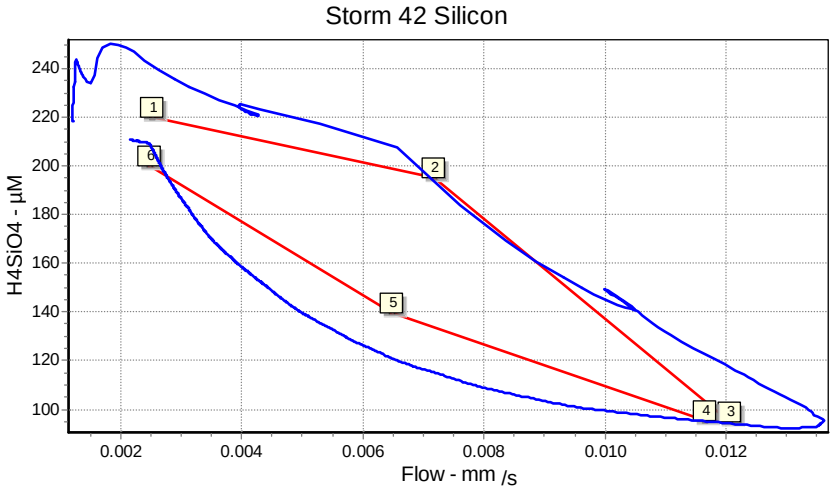

Miscellaneous Info:
Clockwise
API: 47.1
Total Rain: 23 mm
Max Flow Lower Gage: 93 L/sec

Rainfall Elapsed Time by Quartile (min)			
0-25%	25-50%	50-75%	75-100%
44	29	45	123

Figure 40. Results of DEMMA of Storm 4 (November 28-29, 1994).

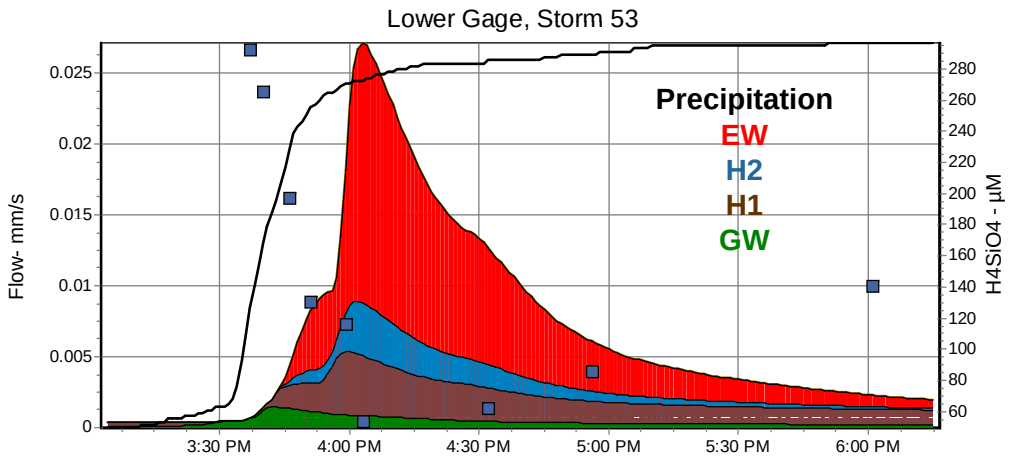

Storm 53, September 21, 1996			
	% Runoff	Cl^- (µeq/L)	H_4SiO_4 (µM)
GW	6.5	47.1	444.1
H1	23.2	42.8	205.7
H2	12.0	28.5	119.3
EW	58.3	4.0	0.0
RMSE	N/A	3.1	69.6

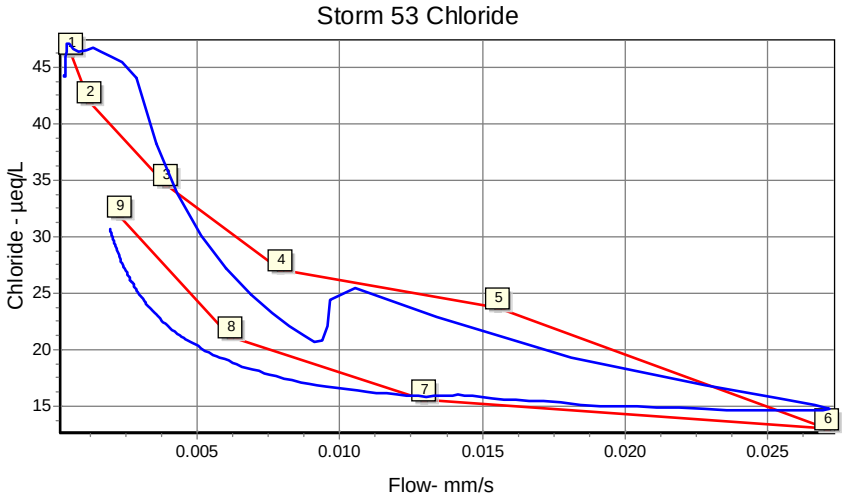

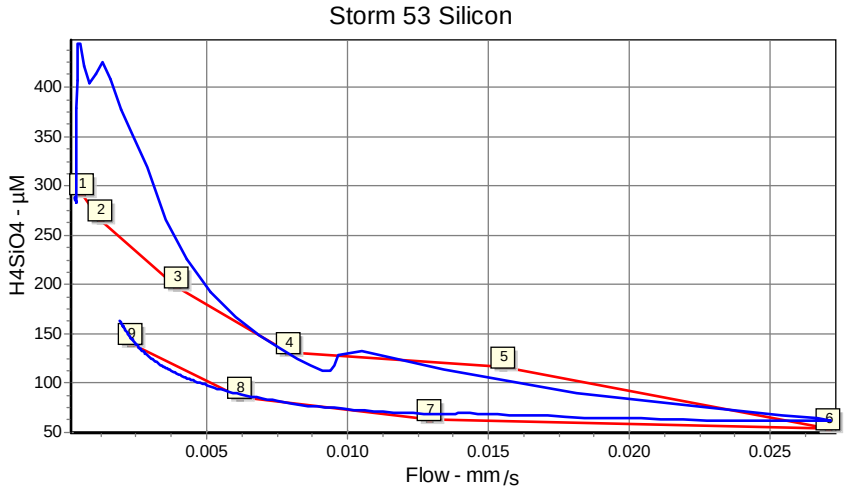

Miscellaneous Info:
Clockwise
API: 48.5
Total Rain: 34 mm
Max Flow Lower Gage: 186 L/sec

Rainfall Elapsed Time by Quartile (min)			
0-25%	25-50%	50-75%	75-100%
25	4	6	124

Figure 41. Results of DEMMA of Storm 53 (September 21, 1996).

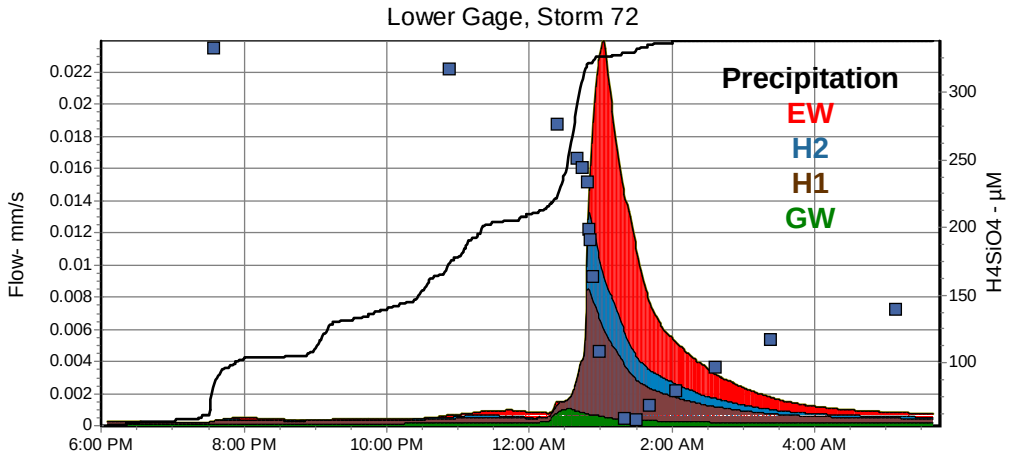

Storm 72, November 1-2, 1999			
	% Runoff	Cl^- (µeq/L)	H_4SiO_4 (µM)
GW	8.6	53.0	387.3
H1	32.1	47.0	217.0
H2	14.3	32.9	103.0
EW	45.0	11.1	0
RMSE	N/A	4.67	35.8

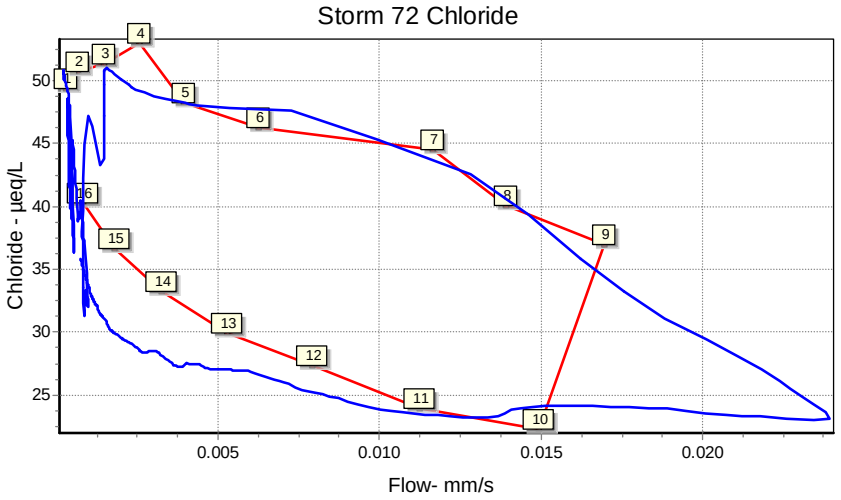

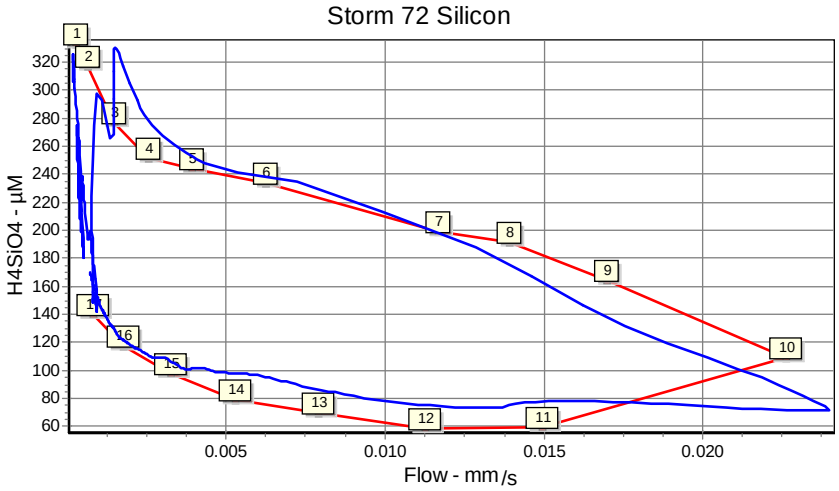

Miscellaneous Info:
Clockwise
API: 11.7
Total Rain: 49 mm
Max Flow Lower Gage: 164 L/sec

Rainfall Elapsed Time by Quartile (min)			
0-25%	25-50%	50-75%	75-100%
170	129	76	85

Figure 42. Results of DEMMA of Storm 72 (November 1-2, 1999).

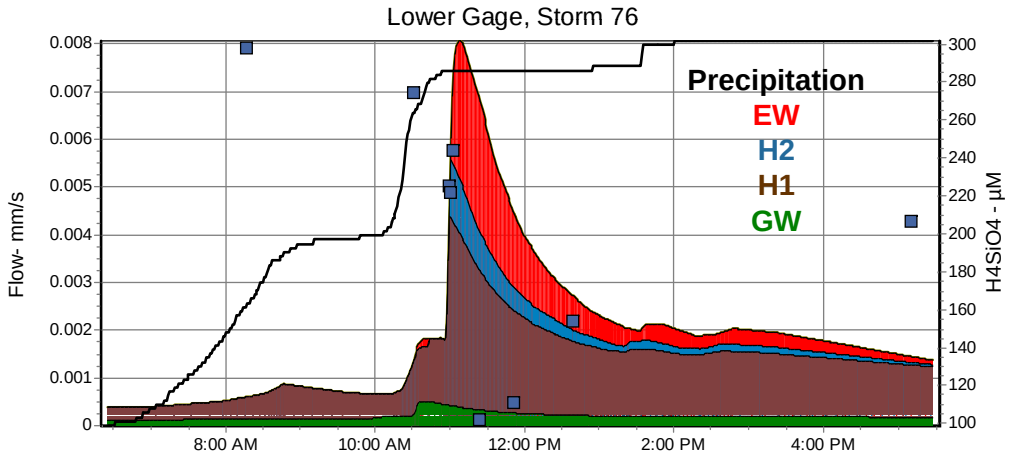

Storm 76, March 16-17, 2000			
	% Runoff	Cl^- (µeq/L)	H_4SiO_4 (µM)
GW	10.8	51.0	411.0
H1	61.4	40.9	207.0
H2	7.7	34.6	88.0
EW	20.5	7.0	17.3
RMSE	N/A	3.4	36.2

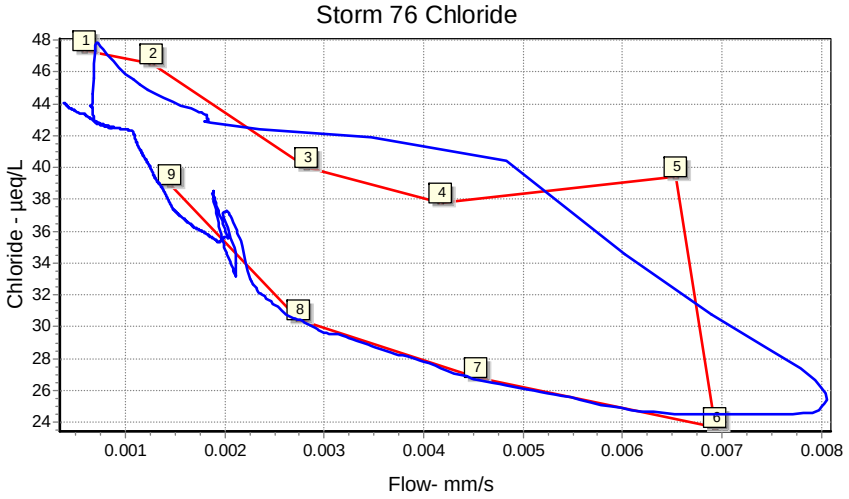

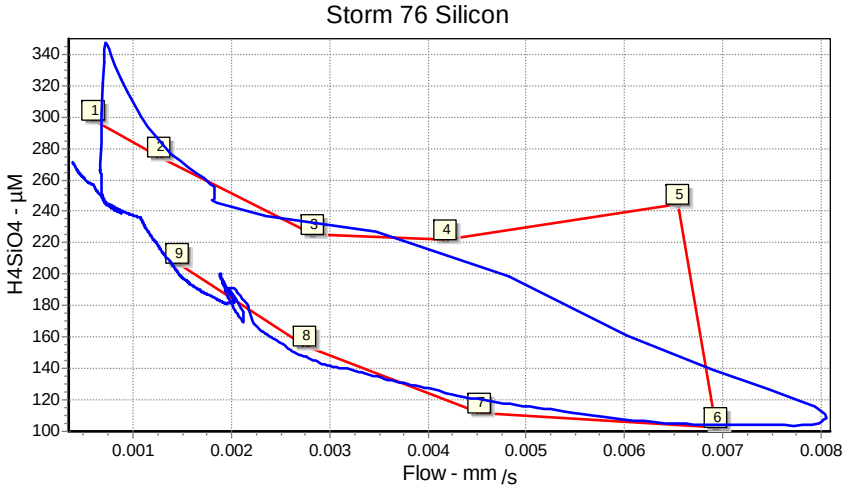

Miscellaneous Info:
Clockwise
API: 18.0
Total Rain: 23 mm
Max Flow Lower Gage: 55 L/sec

Rainfall Elapsed Time by Quartile (min)			
0-25%	25-50%	50-75%	75-100%
92	124	19	215

Figure 43. Results of DEMMA of Storm 76 (March 16-17, 2000).

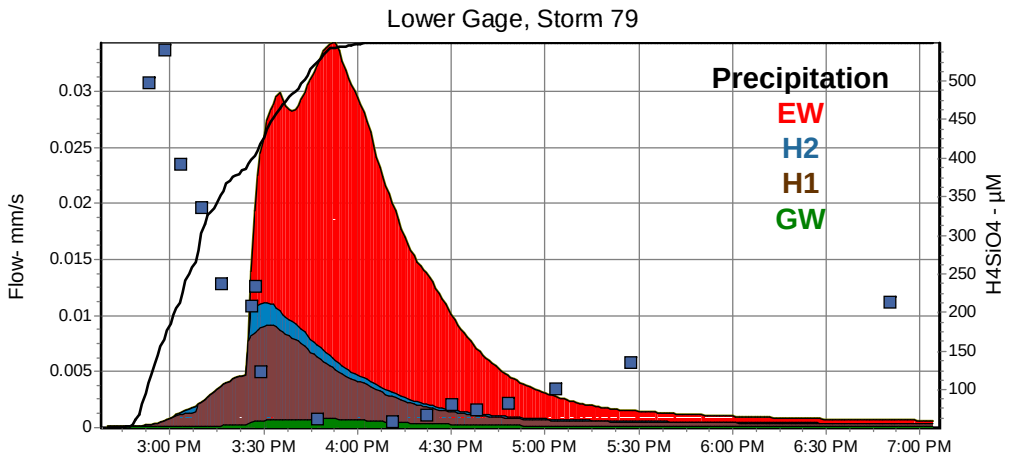

Storm 79, June 19, 2000			
	% Runoff	Cl^- (µeq/L)	H_4SiO_4 (µM)
GW	3.3	50.8	519.0
H1	21.1	28.6	223.0
H2	3.5	27.6	116.0
EW	72.0	9.0	10.2
RMSE	N/A	4.3	88.9

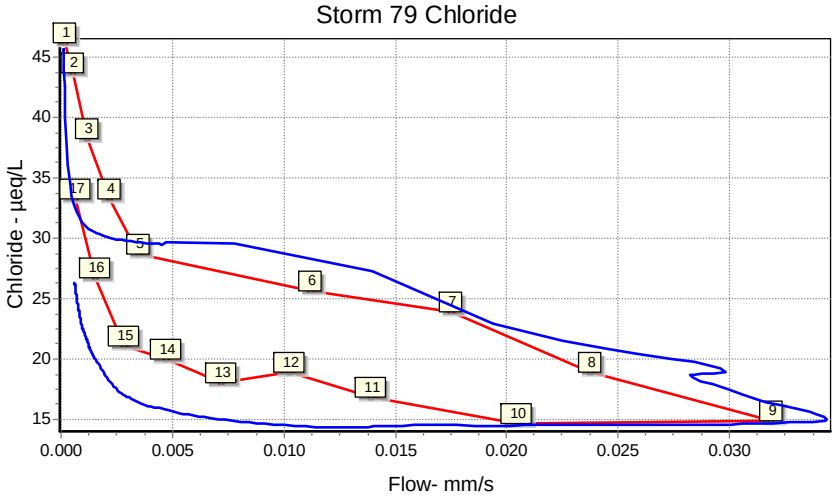

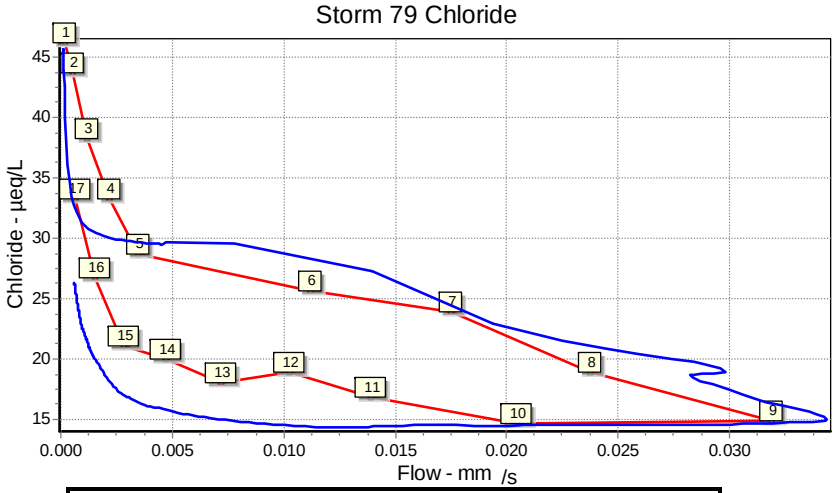

Miscellaneous Info:
Clockwise
API: 20.2
Total Rain: 67 mm
Max Flow Lower Gage: 235 L/sec

Rainfall Elapsed Time by Quartile (min)			
0-25%	25-50%	50-75%	75-100%
13	11	20	32

Figure 44. Results of DEMMA of Storm 79 (June 19, 2000).

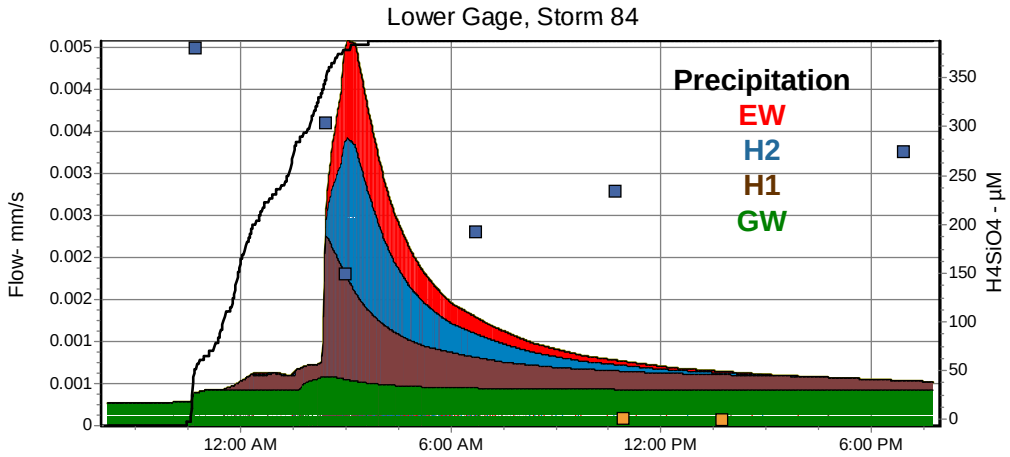

Storm 84, January 29-30 2001			
	% Runoff	Cl^- (µeq/L)	H_4SiO_4 (µM)
GW	42.7	55.0	376.8
H1	26.6	44.1	229.0
H2	18.1	38.0	111.0
EW	12.6	12.1	17.9
RMSE	N/A	1.6	40.0

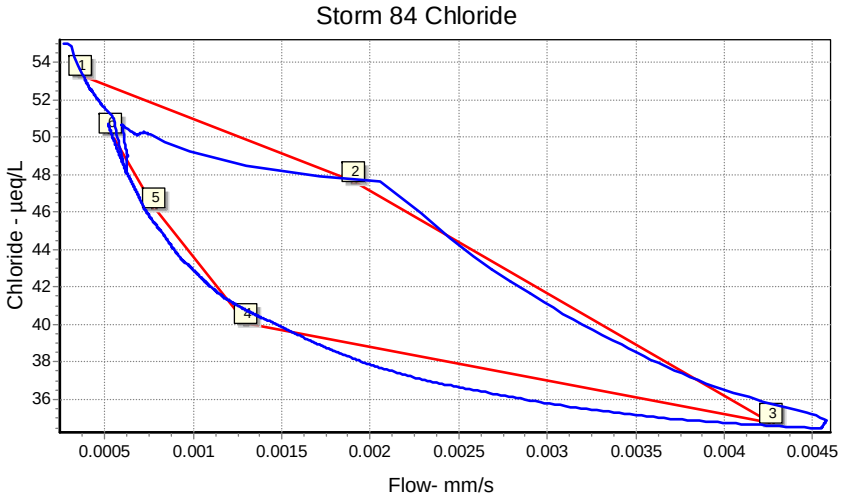

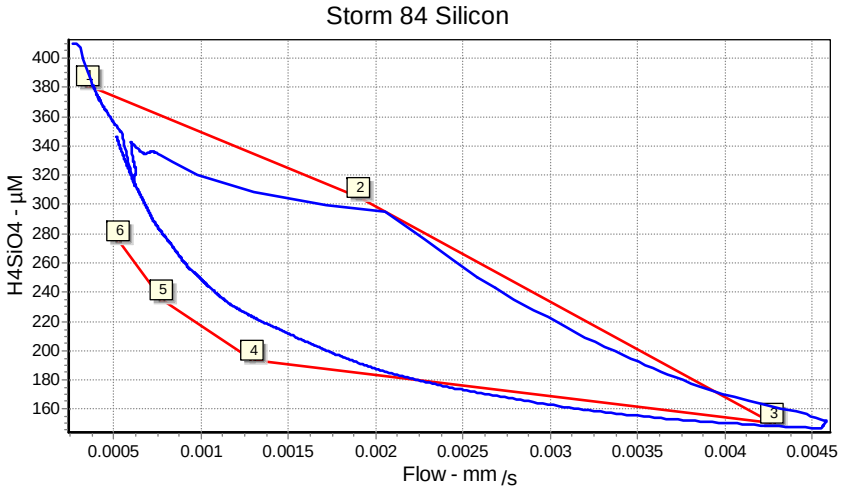

Miscellaneous Info:
Clockwise
API: 17.0
Total Rain: 22 mm
Max Flow Lower Gage: 31 L/sec

Rainfall Elapsed Time by Quartile (min)			
0-25%	25-50%	50-75%	75-100%
61	50	89	112

Figure 45. Results of DEMMA of Storm 84 (January 29-30, 2001).

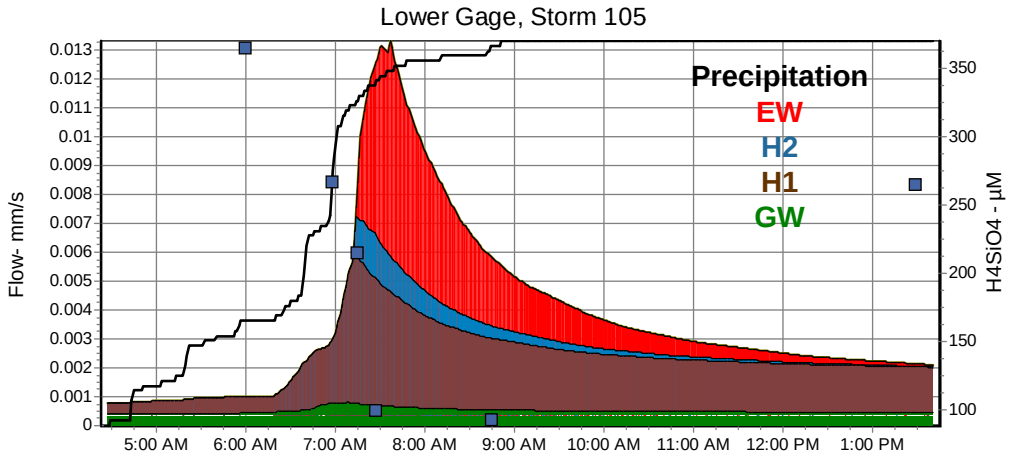

Storm 105, February 22, 2003			
	% Runoff	Cl^- (µeq/L)	H_4SiO_4 (µM)
GW	13.9	46.8	474.0
H1	50.1	40.0	202.0
H2	6.1	35.0	79.0
EW	30	11.0	0.0
RMSE	N/A	1.5	26.7

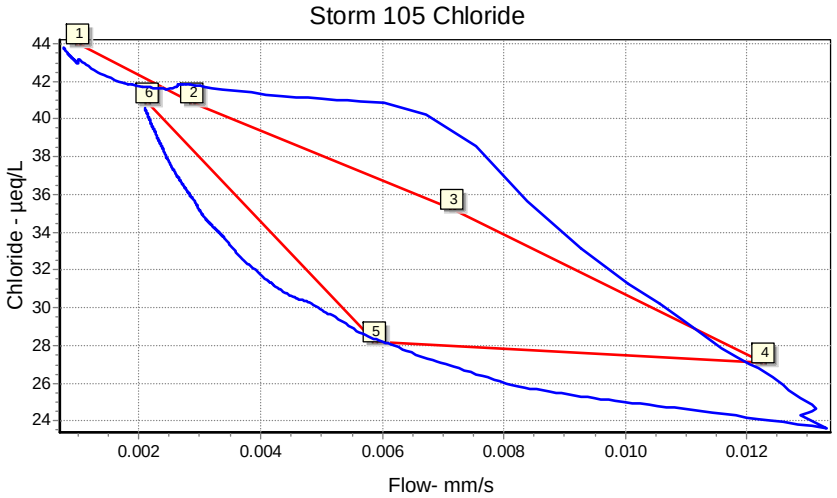

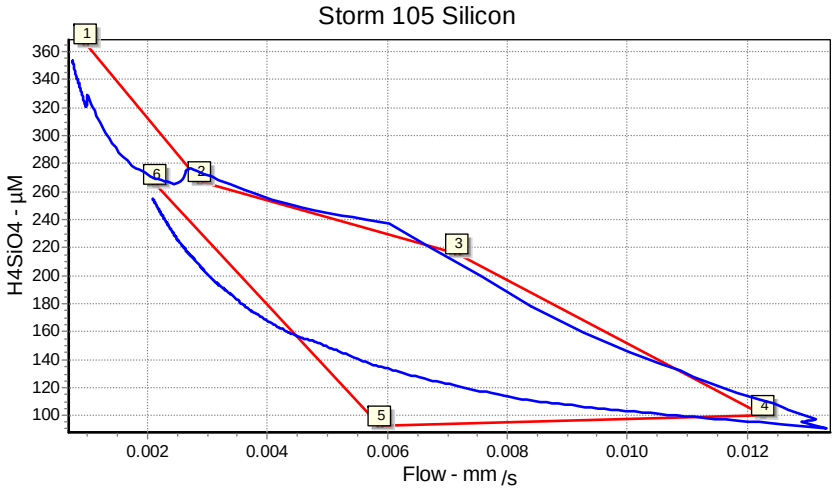

Miscellaneous Info:
Clockwise
API: 34.8
Total Rain: 20 mm
Max Flow Lower Gage: 91 L/sec

Rainfall Elapsed Time by Quartile (min)			
0-25%	25-50%	50-75%	75-100%
86	51	15	110

Figure 46. Results of DEMMA of Storm 105 (February 22, 2003).

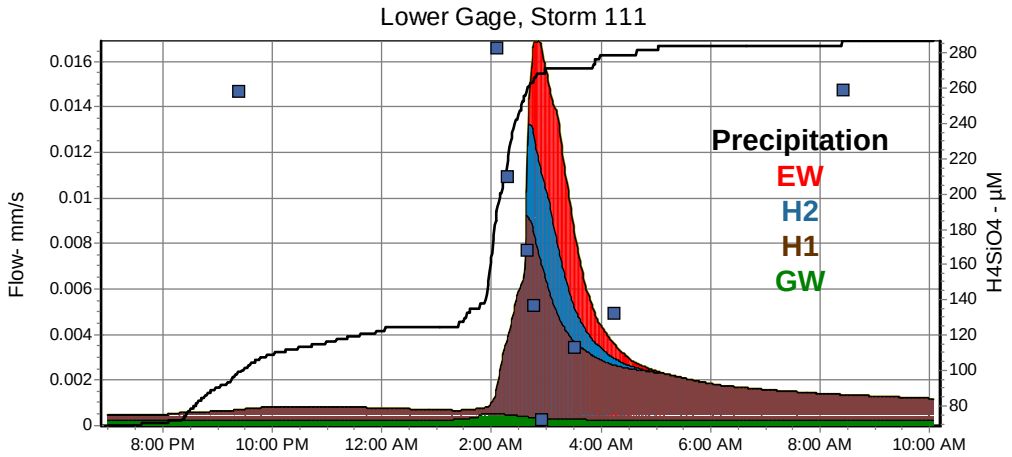

Storm 111, November 18-19, 2003			
	% Runoff	Cl^- (µeq/L)	H_4SiO_4 (µM)
GW	11.2	56.9	413.0
H1	62.9	43.0	182.1
H2	10.4	29.7	77.1
EW	15.5	26.2	7.0
RMSE	N/A	3.6	21.0

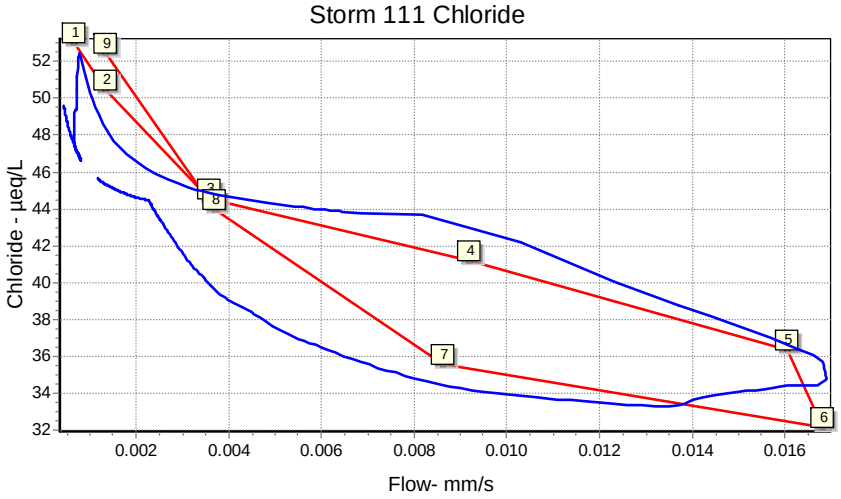

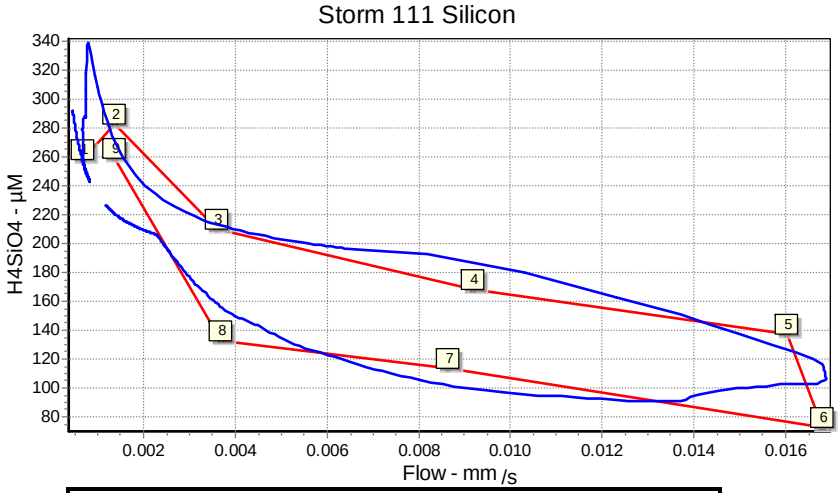

Miscellaneous Info:
Clockwise
API: 13.5
Total Rain: 42 mm
Max Flow Lower Gage: 11 L/sec

Rainfall Elapsed Time by Quartile (min)			
0-25%	25-50%	50-75%	75-100%
267	120	19	361

Figure 47. Results of DEMMA of Storm 111 (November 18-19, 2003).

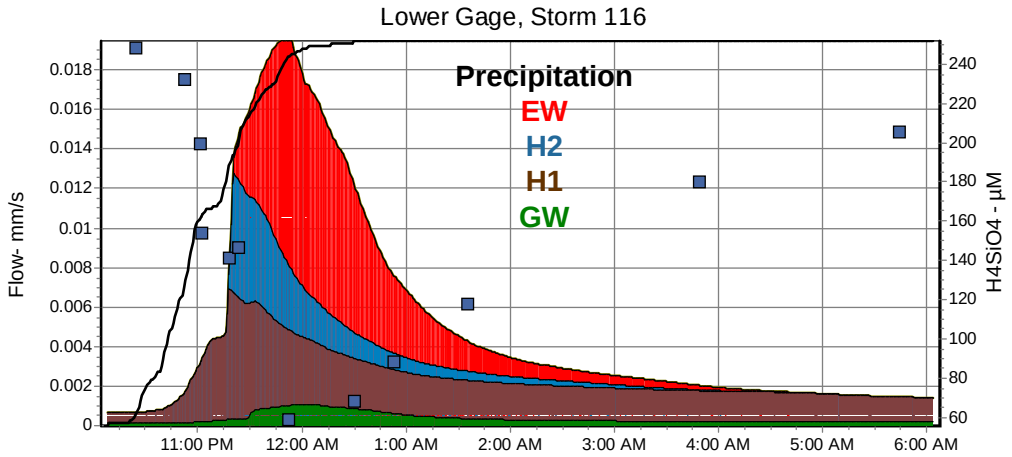

Storm 116, November 2-3, 2004			
	% Runoff	Cl^- (µeq/L)	H_4SiO_4 (µM)
GW	7.1	52.1	418.0
H1	41.2	36.9	176.1
H2	13.6	26.1	66.0
EW	38.1	8.0	3.0
RMSE	N/A	3.0	21.3

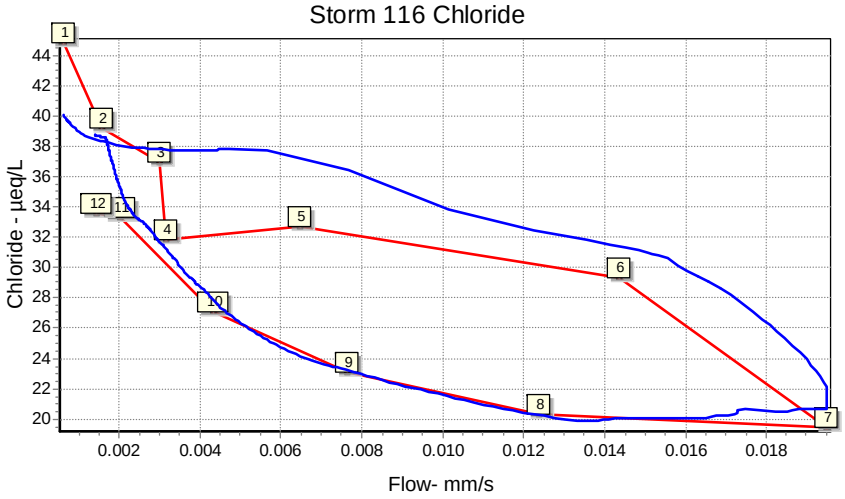

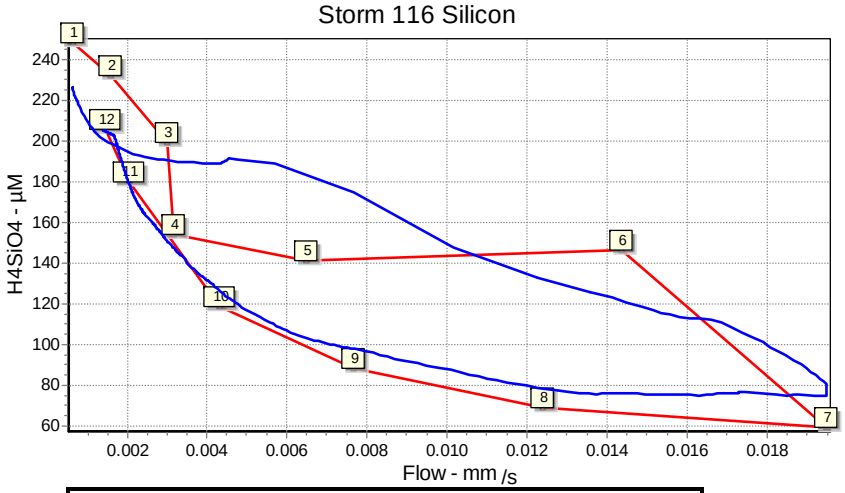

Miscellaneous Info:
Clockwise
API: 13.7
Total Rain: 36 mm
Max Flow Lower Gage: 133 L/sec

Rainfall Elapsed Time by Quartile (min)			
0-25%	25-50%	50-75%	75-100%
36	13	27	65

Figure 48. Results of DEMMA of Storm 116 (November 2-3, 2004).

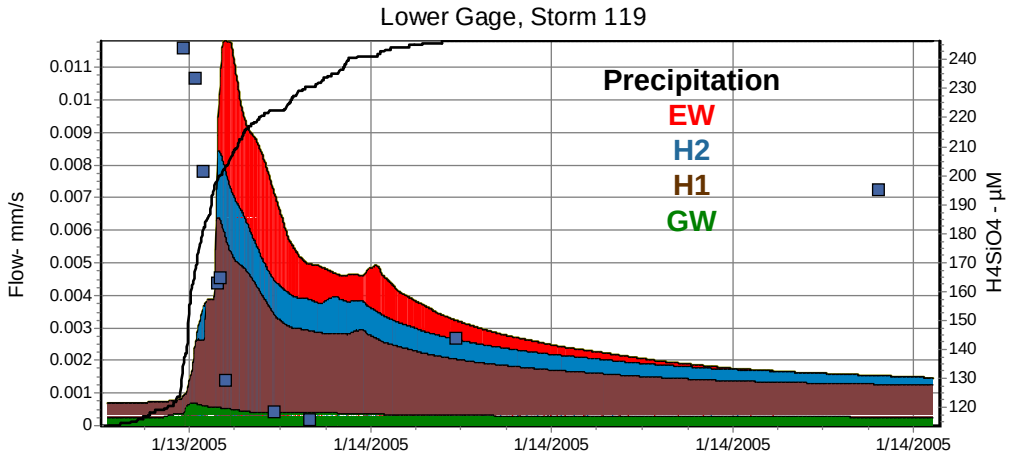

Storm 119, January 13-14, 2005			
	% Runoff	Cl^- (µeq/L)	H_4SiO_4 (µM)
GW	10.5	46.9	386
H1	54.3	37.9	179.7
H2	17.4	29.0	103.0
EW	17.8	18.1	18.0
RMSE	N/A	1.9	15.3

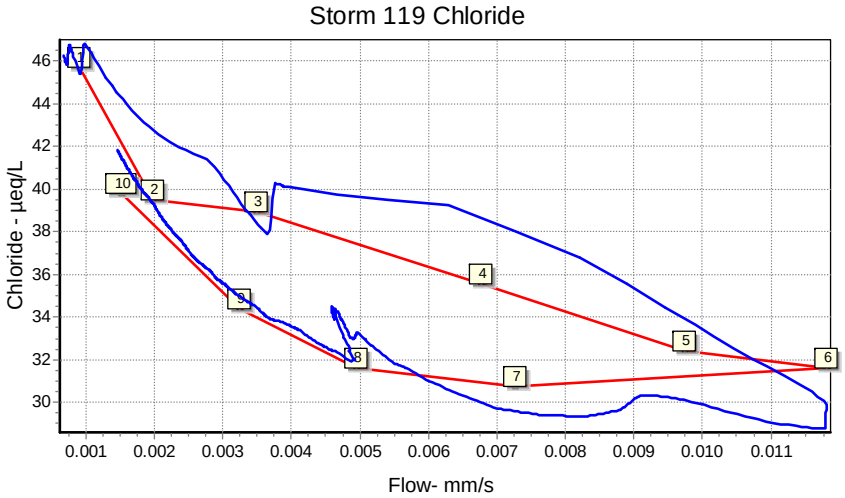

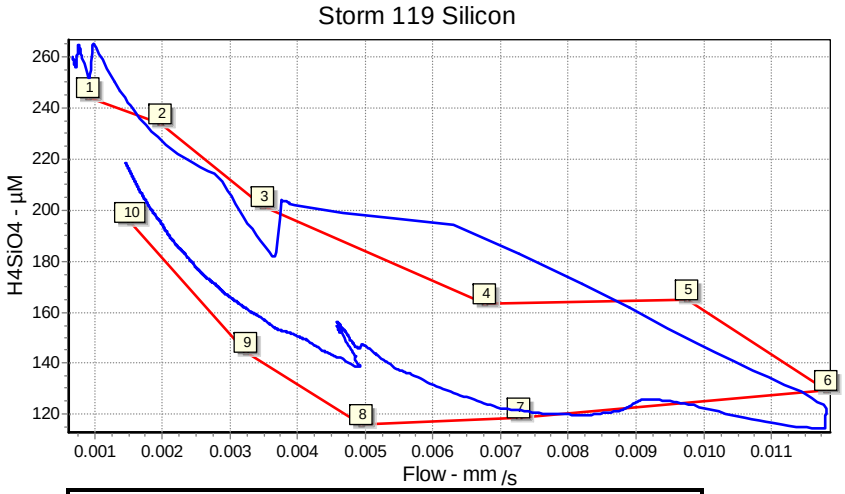

Miscellaneous Info:
Clockwise
API: 10.6
Total Rain: 45 mm
Max Flow Lower Gage: 81 L/sec

Rainfall Elapsed Time by Quartile (min)			
0-25%	25-50%	50-75%	75-100%
136	28	78	398

Figure 49. Results of DEMMA of Storm 119 (January 13-14, 2005).

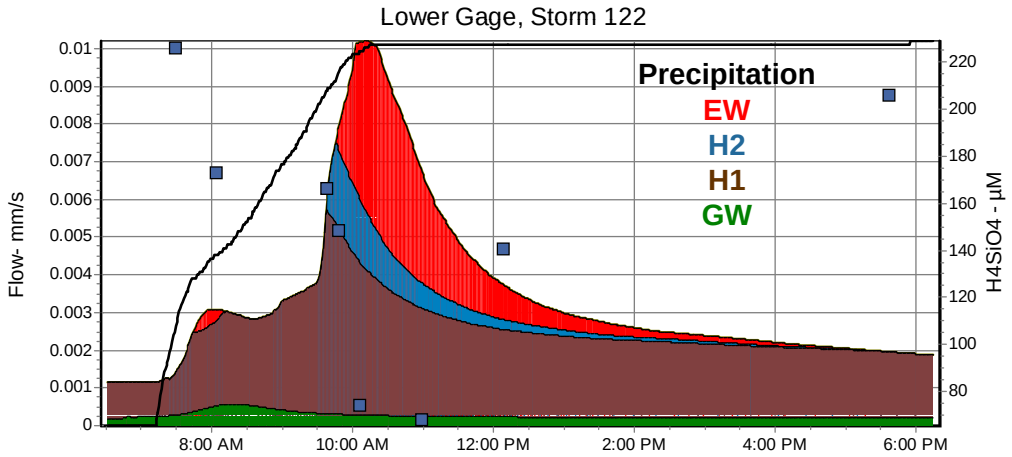

Storm 122, April 30, 2005			
	% Runoff	Cl^- (µeq/L)	H_4SiO_4 (µM)
GW	7.7	53.7	408.0
H1	66.2	24.7	155.7
H2	6.8	21.1	87.2
EW	19.4	4.9	0.0
RMSE	N/A	1.4	16.4

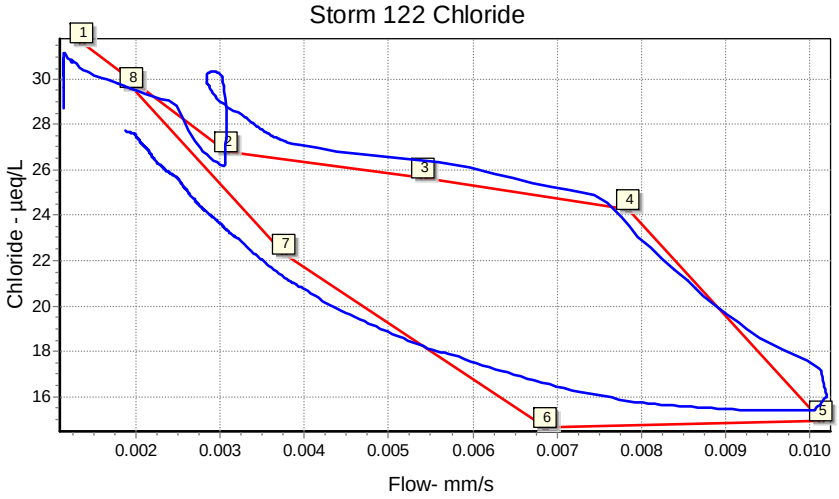

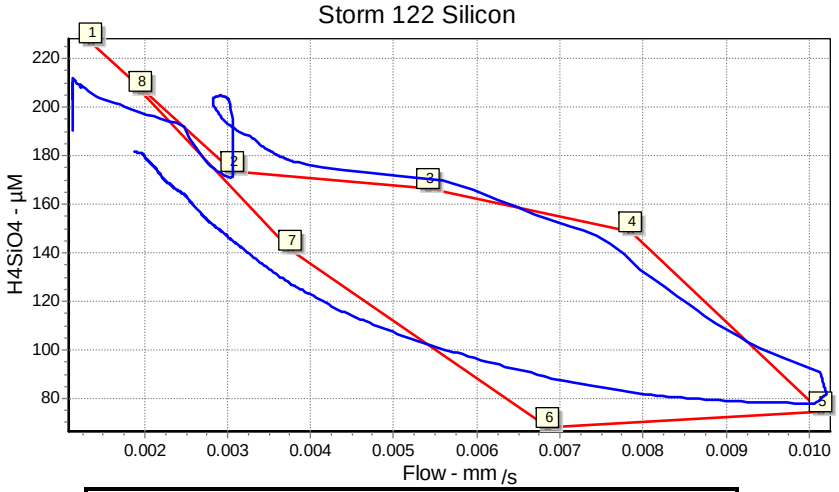

Miscellaneous Info:
Clockwise
API: 28.2
Total Rain: 29 mm
Max Flow Lower Gage: 70 L/sec

Rainfall Elapsed Time by Quartile (min)			
0-25%	25-50%	50-75%	75-100%
16	53	55	519

Figure 50. Results of DEMMA of Storm 122 (April 30, 2005).

APPENDIX B: ANALYZED STORMS WITH COUNTER-CLOCKWISE HYSTERESIS

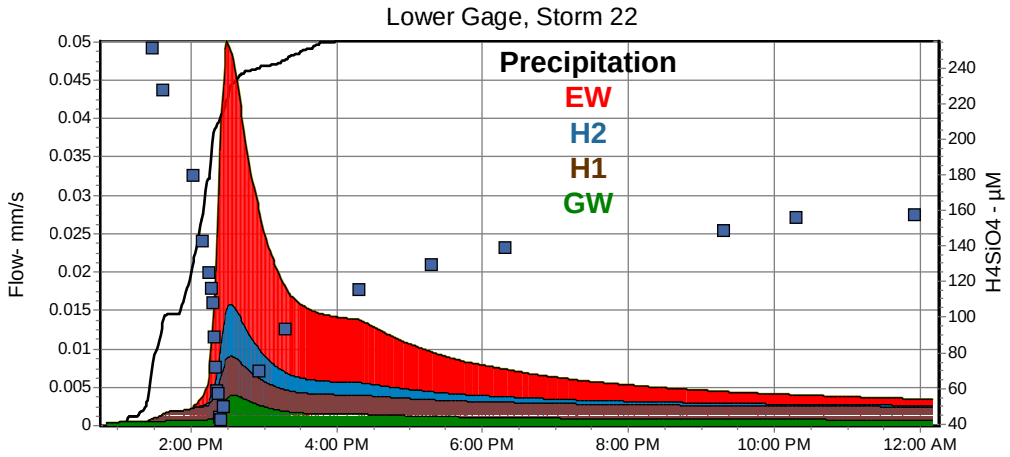

Storm 22, April 23-24, 1988			
	% Runoff	Cl^- (µeq/L)	H_4SiO_4 (µM)
GW	12.8	50.1	424.8
H1	23.3	44.3	194.1
H2	10.5	29.1	67.2
EW	53.3	5.9	0.0
RMSE	N/A	31.7	128.6

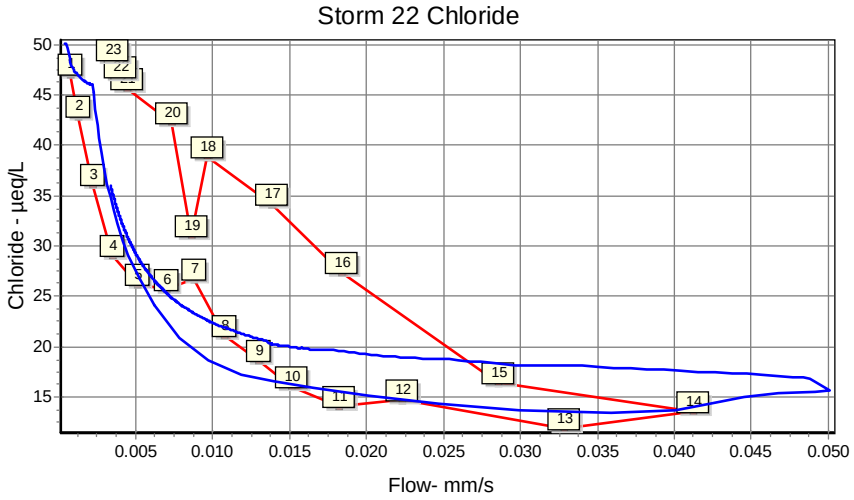

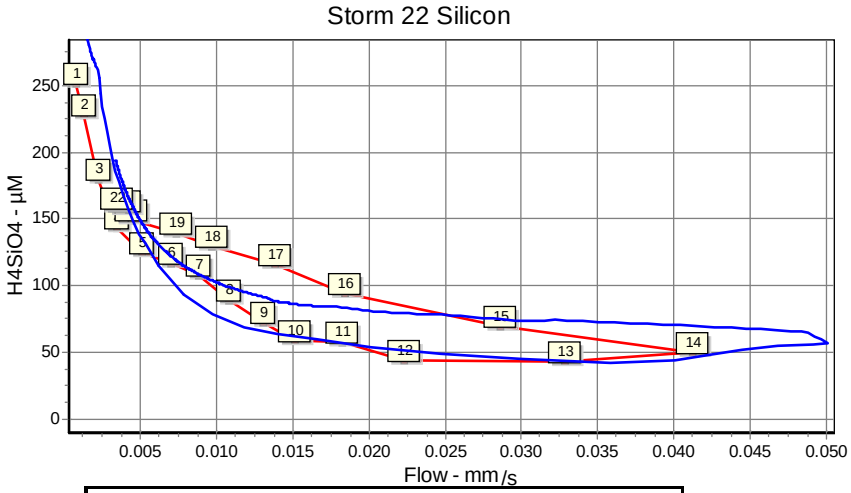

Miscellaneous Info:
Counterclockwise
API: 40.7
Total Rain: 54 mm
Max Flow Lower Gage: 342 L/sec

Rainfall Elapsed Time by Quartile (min)			
0-25%	25-50%	50-75%	75-100%
29	32	11	100

Figure 51. Results of DEMMA of Storm 22 (April 23-24, 1988).

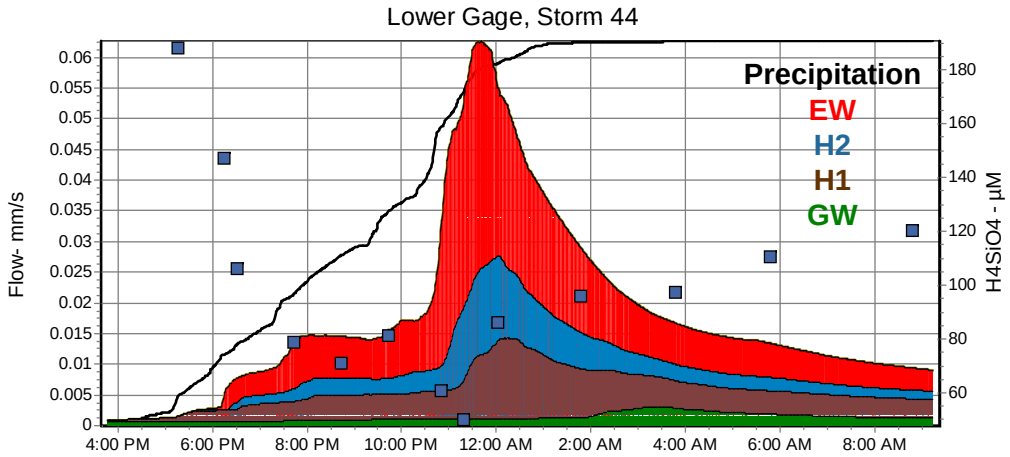

Storm 44, February 10-11, 1995			
	% Runoff	Cl^- (µeq/L)	H_4SiO_4 (µM)
GW	7.4	50	431
H1	25.5	45.1	187.1
H2	18.6	30	92
EW	48.5	5	4.1
RMSE	N/A	3.5	28.6

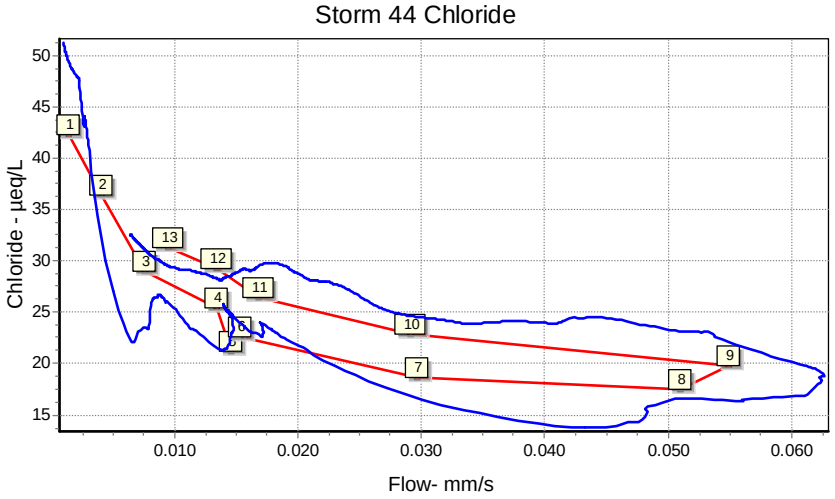

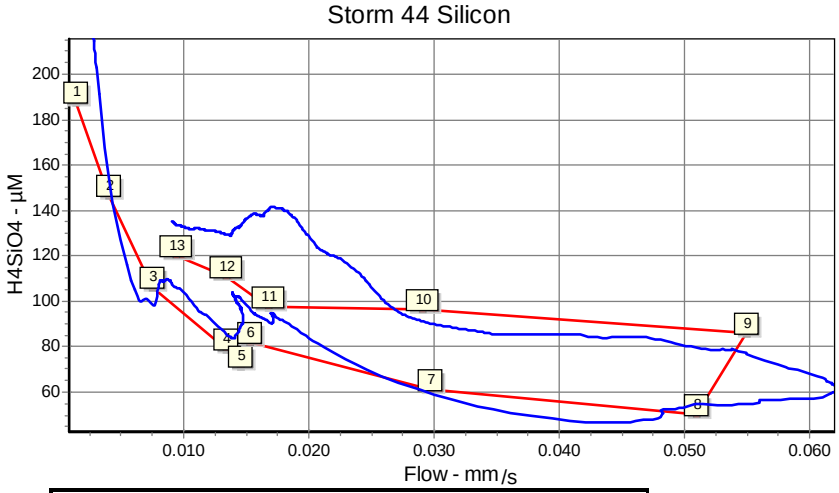

Miscellaneous Info:
Counterclockwise
API: 10.1
Total Rain: 74 mm
Max Flow Lower Gage: 428 L/sec

Rainfall Elapsed Time by Quartile (min)			
0-25%	25-50%	50-75%	75-100%
171	143	79	288

Figure 52. Results of DEMMA of Storm 44 (February 10-11, 1995).

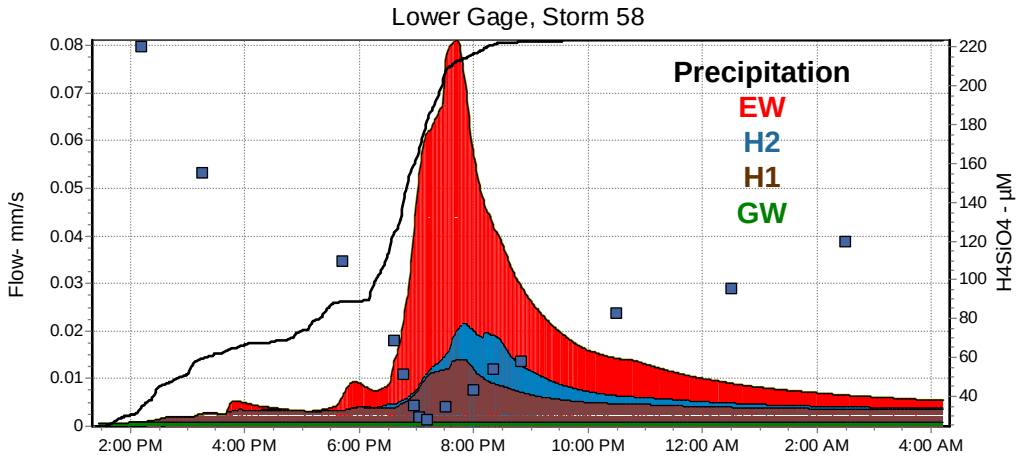

Storm 58, April 27-28, 1997			
	% Runoff	Cl^- (µeq/L)	H_4SiO_4 (µM)
GW	5.5	50	417
H1	25.7	39	183
H2	9.9	26.5	52
EW	58.9	4	0
RMSE	N/A	4.2	55.6

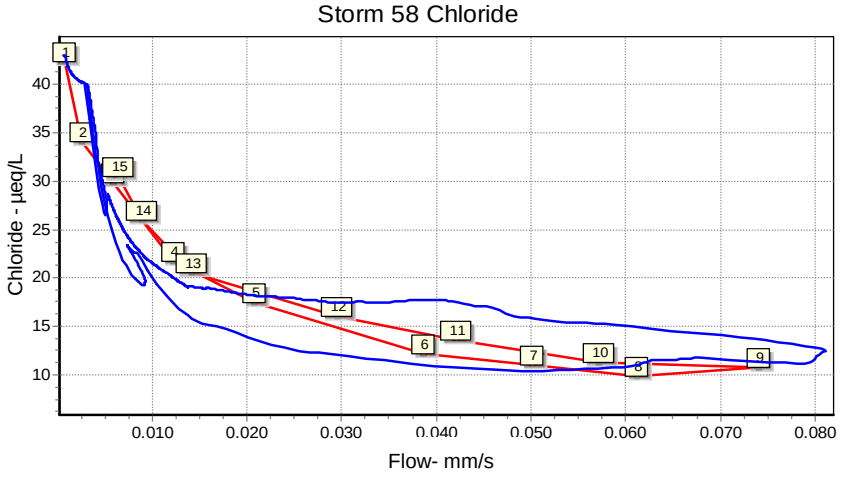

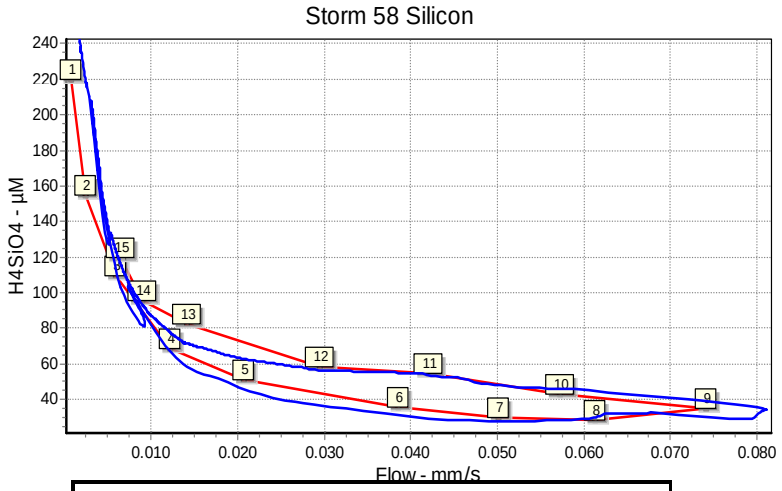

Miscellaneous Info:
Counterclockwise
API: 31.8
Total Rain: 76 mm
Max Flow Lower Gage: 554 L/sec

Rainfall Elapsed Time by Quartile (min)			
0-25%	25-50%	50-75%	75-100%
211	90	30	146

Figure 53. Results of DEMMA of Storm 58 (April 27-28, 1997).

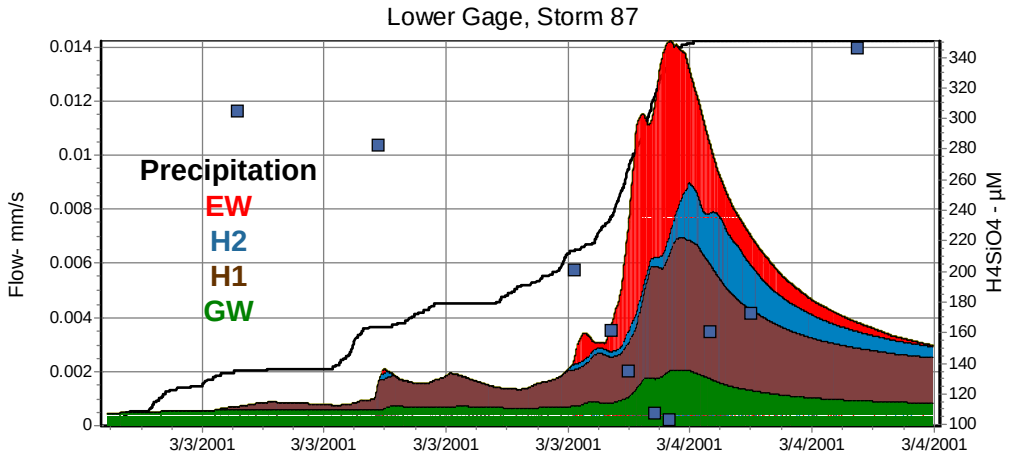

Storm 87, March 2-4, 2001			
	% Runoff	Cl^- (µeq/L)	H_4SiO_4 (µM)
GW	25.2	46	402.0
H1	41.2	41.6	187.0
H2	11.3	29.8	86.0
EW	22.4	6.4	5.1
RMSE	N/A	3.6	51.5

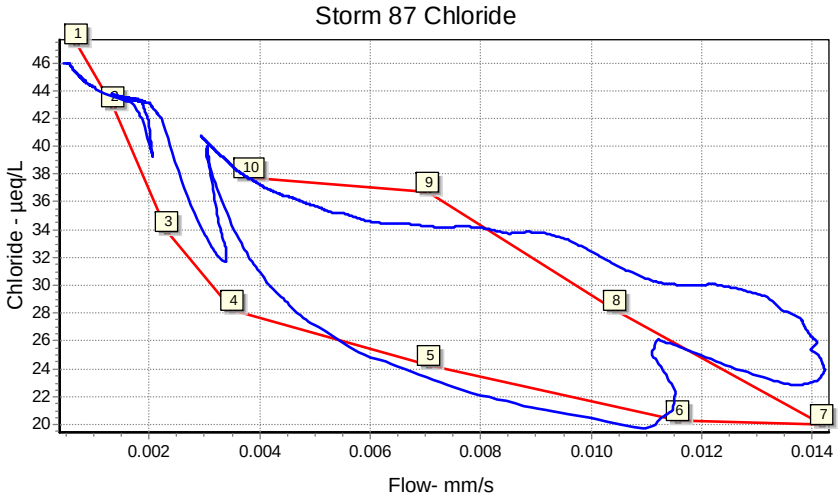

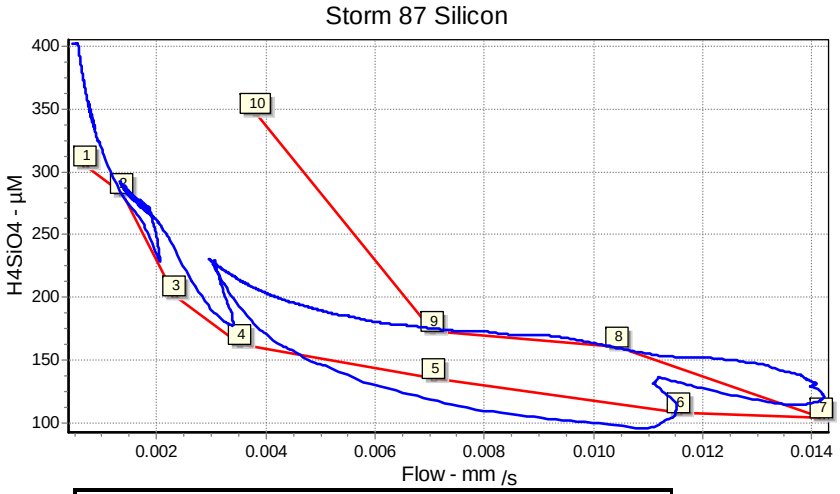

Miscellaneous Info:
Counterclockwise
API: 39.8
Total Rain: 51 mm
Max Flow Lower Gage: 97 L/sec

Rainfall Elapsed Time by Quartile (min)			
0-25%	25-50%	50-75%	75-100%
749	693	132	151

Figure 54. Results of DEMMA of Storm 87 (March 2-4, 2001).

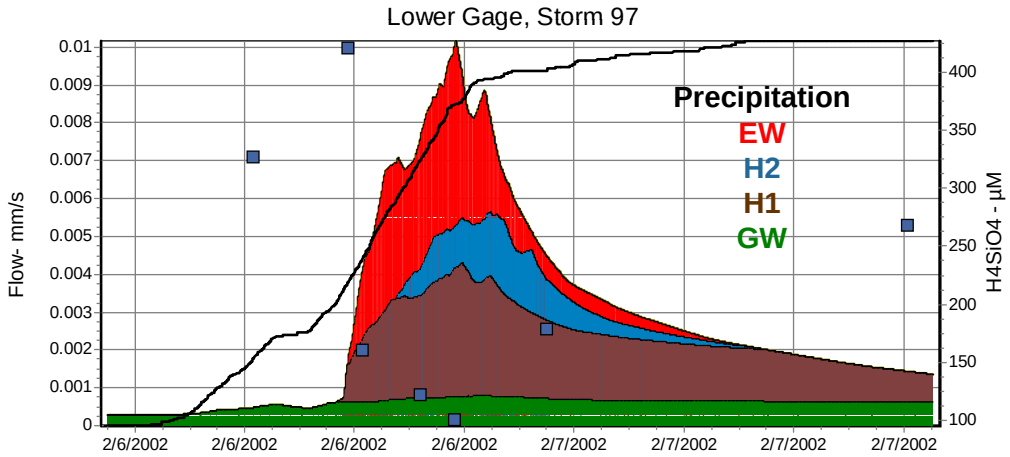

Storm 97, February 5-7, 2002			
	% Runoff	Cl^- (µeq/L)	H_4SiO_4 (µM)
GW	20.9	50.0	391.0
H1	44.4	47.1	207.2
H2	11.0	32.0	85.0
EW	23.7	14.0	5.0
RMSE	N/A	2.9	64.7

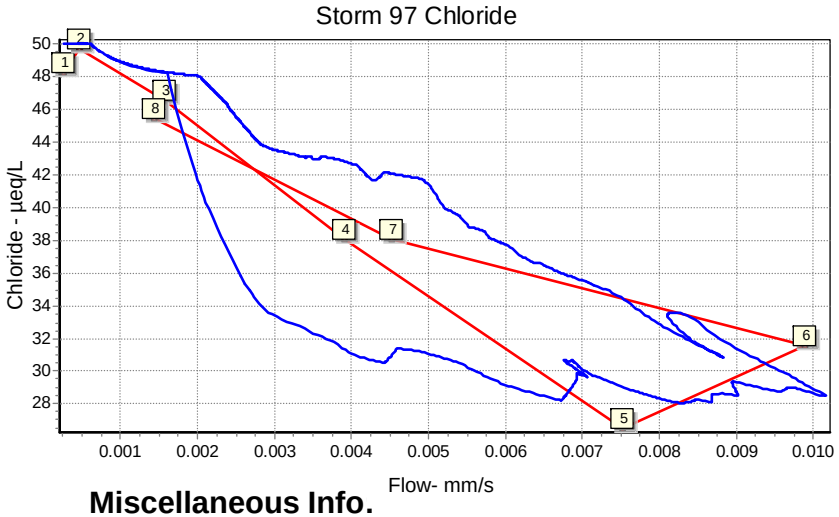

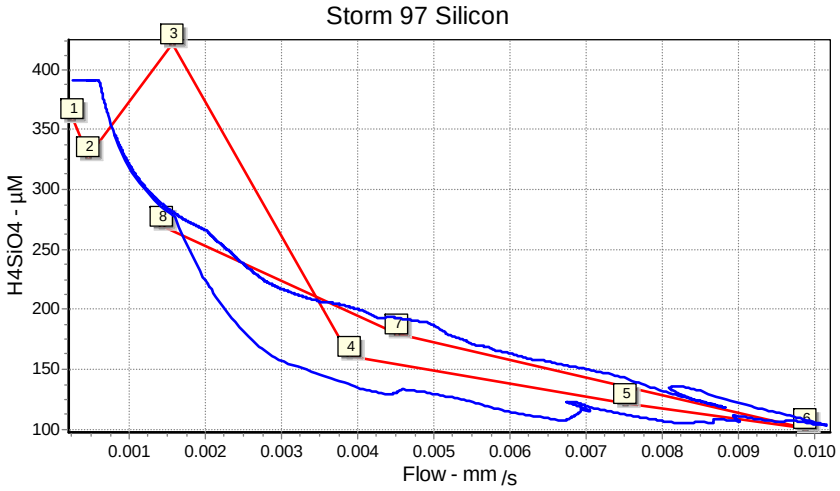

Miscellaneous Info.
Counterclockwise
API: 27.2
Total Rain: 59 mm
Max Flow Lower Gage: 69 L/sec

Rainfall Elapsed Time by Quartile (min)			
0-25%	25-50%	50-75%	75-100%
524	211	193	1020

Figure 55. Results of DEMMA of Storm 97 (February 5-7, 2002).

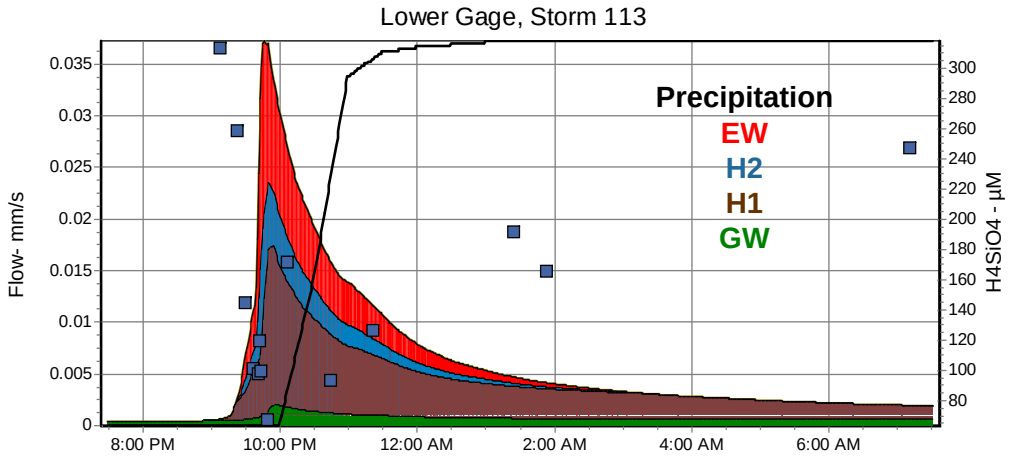

Storm 113, June 16-17, 2004			
	% Runoff	Cl^- (µeq/L)	H_4SiO_4 (µM)
GW	12.3	46	416
H1	53.6	37.3	209
H2	11.2	21	124.9
EW	22.8	9	0
RMSE	N/A	2.8	35.2

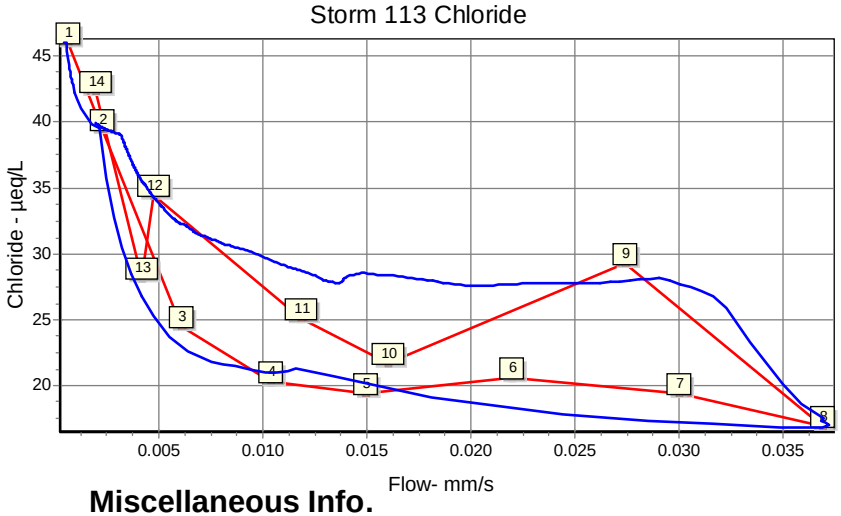

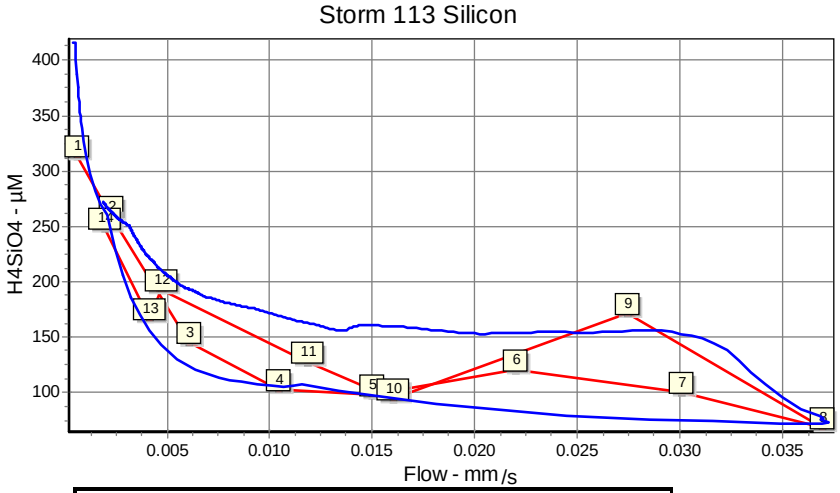

Miscellaneous Info.
Counterclockwise
API: 60.8
Total Rain: 38 mm
Max Flow Lower Gage: 254 L/sec
Erroneous Rainfall data

Rainfall Elapsed Time by Quartile (min)			
0-25%	25-50%	50-75%	75-100%
19	17	15	128

Figure 56. Results of DEMMA of Storm 113 (June 16-17, 2004).